

UNCLASSIFIED

AD NUMBER	
AD224419	
CLASSIFICATION CHANGES	
TO:	UNCLASSIFIED
FROM:	SECRET
LIMITATION CHANGES	
TO: Approved for public release; distribution is unlimited.	
FROM: Distribution authorized to U.S. Gov't. agencies and their contractors; Administrative/Operational Use; 1955. Other requests shall be referred to Navy Electronics Coomand, San Diego, CA.	
AUTHORITY	
15 May 1964 per doc markings ; NEL ltr 31 Dec 1985	

THIS PAGE IS UNCLASSIFIED

THIS REPORT HAS BEEN DELIMITED
AND CLEARED FOR PUBLIC RELEASE
UNDER DOD DIRECTIVE 5200.20 AND
NO RESTRICTIONS ARE IMPOSED UPON
ITS USE AND DISCLOSURE.

DISTRIBUTION STATEMENT A

APPROVED FOR PUBLIC RELEASE;
DISTRIBUTION UNLIMITED.

UNCLASSIFIED

AD 2 2 4 4 1 9

DEFENSE DOCUMENTATION CENTER

FOR

SCIENTIFIC AND TECHNICAL INFORMATION

CAMERON STATION, ALEXANDRIA, VIRGINIA

CLASSIFICATION CHANGED
TO UNCLASSIFIED

FROM SECRET RESTRICTED DATA L

PER AUTHORITY LISTED IN

DD TAB NO U64-10 PBno. 150

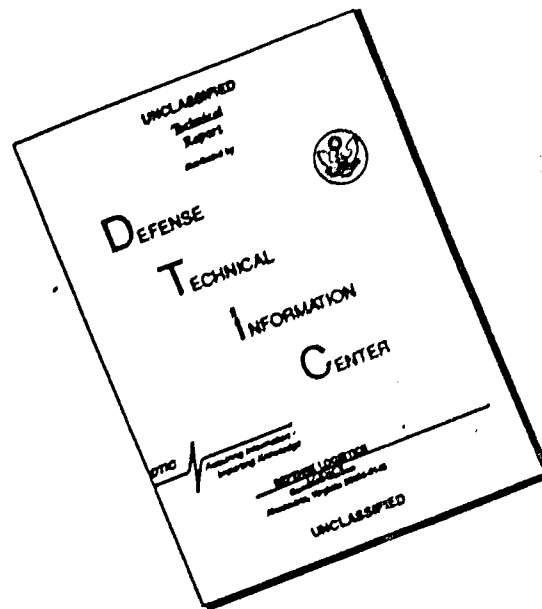
DATE 15 May 64 - -



UNCLASSIFIED

NOTICE: When government or other drawings, specifications or other data are used for any purpose other than in connection with a definitely related government procurement operation, the U. S. Government thereby incurs no responsibility, nor any obligation whatsoever; and the fact that the Government may have formulated, furnished, or in any way supplied the said drawings, specifications, or other data is not to be regarded by implication or otherwise as in any manner licensing the holder or any other person or corporation, or conveying any rights or permission to manufacture, use or sell any patented invention that may in any way be related thereto.

DISCLAIMER NOTICE



THIS DOCUMENT IS BEST QUALITY AVAILABLE. THE COPY FURNISHED TO DTIC CONTAINED A SIGNIFICANT NUMBER OF PAGES WHICH DO NOT REPRODUCE LEGIBLY.

NOTICE: When government or other drawings, specifications or other data are used for any purpose other than in connection with a definitely related government procurement operation, the U. S. Government thereby incurs no responsibility, nor any obligation whatsoever; and the fact that the Government may have formulated, furnished, or in any way supplied the said drawings, specifications, or other data is not to be regarded by implication or otherwise as in any manner licensing the holder or any other person or corporation, or conveying any rights or permission to manufacture, use or sell any patented invention that may in any way be related thereto.

NOTICE:

THIS DOCUMENT CONTAINS INFORMATION
AFFECTING THE NATIONAL DEFENSE OF
THE UNITED STATES WITHIN THE MEAN-
ING OF THE ESPIONAGE LAWS, TITLE 18,
U.S.C., SECTIONS 793 and 794. THE
TRANSMISSION OR THE REVELATION OF
ITS CONTENTS IN ANY MANNER TO AN
UNAUTHORIZED PERSON IS PROHIBITED
BY LAW.

USMIO

RESTRICTED DATA

SECRET

WT-1104

Copy No. 145 A

Restricted Data

WDO

Technical Library
100000

Operation

TEAPOT

NEVADA TEST SITE

February - May 1955

Project 1.5

FRESHOCK SOUND VELOCITIES NEAR
THE GROUND IN THE VICINITY OF
AN ATOMIC EXPLOSION

AIR FORCE
BALLISTIC MISSILE DIVISION

TECHNICAL LIBRARY

Document No. 341057

Copy No. 1



RESTRICTED DATA

This document contains restricted data as defined in the Atomic Energy Act of 1951. Its transmittal or the disclosure of its contents in any manner to an unauthorized person is prohibited.

EXCLUDED FROM AUTOMATIC
REGRADING; DOD DIR 5200.10
DOES NOT APPLY

HEADQUARTERS FIELD COMMAND, ARMED FORCES SPECIAL WEAPONS PROJECT
SANDIA BASE, ALBUQUERQUE, NEW MEXICO

RESTRICTED DATA

SECRET

Inquiries relative to this report may be made to

Chief, Armed Forces Special Weapons Project
Washington, D. C.

If this report is no longer needed, return to
AEC Technical Information Service Extension
P. O. Box 401
Oak Ridge, Tennessee

RESTRICTED DATA 7-6100

146 76
14307

(4) NA 5 630500

SECRET

This document consists of 76 pages.

No. 145 of 210 copies, Series A

WT-1104

OPERATION TEAPOT—PROJECT 1.5

7 NA

Report to the Test Director

6
PRESHOCK SOUND VELOCITIES NEAR
THE GROUND IN THE VICINITY OF
AN ATOMIC EXPLOSION, [U]

9 NA
11 [1755]

10 1/2

R. C. McLoughlin,

12 76p

Navy Electronics Laboratory
San Diego, California

13 NA

14 17 NA

"This document contains information affecting the National
Defense, the disclosure of which in any manner to an unauthorized
person is prohibited by law."

1. 100

11 WT-1104

RESTRICTED DATA

This document contains restricted data as
defined in the Atomic Energy Act of 1954.
Its transmittal or the disclosure of its
contents in any manner to an unauthorized
person is prohibited.

20 S-RED

21 1/2 1.5 L-1

SECRET

RESTRICTED DATA

SECRET

SUMMARY OF SHOT DATA, OPERATION TEAPOT

Shot	Code Name	Date	Time*	Area	Type	Latitude and Longitude of Zero Point	
1	Waap	18 February	1204	T-7-4 ¹	762-ft Air	01° 00' 11.000"	114° 01' 10.000"
2	Moth	22 February	0515	T-3	300-ft Tower	01° 01' 02.004"	114° 01' 10.001"
3	Tusia	1 March	0530	T-9b	300-ft Tower	01° 02' 01.020"	114° 01' 01.001"
4	Tork	7 March	0520	T-2	500-ft Tower	01° 00' 10.004"	114° 01' 01.004"
5	Hornet	12 March	0520	T-3a	300-ft Tower	01° 01' 00.003"	114° 01' 01.004"
6	Bee	22 March	0505	T-7-1a	500-ft Tower	01° 00' 01.001"	114° 01' 00.004"
7	ISS	23 March	1230	T-16a	67-ft Underground	01° 00' 00.000"	114° 02' 01.000"
8	Apple	24 March	0455	T-8	500-ft Tower	01° 00' 00.000"	114° 00' 00.000"
9	Waap	29 March	1604	T-7-0 ²	740-ft Air	01° 00' 11.000"	114° 01' 10.000"
10	HA	6 April	1000	T-5 ³	36 620-ft MSL Air	01° 01' 01.001"	114° 03' 20.004"
11	Post	9 April	0430	T-9c	300-ft Tower	01° 01' 10.000"	114° 01' 00.000"
12	M.T.	15 April	1115	FF	400-ft Tower	01° 01' 02.001"	114° 00' 00.004"
13	Apple 2	5 May	0510	T-1	500-ft Tower	01° 00' 11.001"	114° 00' 00.001"
14	Zuchtni	15 May	0500	T-7-1a	500-ft Tower	01° 00' 01.000"	114° 01' 10.004"

* Approximate local time: PST prior to 24 April; PDT after 24 April

¹ Actual zero point 36 feet north, 426 feet west of T-7-4

² Actual zero point 91 feet north, 62 feet west of T-7-4

³ Actual zero point 36 feet south, 397 feet west of T-5


SECRET



ABSTRACT

Preshock velocity of sound waves in air were measured at elevations of $1\frac{1}{2}$, 3, and 6 feet above grade level at 1,000- and 2,000-foot ranges during Shot 12 over desert soil, water, asphalt, concrete, fir boughs, and Ivy.

Twenty-three of the original twenty-four channels recorded velocity from less than 20 msec after detonation to shock-wave arrival. The sound velocities at elevations from $1\frac{1}{2}$ to 6 feet above grade level were very similar and averaged around 5 percent above ambient in most cases. Velocities measured over asphalt, water, desert soil, and concrete were very similar in amplitude. Maximum velocities occurring just before shock arrival were similar at the 1,000- and 2,000-foot ranges. Air sound velocities were measured over fir boughs and Ivy. Velocities measured above the fir boughs were the highest recorded, reaching 18 percent above ambient at the $1\frac{1}{2}$ -foot elevation. Velocities over the Ivy plot were similar to those over the fir boughs, however, the medium over the Ivy appeared to be more turbulent, and consequently some data were unreadable.



FOREWORD

This report presents the final results of one of the 56 projects comprising the Military Effects Program of Operation Teapot, which included 14 test detonations at the Nevada Test Site in 1955.

For overall Teapot military-effects information, the reader is referred to the "Summary Report of the Technical Director, Military Effects Program," WT-1153, which includes the following: (1) a description of each detonation including yield, zero-point location and environment, type of device, ambient atmospheric conditions, etc.; (2) a discussion of project results, (3) a summary of the objectives and results of each project, (4) a listing of project reports for the Military Effects Program.

PREFACE

The author hereby thanks Maj H. T. Bingham, Director, Program 1; CDR W. M. McLellan, Director, Program 3; Lt Col J. J. Haley, Chief, Requirements Branch; and his assistant, LCDR A. P. Minwegen for the wholehearted cooperation they rendered to Project 1.5 at all times.

Special praises are due G. O. Pickens, L. C. Thompson and R. H. Wells, Navy Electronics Laboratory engineers for their capable work on the Project 1.5 instrumentation.

The author gratefully acknowledges the fine support given by all people who participated in the project.

CONTENTS

ABSTRACT	3
FOREWORD	4
PREFACE	4
CHAPTER 1 OBJECTIVES	9
1.1 Desert Soil Surface	9
1.2 Asphalt Surface	9
1.3 Water Surface	9
1.4 Special Surfaces	10
CHAPTER 2 RESULTS	11
2.1 Desert Sand, Asphalt, and Water, 1,000-Foot Ground Range	11
2.2 Desert Sand, Asphalt, and Concrete, 2,000-Foot Ground Range	11
2.3 Fir Boughs and Ivy	12
CHAPTER 3 INSTRUMENTATION AND REMARKS	22
3.1 Basic Sound Velocity Meter	22
3.2 Changes in Instrumentation	23
3.3 Preliminary Electronics Test	24
3.4 Transducers and the Air Path	24
3.5 Attenuation of the Acoustic Signal in the Air Gap	26
3.6 Other Measurements of Velocity	31
3.7 Attenuation of Acoustic Signals Caused by Heating Various Parts of the Microphone	32
CHAPTER 4 DISCUSSION	35
4.1 Calculations of Preshock Sound Velocity from Peak-Pressure, Shock-Velocity, and Precursor-Angle Data	36
4.2 Project 1.5 Sound-Velocity Data	39
4.2.1 Teapot Instruments	39
4.2.2 Data Comparisons with Previous Precursor Shots	39
CHAPTER 5 CONCLUSIONS AND RECOMMENDATIONS	42
APPENDIX A INSTRUMENTATION	43
A.1 Background	43
A.2 Basic Instrumentation	43
A.2.1 Master Generator	43
A.2.2 Transducer Power Amplifiers	43
A.2.3 Mike-to-Line Amplifiers	43
A.3 Discussion	44

APPENDIX B	PHASE AND AMPLITUDE CHANGES DUE TO INTERFERENCE OF SOUND WAVES	46
APPENDIX C	OPERATIONS	48
APPENDIX D	CALCULATIONS OF ATTENUATION OF SOUND IN AIR	50
APPENDIX E	ATTENUATION OF ACOUSTIC SIGNALS MEASURED IN SHOT 12	52
APPENDIX F	RECORDINGS OF RAW DATA MADE BY PROJECT 1.5 SOUND VELOCITY METERS	56
REFERENCES		73

TABLES

3.1	Results of Test of Project 1.5 Velocity Meter in Paint Oven	32
4.1	Blast Velocities and Corresponding Air Temperatures	37
4.2	Blast Velocities	38
4.3	Wave Front Angle Comparison	39
4.4	Preshock Sound Velocities	40

FIGURES

1.1	Blast line layout showing positions of Project 1.5 (NEL) sound velocity meters	10
2.1	Preshock air sound velocity versus time, 1,000-foot range, over desert, asphalt and water surfaces	12
2.2	Preshock air sound velocity versus time, 1,000-foot range, over desert surface	13
2.3	Preshock air sound velocity versus time, 1,000-foot range, over asphalt surface	14
2.4	Preshock air sound velocity versus time, 1,000-foot range, over water surface	15
2.5	Preshock air sound velocity versus time, 2,000-foot range, over desert, asphalt and concrete surfaces	16
2.6	Preshock air sound velocity versus time, 2,000-foot range, over desert surface	17
2.7	Preshock air sound velocity versus time, 2,000-foot range, over asphalt surface	18
2.8	Preshock air sound velocity versus time, 2,000-foot range, over a 20-by-30-foot plot of concrete	19
2.9	Preshock air sound velocity versus time, 2,000-foot range, over a 20-by-30-foot plot of white fir boughs	20
2.10	Preshock air sound velocity versus time, 2,000-foot range, over a 20-by-30-foot plot of ivy	21
3.1	Sound velocity meter transducers used on Upshot-Knothole	23
3.2	Directivity pattern of Altec-Lansing 802-C loudspeaker at frequency 3.2 kc with attached horn	26

3.3	Effect of directivity patterns on direct and indirect signals	27
3.4	Sound velocity meter three feet above flaming gasoline	29
3.5	Measured sound velocities and signal amplitudes three feet above flaming gasoline line	30
3.6	Effect of burning copper screen in horn throat on microphone	33
3.7	Effect of applying a blowtorch flame to horn of microphone	33
3.8	Signal amplitude versus time for condition where blowtorch is played over microphone horn	34
A.1	Electronics for one typical field station, three channels	44
A.2	Recorded acoustic signal showing effects of electromagnetic transient at detonation	45
C.1	Model of NEL instrument shelter with dimensions of full-size shelter depicted	48
C.2	Model of NEL instrument shelter	49
C.3	Details of NEL instrument shelter model	49
E.1	Relative sound pressure amplitude versus time, 1,000-foot desert	52
E.2	Relative sound pressure amplitude versus time, 1,000-foot asphalt	52
E.3	Relative sound pressure amplitude versus time, 1,000-foot water	53
E.4	Relative sound pressure amplitude versus time, 2,000-foot desert	53
E.5	Relative sound pressure amplitude versus time, 2,000-foot asphalt	54
E.6	Relative sound pressure amplitude versus time, 2,000-foot concrete	54
E.7	Relative sound pressure amplitude versus time, 2,000-foot fir bough	55
E.8	Relative sound pressure amplitude versus time, 2,000-foot ivy	55
F.1	Channel 10, desert, 1,000-foot ground range, 1½-foot elevation	56
F.2	Channel 11, desert, 1,000-foot ground range, 3-foot elevation	56
F.3	Channel 12, desert, 1,000-foot ground range, 6-foot elevation	57
F.4	Channel 19, desert, 2,000-foot ground range, 1½-foot elevation	57
F.5	Channel 20, desert, 2,000-foot ground range, 3-foot elevation	58
F.6	Channel 21, desert, 2,000-foot ground range, 6-foot elevation	59
F.7	Channel 4, asphalt, 1,000-foot ground range, 1½-foot elevation	60
F.8	Channel 5, asphalt, 1,000-foot ground range, 3-foot elevation	60
F.9	Channel 6, asphalt, 1,000-foot ground range, 6-foot elevation	60
F.10	Channel 7, asphalt, 2,000-foot ground range, 1½-foot elevation	61
F.11	Channel 8, asphalt, 2,000-foot ground range, 3-foot elevation	62
F.12	Channel 9, asphalt, 2,000-foot ground range, 6-foot elevation	63
F.13	Channel 2, water, 1,000-foot ground range, 3-foot elevation	63
F.14	Channel 3, water, 1,000-foot ground range, 6-foot elevation	63
F.15	Channel 22, concrete, 2,000-foot ground range, 1½-foot elevation	64
F.16	Channel 23, concrete, 2,000-foot ground range, 3-foot elevation	65
F.17	Channel 24, concrete, 2,000-foot ground range, 6-foot elevation	66
F.18	Channel 16, white fir boughs, 2,000-foot ground range, 1½-foot elevation	67
F.19	Channel 17, white fir boughs, 2,000-foot ground range, 3-foot elevation	68
F.20	Channel 18, white fir boughs, 2,000-foot ground range, 6-foot elevation	69
F.21	Channel 13, broad leaf cover (ivy), 2,000-foot ground range, 1½-foot elevation	70

F.22	Channel 14, broad leaf cover (ivy), 2,000-foot ground range,	
	3-foot elevation -----	71
F.23	Channel 15, broad leaf cover (ivy), 2,000-foot ground range,	
	6-foot elevation -----	72

SECRET

Chapter 1

OBJECTIVES

The primary objective was to determine preshock air sound velocities at elevations up to 6 feet above the ground in the region where the precursor wave existed. It was felt that this information would be valuable in explaining the generation of the precursor. Shot 12 was a 24-kt device detonated on a tower at 400-foot elevation and, consequently, fulfilled the conditions for a precursor-generating shot (Reference 4).

Measurements of preshock air sound velocity were made over three different blast lines: (1) a regular Frenchman Flat desert blast line, (2) an asphalt-covered blast line, and (3) a water-covered blast line. Velocity meters were situated at the 1,000- and 2,000-foot ranges on the first two lines and only at the 1,000-foot range on the third (see Figure 1-1).

Also, measurements of preshock air sound velocity were made over three special surface plots situated in the vicinity of the 2,000-foot station on the desert line. One plot was composed of concrete, a second of white fir boughs and a third of broad leaf cover or Ivy. The dimensions of all plots were 20 by 30 feet with the shorter dimension oriented along the blast line.

1.1 DESERT SOIL SURFACE

On previous tests (References 1, 2, and 3) data were gathered on air sound velocities and air temperatures from 1 $\frac{1}{2}$ to 54 feet above desert soil. In general, there were negligible preshock air-temperature and/or sonic-velocity changes above the 10-foot level over Nevada soil. Below the 10-foot level, the velocities and temperatures were known to be above ambient, but no gradient had been established. Also, only meager data of this type had ever been taken in the zone of interest on previous precursor-generating shots.

1.2 ASPHALT SURFACE

Asphalt is a convenient ground cover which tends to absorb most of the thermal radiation incident upon it. It tends to emit smoke and also to impart its heat energy to the air by conduction and convection. The preshock air sound velocities over this surface are of interest in explaining blast-wave performances over dust-free, thermal-absorbing surfaces.

1.3 WATER SURFACE

Water is probably the cheapest and most feasible highly reflecting surface available. It was expected that the air above the water surface would not change in temperature, since the surface itself would not absorb thermal radiation and, hence, could not transfer its heat to the air by conduction or convection.

1.4 SPECIAL SURFACES

In Upshot-Knothole Shot 9, air sound velocities were measured over three different plots of white fir boughs. Plot dimensions were 40 by 28 feet. Velocities measured were two to three times ambient.

A similar plot of white fir boughs was set up at 2,000-foot range on the desert line in Teapot Shot 12. Also, a plot of broad leaf cover or ivy and a plot of ordinary concrete

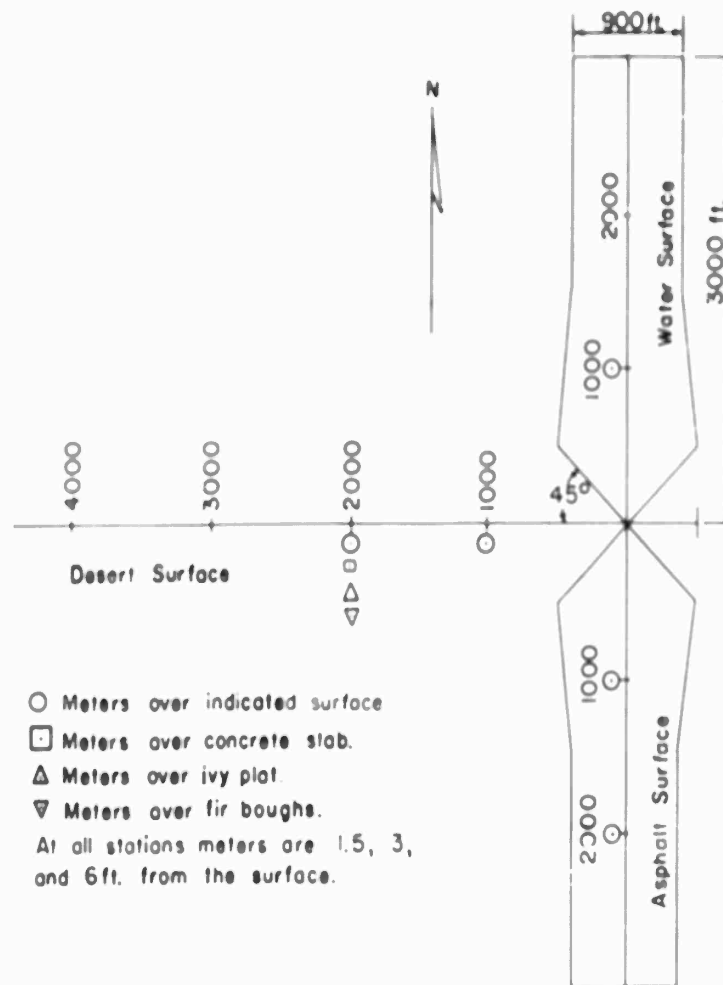


Figure 1.1 Blast line layout showing positions of Project 1.5 (NEL) sound velocity meters.

were situated at the same location. Dimensions of these plots were 30 by 20 feet.

Thermal effects on these special surfaces are apt to be quite different from those occurring on the ordinary desert terrain. Consequently, for a relatively small cost, comparisons of preshock air sound velocities over different plots can be made. This in turn might indicate variations in blast-wave performance over the various surfaces.

Chapter 2

RESULTS

The graphs of Figures 2.1 through 2.10 depict the recorded values of the velocity of sound in air from zero time (time of detonation) to the arrival of the shock wave for 23 of the original 24 channels. The 1 1/2-foot elevation meter at the 1,000-foot range on the water line failed at detonation.

The points that appear on the curves are the actual values taken directly from the raw data — no averaging of any sort has been done. Discrepancies between these curves and those in the preliminary Project 1.5 report (ITR-1104), resulted, since for this report travel times across the air path have been read with the greater accuracy of the 3,200-cps carrier instead of the 100-cps modulating signal.

In order to roughly compare air-sound-velocity change with air-temperature change, the conversion 2 ft/s/°C may be used with the mental reservation that it applies strictly to clean air whose chemical composition does not change.

2.1 DESERT SAND, ASPHALT, AND WATER, 1,000-FOOT GROUND RANGE

Figure 2.1 depicts the change in the air sound velocity from detonation to shock arrival at elevations of 1 1/2, 3 and 6 feet above sand, asphalt, and water surfaces at a ground range of 1,000 feet. These curves indicate a velocity increase rate of approximately 1 ft/sec/msec irrespective of elevation. The magnitude of the velocity change also seems to be independent of the surface. The fact that the sound velocity over the water is higher than over the other surfaces is not considered significant. This velocity differential represents approximately 0.2 msec out of 5.0 msec total signal travel time from one diaphragm to the other, 6 feet away. It is possible that the greater reflectance of the water surface caused the microphone horns in the instruments on the water line to receive more radiation than those on the other lines. A small high-temperature region close to the transducer horns could easily account for the indicated change in transit time.

The same curves shown in Figure 2.1 are plotted individually in Figures 2.2 through 2.4; these include the shock-arrival instants in each case.

2.2 DESERT SAND, ASPHALT, AND CONCRETE; 2,000-FOOT GROUND RANGE

In Figure 2.5 preshock air sound velocities over desert soil, asphalt, and concrete surfaces at 2,000-foot ground range are plotted versus time. The first velocity increases occur about 70 msec after detonation at this range compared with 40 to 50 msec at the 1,000-foot ground range. After this the rate of increase at the three elevations at 2,000-foot range is approximately 0.8 ft/sec/msec. After 250 msec there is little velocity increase at any elevation or over any of the three surfaces. At neither the 1,000-foot nor the 2,000-foot range do the velocity magnitudes reach 1,300 ft/sec at any elevation or over any surface so far considered.

In Figures 2.6 through 2.8 the same curves depicted in Figure 2.5 are presented along with the respective shock-arrival times.

2.3 FIR BOUGHS AND IVY

Preshock air sound velocities over a surface of white fir boughs and an ivy surface are depicted for elevations of $1\frac{1}{2}$, 3, and 6 feet in Figures 2.9 and 2.10, respectively.

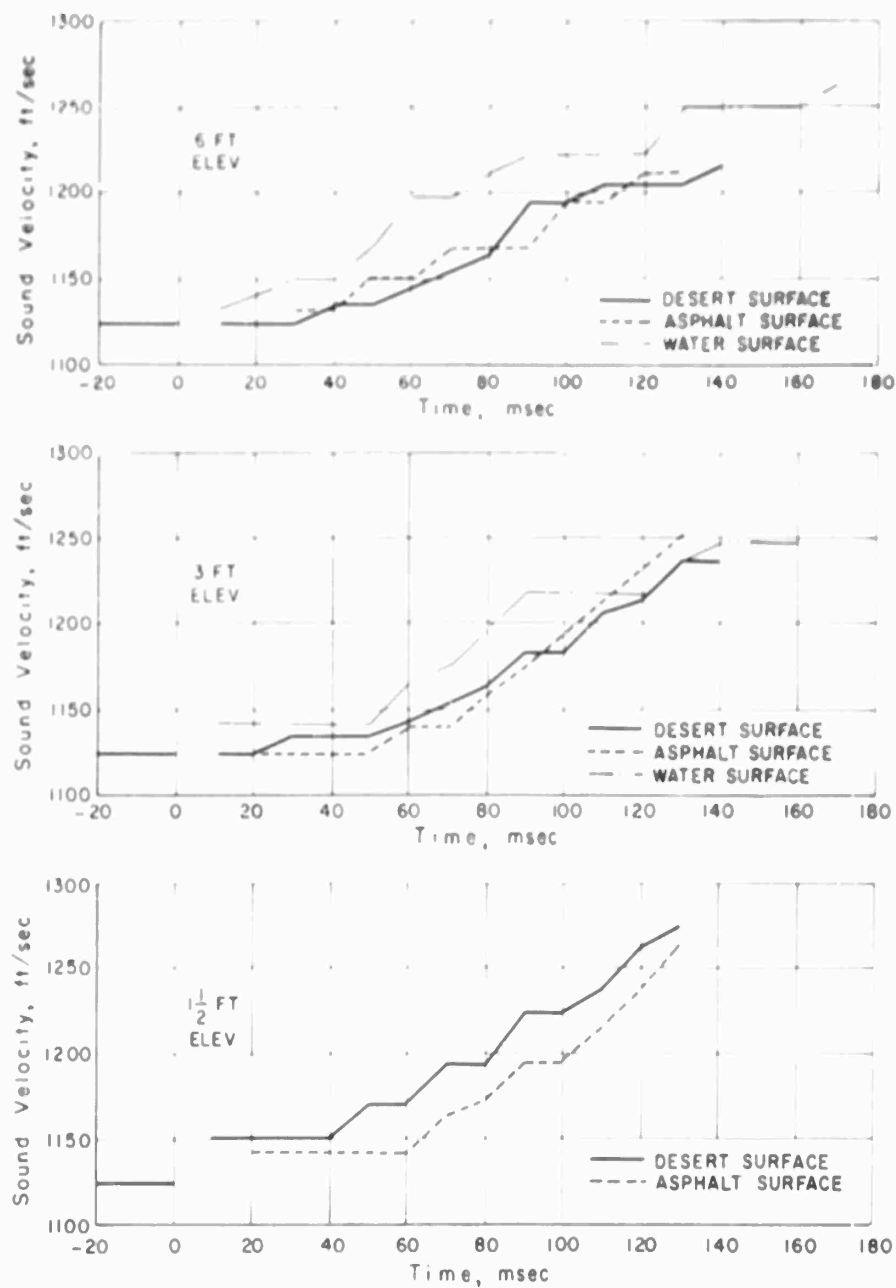


Figure 2.1 Preshock air sound velocity versus time, 1000-foot range, over desert, asphalt and water surfaces.

Judging from the distortion of the recorded signals (Appendix F), extreme turbulence existed over the Ivy plot, much more, in fact, than over any other surface. The velocity recorded over the white fir boughs at $1\frac{1}{2}$ -foot elevation was the highest recorded on any channel—it exceeded 1,300 ft/sec. This does not imply, however, that an equally high velocity did not occur over the Ivy plot where the medium was so turbulent that the recorded sound wave was too distorted for any velocity determination to be made.

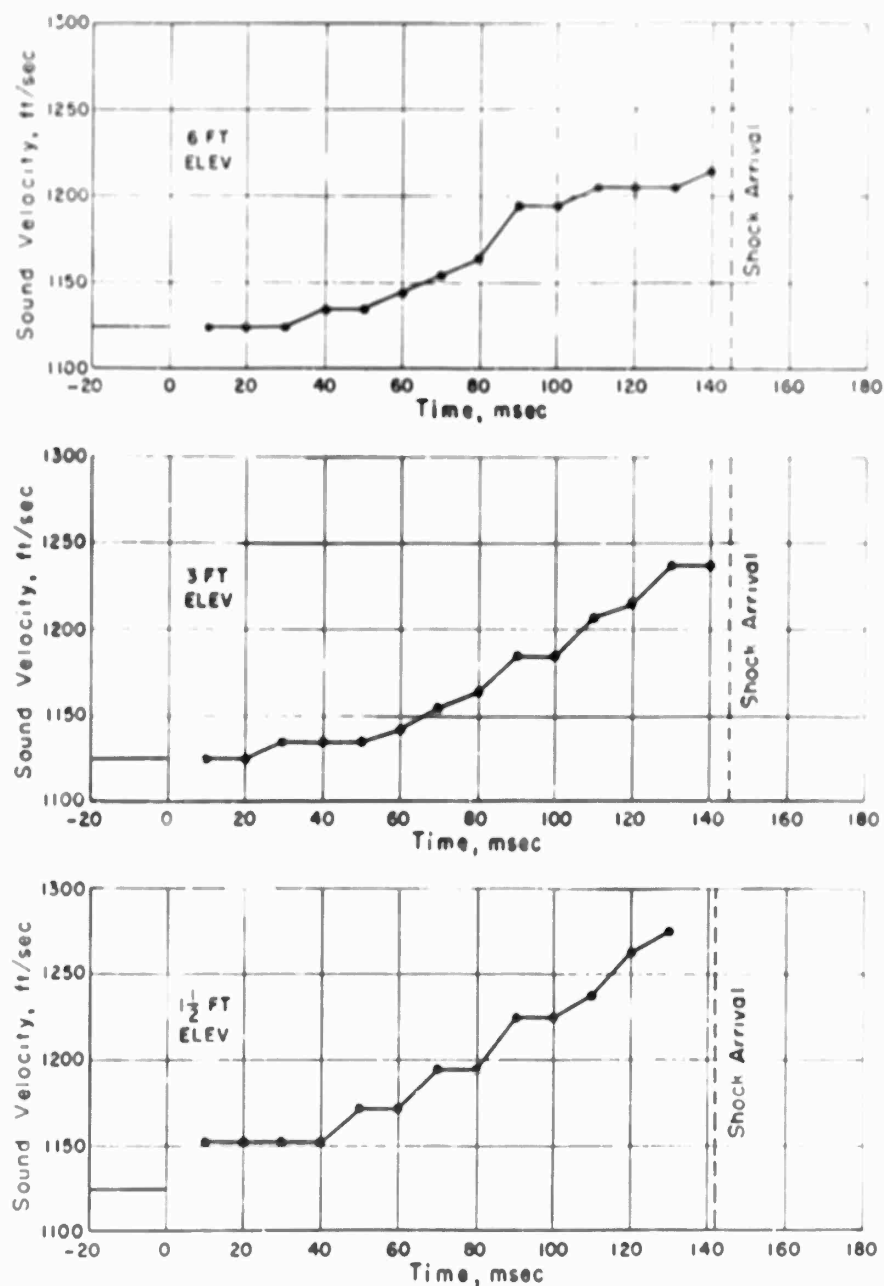


Figure 2.2 Preshock air sound velocity versus time, 1000-foot range, over desert surface.

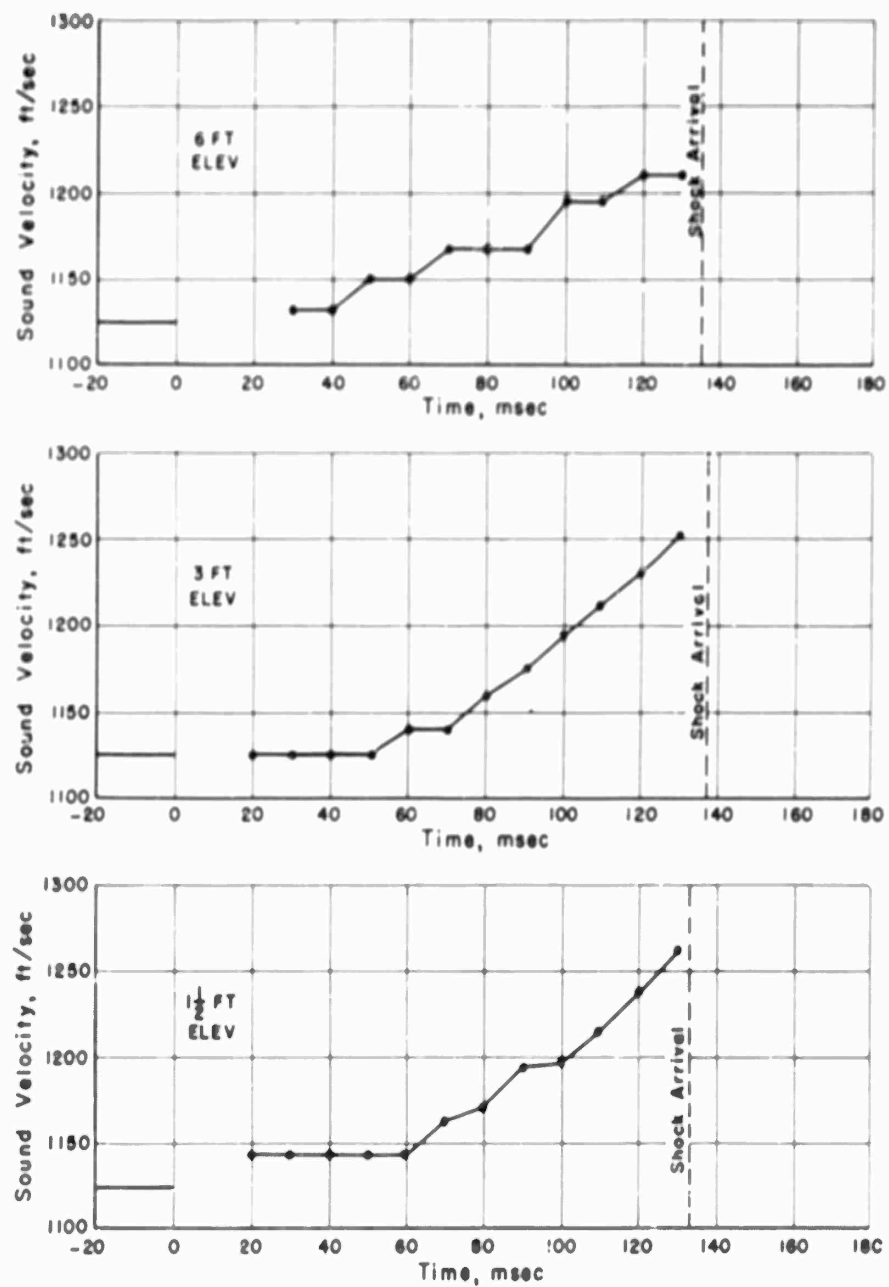


Figure 2.3 Preshock air sound velocity versus time, 1000-foot range, over asphalt surface.

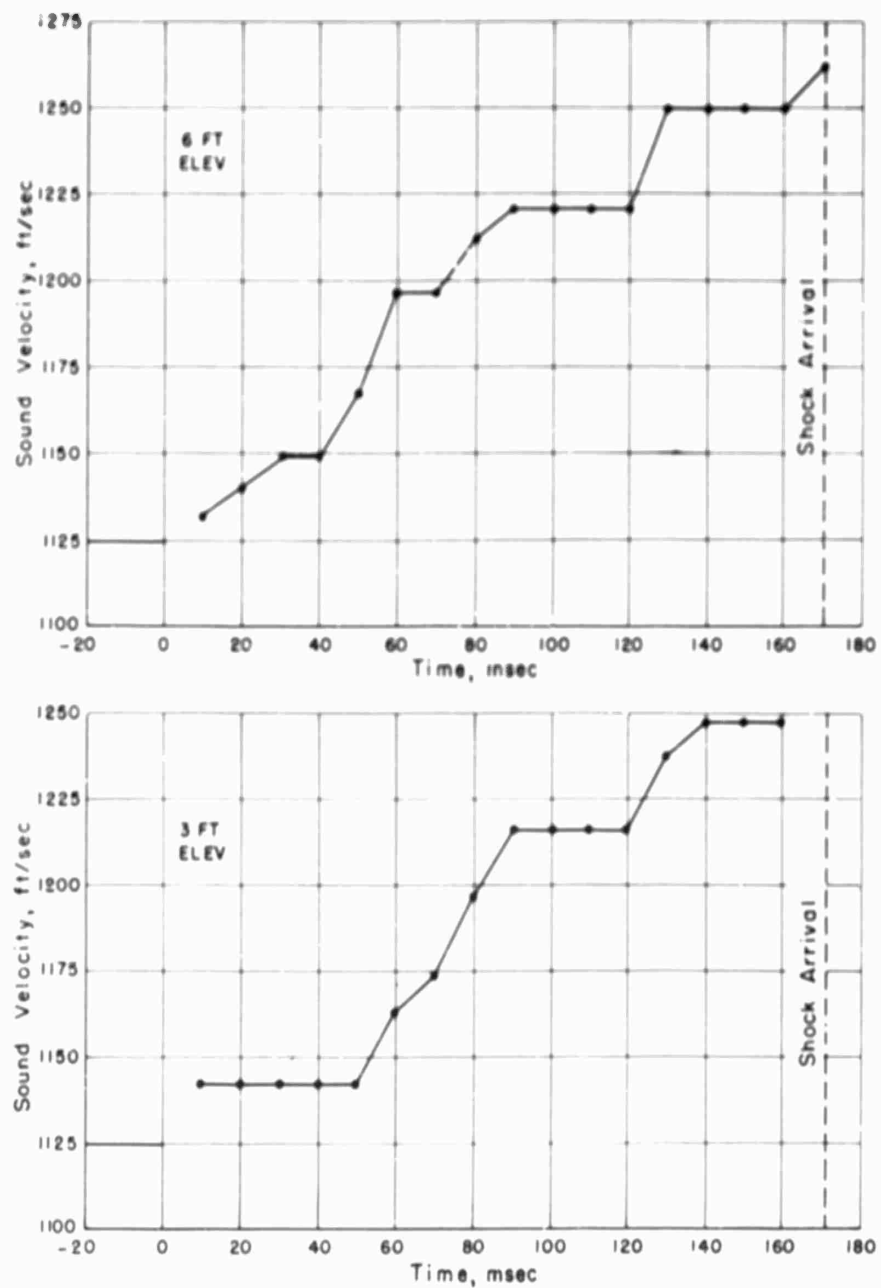


Figure 2.4 Preshock air sound velocity versus time, 1000-foot range, over water surface.

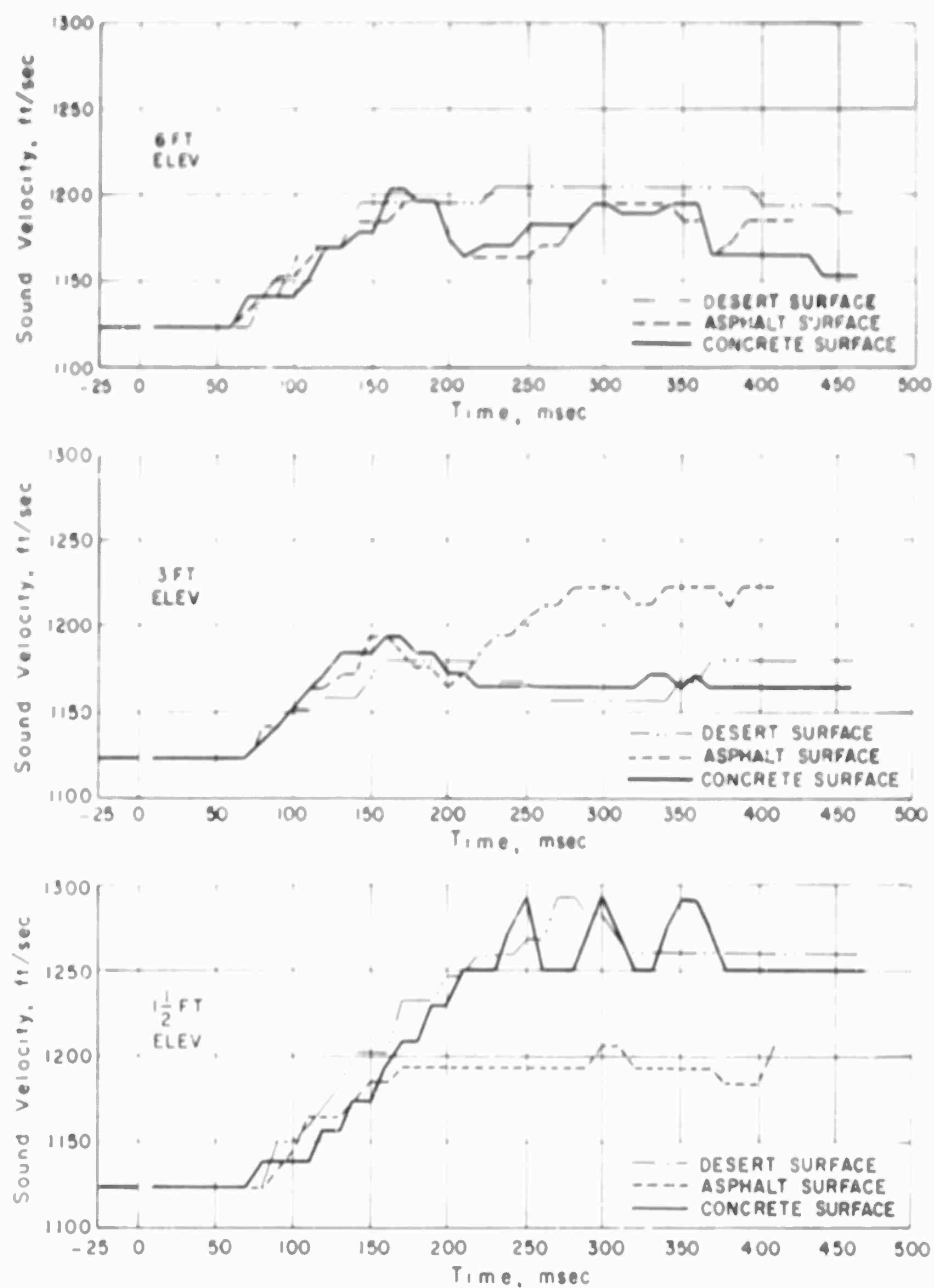


Figure 2.5 Preshock air sound velocity versus time, 2000-foot range, over desert, asphalt and concrete surfaces.

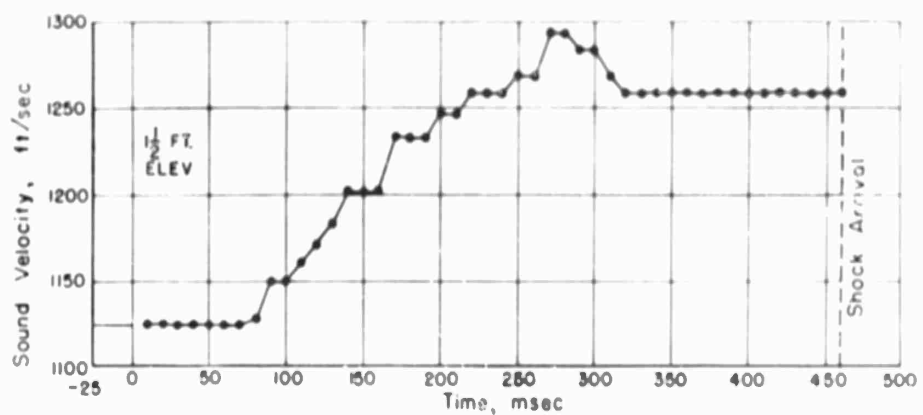
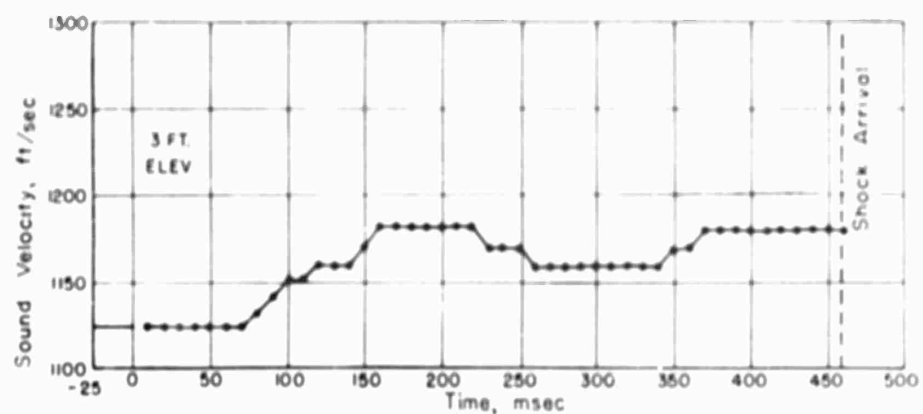
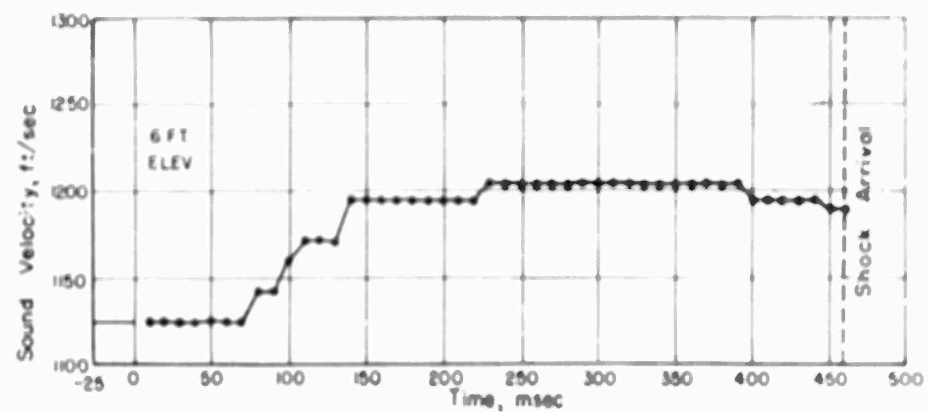


Figure 2.6 Preshock air sound velocity versus time, 2000-foot range, over desert surface.

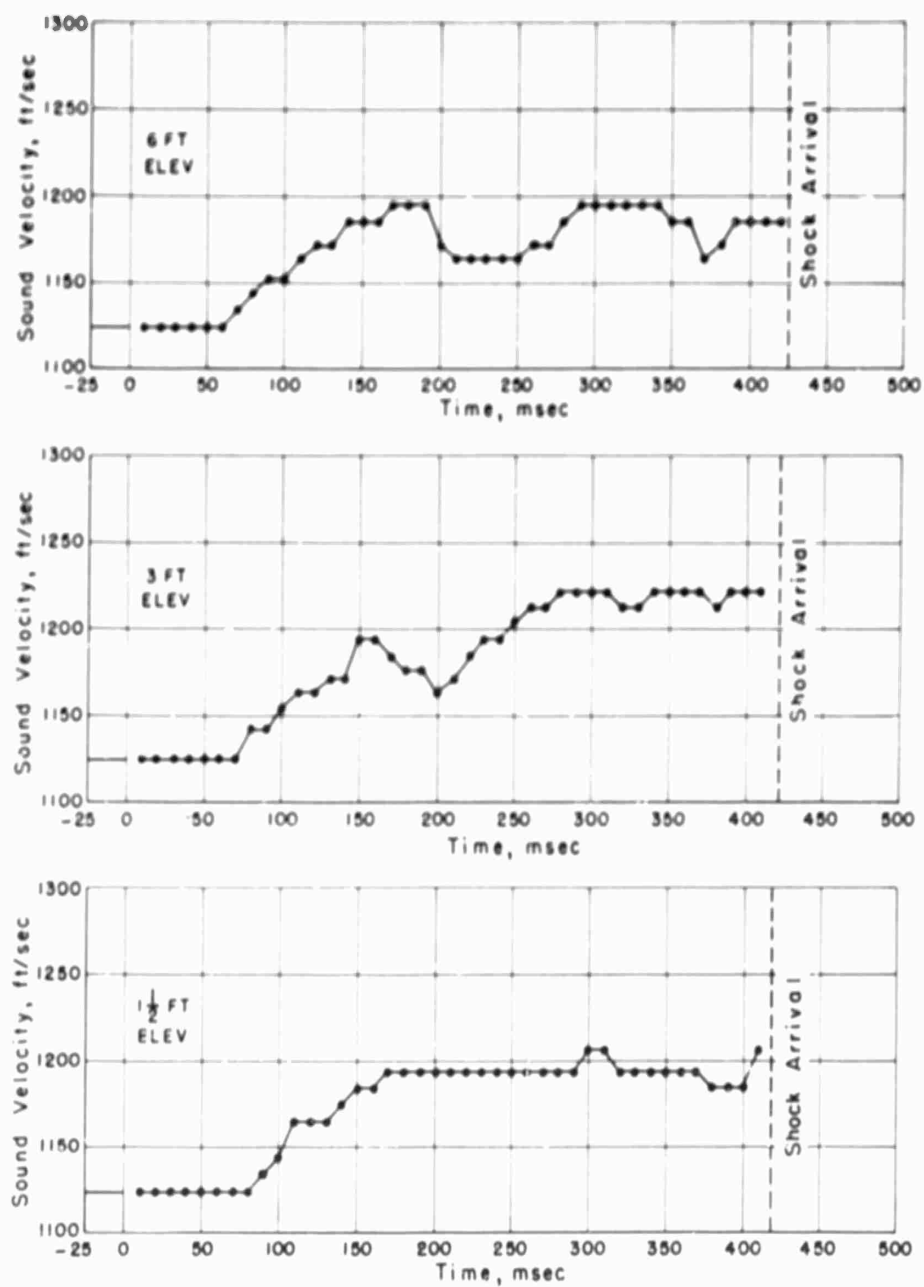


Figure 2.7 Preshock air sound velocity versus time, 2000-foot range, over asphalt surface.

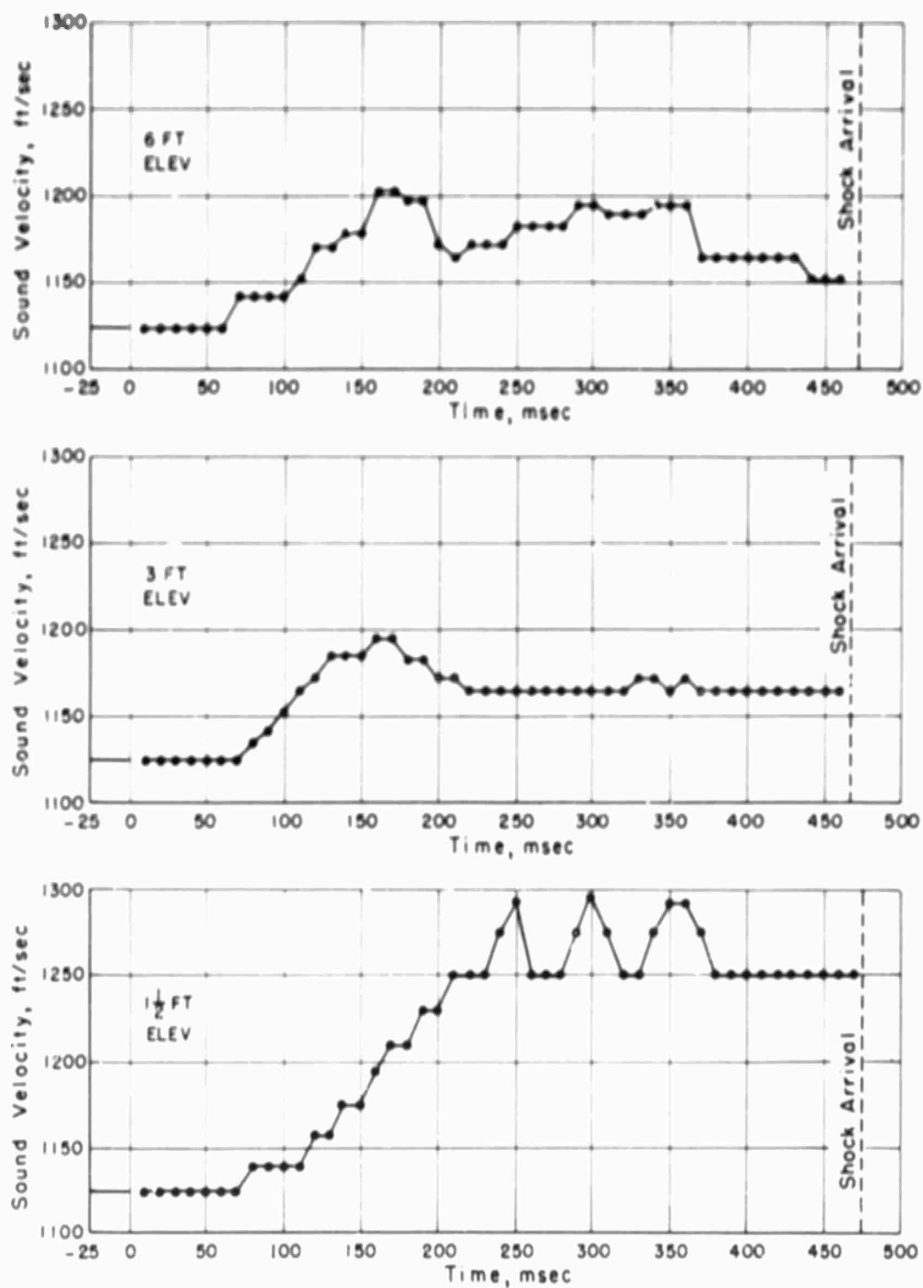


Figure 2.8 Preshock air sound velocity versus time, 2000-foot range, over a 20-by-30-foot plot of concrete.

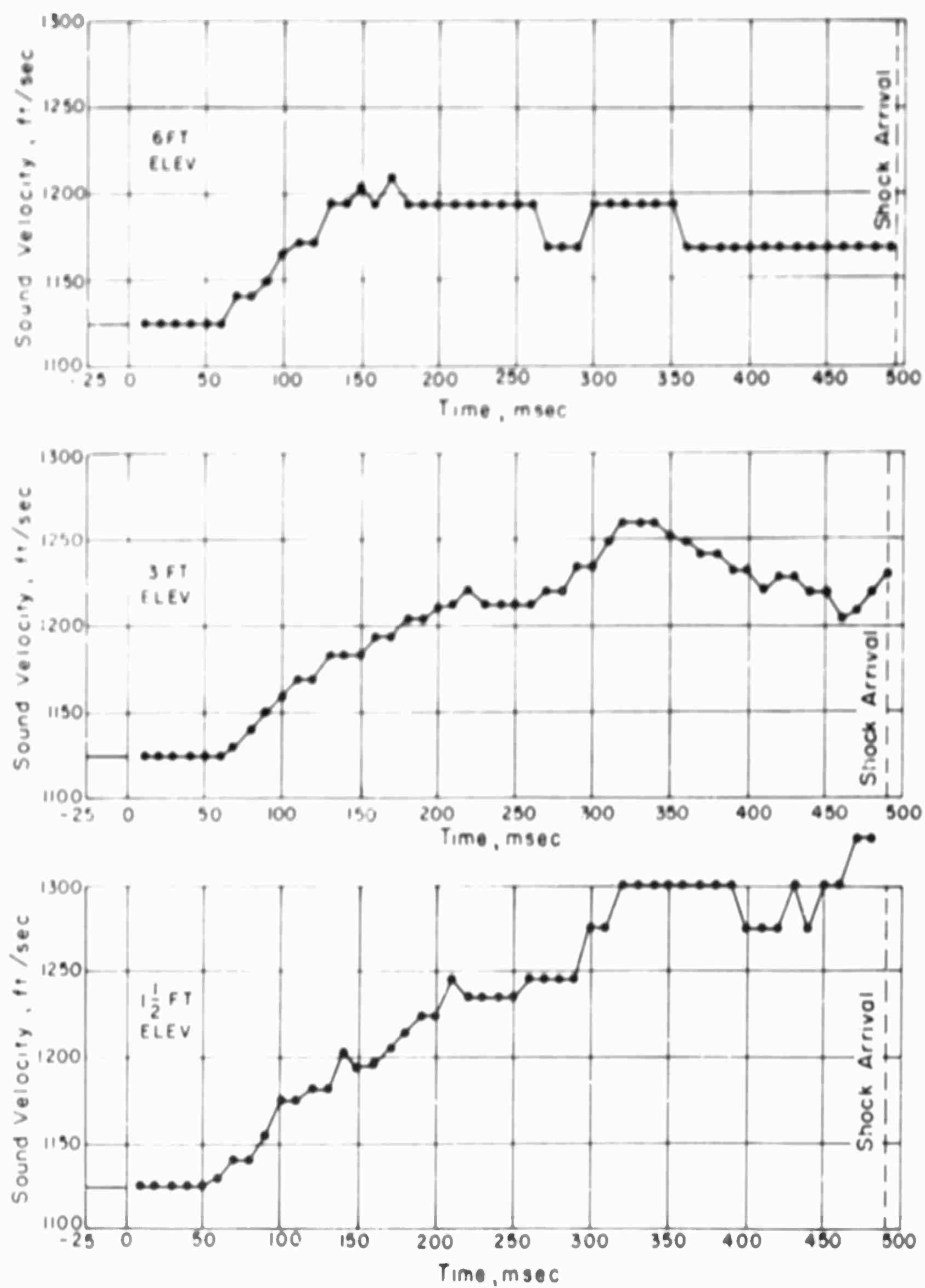


Figure 2.9 Preshock air sound velocity versus time, 2000-foot range, over a 20-by-30-foot plot of white fir boughs.

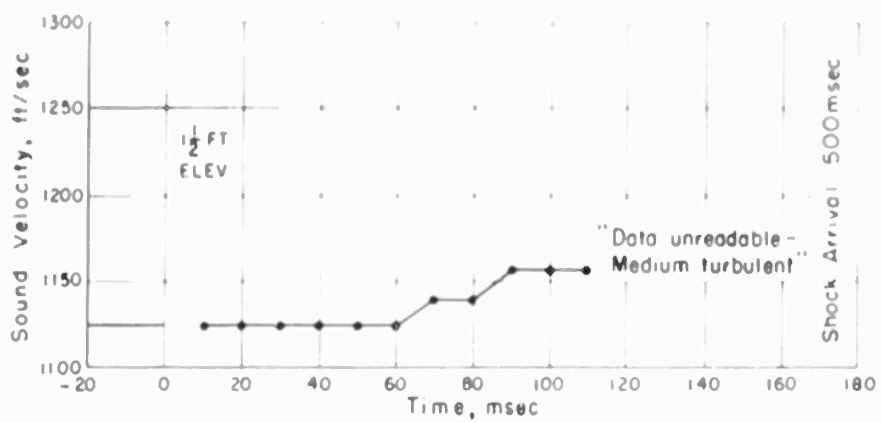
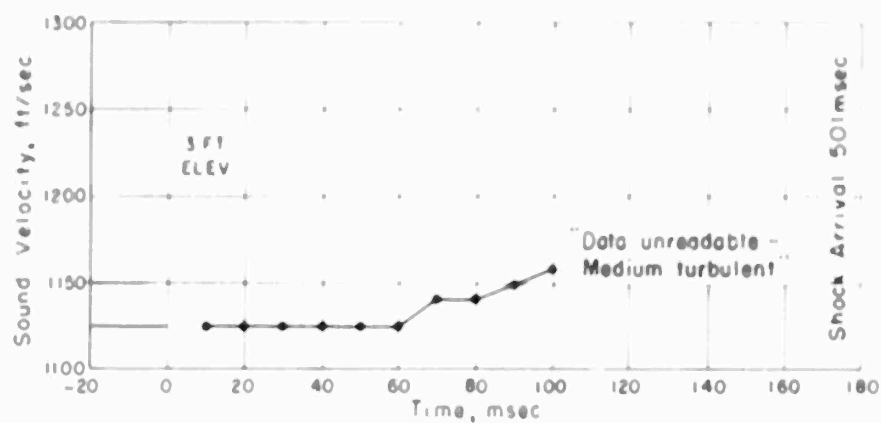
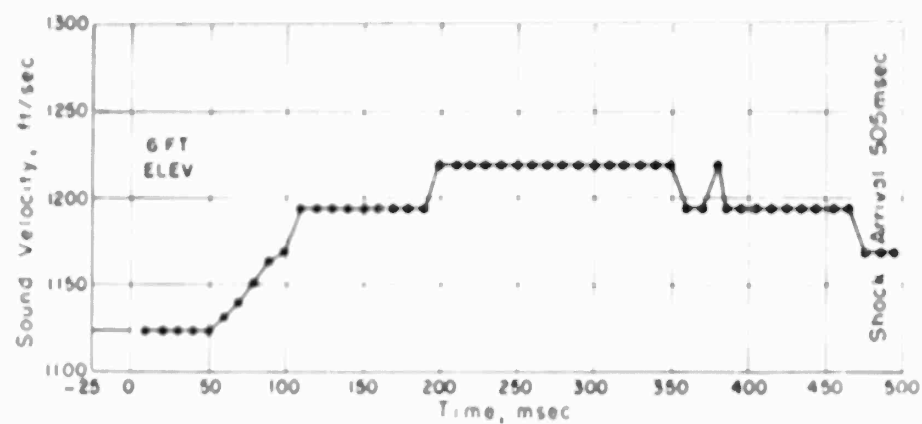


Figure 2.10 Preshock air sound velocity versus time, 2000-foot range, over a 20-by-30-foot plot of ivy.

Chapter 3

INSTRUMENTATION AND REMARKS¹

The data taken by Project 1.5 during Shot 12 were consistent in themselves, but were not consistent with temperature data taken over the same surfaces by Project 8.4e. Also, neither project's data were compatible with current blast-wave theory as applied to the pressure data taken by other projects (References 5, 6, and 8).

The preshock sound velocities measured by Project 1.5 were about half as large as those predicted from peak pressure, shock arrival, and precursor angle photographic data. It therefore seems appropriate to examine the 1.5 instruments and determine if the records obtained were reasonably correct, or if perhaps there were some basic deficiencies in the instruments and the results obtained therefore not a true representation of the physical picture.

On this basis, an attempt will be made in this chapter to answer the questions asked about these instruments by many interested parties since the contradictory data were first reported in the preliminary report. In addition, the results of several supplementary tests of the instruments will be discussed.

3.1 BASIC SOUND VELOCITY METER

The basic sound velocity meter used on Teapot was the same type as that previously used by Navy Electronics Laboratory (NEL) in measurements made at Tumbler and Upshot-Knothole; it consisted of two transducers, one used as a loudspeaker, the other as a microphone. The distance between the transducer diaphragms was fixed at 6 feet. The acoustic signal which traveled between these transducers was a 3,200-cps carrier, amplitude-modulated by a 100-cps sinusoid (see Figure 3.1).

The signal from the microphone terminals was compared in time delay with the signal entering the terminals of the loudspeaker. The difference, when the correct phase adjustments were made, was the time of travel between the diaphragms. The quotient of the interdiaphragm distance and the interdiaphragm travel time was the velocity of sound in the medium between diaphragms, assuming a straight-line acoustic path between diaphragms. The aforementioned phase adjustments were made because the carrier had to pass through inductive, capacitive, and resistive elements and their equivalents in the various electronic circuits. These caused a phase shift of the carrier (the phase shift in the modulating signal was $1/32$ of this). Although the shift was very small, it was nevertheless corrected by use of a phase-shifting network.

The transducers were Model 802-C Altec-Lansing high-frequency driver units capable of operating both as loudspeakers and as microphones over the range from 1 to 10 kc. Adequate directionality was obtained by coupling both transducers to the air medium by means of conical horns. These horns had 1-inch throats, a total flare angle of $2 \arctan \frac{2}{3}$ and mouths 9 inches in diameter; these were adequate to prevent acoustic crosstalk between adjacent field channels.

¹ Further details of instrumentation are included in Appendix A.

Admittedly, part of the measured medium was inside the horns and transducers; however, this amount was small in comparison with the total path length, and the error introduced was small (less than 2 percent for the velocities measured).

3.2 CHANGES IN INSTRUMENTATION

To eliminate a bothersome transient condition which occurred for as much as $\frac{1}{2}$ second after detonation on the close-in NEL velocity meters on previous tests, several major modifications were made:

1. The AVC (automatic-volume-control) system used in previous tests was eliminated. Its function was to boost the microphone output voltage when the microphone's

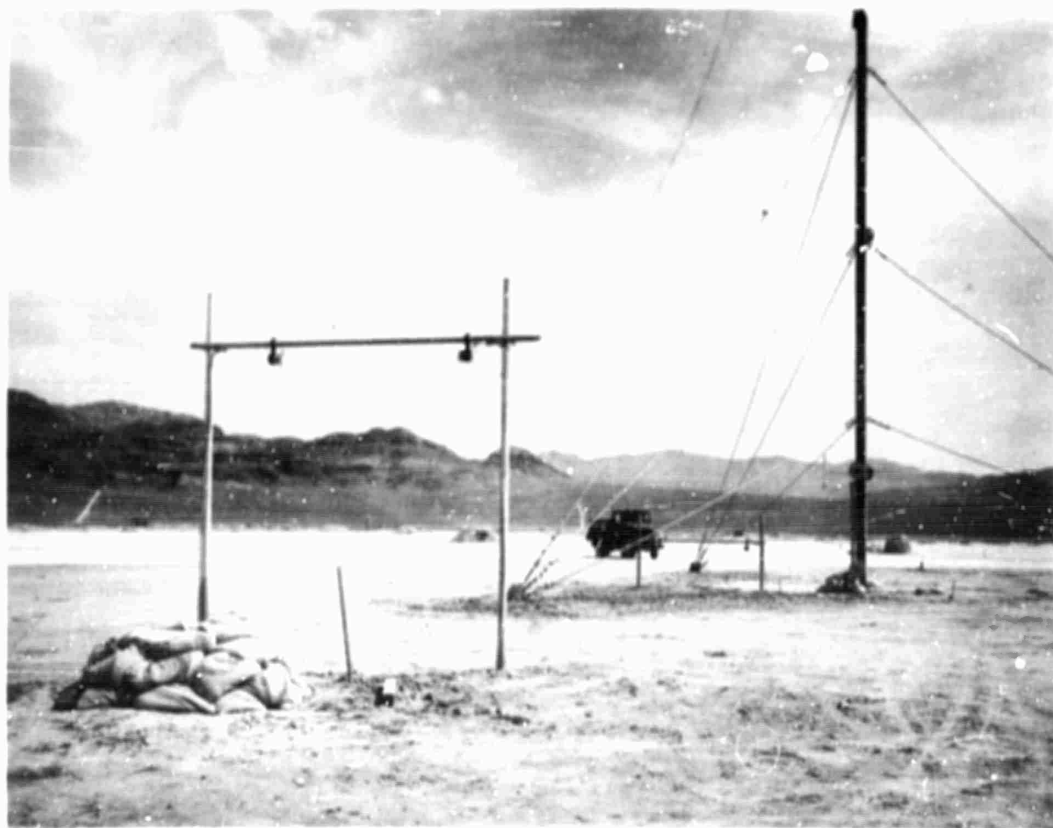


Figure 3.1 Sound velocity meter transducers used on Upshot-Knothole. (These are same as used on Teapot, except for higher elevation and smaller diameter horn on microphone).

input acoustic signal became weak. Although the AVC performed satisfactorily in the job for which it was designed, it tended to maintain high voltage levels for long periods when once triggered by the electromagnetic transient at weapon detonation, which led to spurious velocity readings.

2. Carefully designed line-balancing transformers were used to suppress longitudinal currents induced on the lines at detonation.

3. The number of components per channel was drastically reduced. Whereas 20 vacuum tubes per channel were used before, only 5 were used on Teapot. This increased the probability of operating throughout a test without failure.

4. Design changes enabled NEL to move most of the fragile electronic equipment

from the blast-line instrument shelters which were within 2,000 feet of ground zero back to the recording van 7,000 feet from ground zero. This protected the electronics from both the seismic shock and the intense electromagnetic transient at detonation.

5. Band-pass filters were used at the terminations of all the long transmission lines to pass the carrier and side bands, and yet eliminate much of the side-band electrical noise.

6. The actual modulated carrier that crossed the air gap was recorded on magnetic tape together with a series of reference spikes. The shifts in time position of this carrier referred to these spikes conveyed the information of variations in time delay across the air gap.

In previous tests the carrier was demodulated and the resulting 100-cycle signal was converted into a series of spikes at the positive-slope zero crossings. The signal spikes of one polarity were recorded on magnetic tape with reference spikes of opposite polarity. Shifts in time positions of the signal spikes denoted the variations in time delay across the air gap. The Teapot system, which recorded the basic sound signal rather than a spike derived from this signal, is felt to be superior because better insight into the system's operation is afforded.

3.3 PRELIMINARY ELECTRONICS TEST

On 29 March 1955, a test of the system was made on Shot 8 to determine the effectiveness of the aforementioned instrumentation changes before using the equipment on Shot 12. Five complete channels of instrumentation were set up at Area T-4 in Yucca Flat at a ground range of 2,750 feet. In addition, a sixth channel was established which was complete in every detail except one; the 4-terminal network of two transducers, coupled by horns to the air medium, was replaced by an electrical 4-terminal network which had the same transmission characteristics as the other under ambient conditions. The results of the six channels on this test were: (1) no objectionable transients occurred at detonation on any channels; the transients that did occur were of short duration, approximately 0.02 second long; (2) no significant air-sound-velocity changes occurred; (3) on the five regular channels the pressure amplitude of the sound signal through the air decreased markedly after detonation; in fact, the one meter at $1\frac{1}{2}$ -foot elevation dropped to a level of $\frac{1}{10}$ the ambient sound-pressure amplitude; and (4) the "dummy-air-path" channel (sixth channel) did not show any variations in signal amplitude whatsoever.

It was concluded from this experiment that: (1) the removal of the AVC had eliminated the serious transient problem; (2) the long ground range (2,750 feet) and unexpectedly small weapon magnitude (15 kt) had prevented any noteworthy preshock air-sound-velocity increase; and (3) there was a phenomenon causing attenuation of the original signals--either occurring in the air path or in the transducers themselves but was definitely not in the electronics (see Results 3 and 4 above).

3.4 TRANSDUCERS AND THE AIR PATH

The orientation of the transducers in Shot 12 was along radii from ground zero with the loudspeaker in all cases pointing away from and the microphone pointing toward ground zero. Although in retrospect it would appear wiser to have oriented the transducers across the lines, this was not done in the interest of not changing the test conditions from those of Upshot-Knothole and Tumbler. The reason that the instruments were so oriented on Tumbler in the first place was to measure the post-shock material

velocities in case the instruments were capable of operating in that period, a condition which unfortunately never existed.

A comparison of on-the-line versus across-the-line orientation was made on Upshot-Knothole Shots 9 and 10 for transducers at elevations of 10 feet, and the differences in their preshock performances were inconsequential. One might argue that at the 10-foot elevation little velocity difference should occur anyway for the two cases, since there is practically no sound-velocity change at this elevation.

However, the insides of the microphones' horns and the fine copper screens in their throats were directly exposed to the thermal radiation in both Upshot-Knothole Shot 10 and Teapot Shot 12 and under similar conditions of yield and relative location. In Upshot-Knothole Shot 10 those instruments oriented along the blast line gave the same sort of records as those oriented across the blast line at the same elevations (see Figures 3.15 and 3.16, Reference 2). However, the microphone horns used in Upshot-Knothole were only $\frac{1}{2}$ wavelength (of the carrier) from mouth to throat while those used on Teapot were $1\frac{1}{2}$ wavelengths long. More will be said about this in Section 3.6.

Since the Upshot-Knothole records were derived and not basic raw data, as were the Teapot records, there is no way of telling if there was an amplitude change in the acoustic signals received by the microphones. But even if there was, there was no noteworthy velocity shift in the on-the-line meters as compared with the across-the-line meters. In short, thermal radiation on the horns did not cause any significant sound-velocity changes to occur on the Upshot-Knothole Shot 10 tests under conditions very similar to Teapot Shot 12.

The free-air directivity pattern at 3.2 kc of the loudspeaker and microphone used in the Teapot Shot 12 sound-velocity measurements is shown in Figure 3.2. This pattern was made with a loudspeaker and its horn at an elevation of 50 feet above the ground surface. Because of symmetry the pattern may be rotated about its axis to establish the three-dimensional space pattern (ignore minor variations between the right and left sides of Figure 3.2). The role of the transducer horn is an important one. This is the device which prevents acoustic crosstalk between adjacent channels and minimizes the effectiveness of sound rays crossing the air gap by multiple paths. The danger from this last comes from a signal which crosses the gap at some average velocity over a path length which is unknown. If a single acoustic ray were to travel between transducers by a devious route the sound velocity found by $C = D/t$ would be incorrect, for although the travel time t would be correctly measured, D would not be the straight line distance between diaphragms. Two possible ways for such an event to occur are: by reflection of off-axis acoustic rays from a hard surface such as the ground and by refraction of these rays from a hot-air region where the sound velocity is higher than it is between the transducers.

Let the appropriate data of the directivity pattern of Figure 3.2 be employed in a simple ray diagram as in Figure 3.3 which depicts the $1\frac{1}{2}$ -foot-elevation transducer pair (a more severe condition than for the 3- and 6-foot elevation instruments); to simplify, assume that the zone of transmission from the loudspeaker is a point, and similarly, the zone of reception for the microphone is a point; then assume no inverse first power or inverse square law of sound transmission; also assume perfect reflection from the ground. These last two assumptions are conservative (that is, they err in the direction which hurts the instrument's cause). From Figure 3.2, the sound pressures associated with the two rays meeting at the microphone in Figure 3.3 differ by a factor of 16 in pressure amplitude. It therefore seems reasonable that bundles of acoustic rays leaving a finite-sized loudspeaker horn and arriving at a finite-sized microphone horn (when reflected from an imperfect reflecting surface and spread out by inverse first power or in-

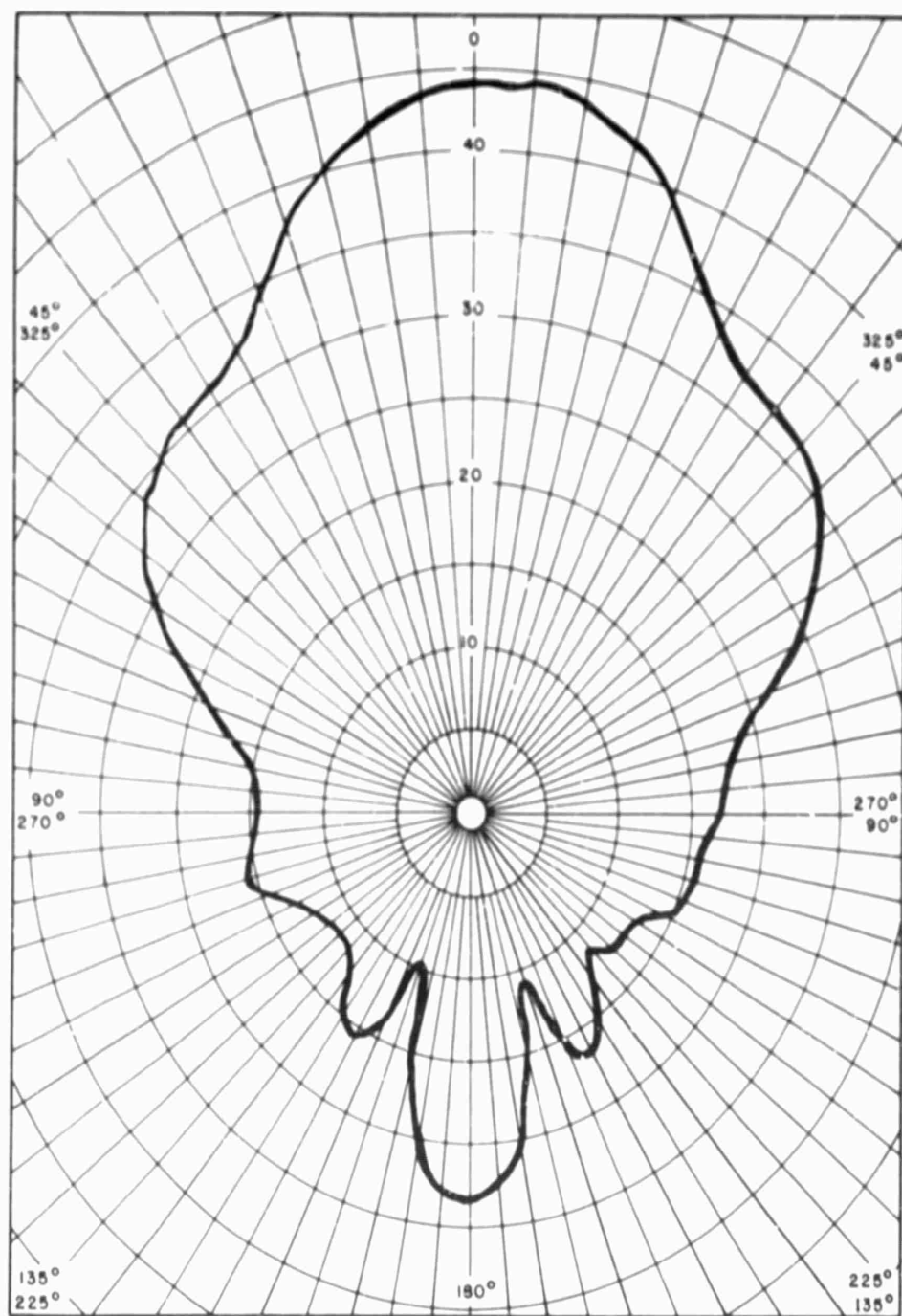


Figure 3.2 Directivity pattern of Altec-Lansing 802-C loudspeaker at frequency 3.2 kc with attached horn. Horn dimensions: 9-inch-diameter mouth; 1-inch-diameter throat; total flare angle $2 \arctan 2/3$. Scale: 1 db/radial division.

verse square law) will produce a pressure of even less than $\frac{1}{16}$ that produced by the direct rays, since the latter do not travel so far and are not absorbed by a reflecting medium. An even more favorable ratio of signal to noise will exist at the higher elevation instruments at 3 and 6 feet.

An argument similar to the reflection case holds for the refraction case.

If the maximum change of amplitude of the straight-path-signal due to long-path signal interference is one part in sixteen, the maximum shift in the phase angle of the carrier is $3\frac{1}{2}$ degrees (see Appendix B). This represents an error in the calculated sound velocity of the acoustic signal across the air path of 0.06 percent of an air tem-

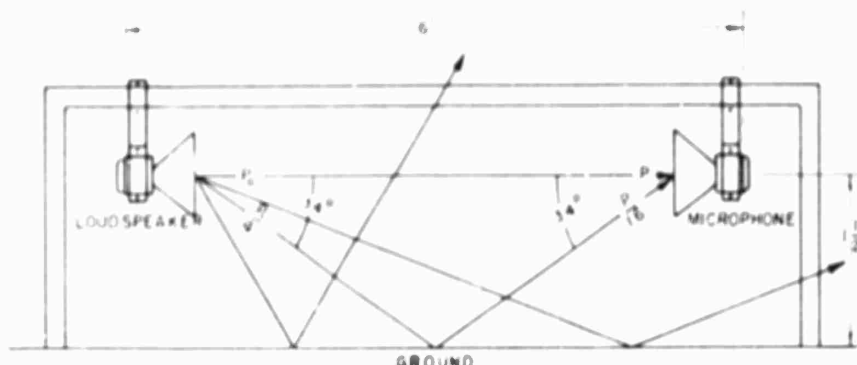


Figure 3.3 Effect of directivity patterns on direct and indirect signals.

perature of 70°C. From this, it appears that long-path signals may enter the microphone, but their contributions to either phase shifts or amplitude variations of minimum path signals are extremely small.

Other observers in this field have expressed the feeling that the strong signal rays near the axis of the loudspeaker might be refracted and travel over path lengths which are about double the direct path length. Assuming that average velocity over these long paths should be double the ambient figure, the velocity meter would read a travel time $t = 2D/2c_0$ which would be the same as the t measured for direct path signals at ambient sound velocity, i. e., $t = D/c_0$. Certainly, one would have a difficult time fabricating such a long-path sound ray in Figure 3.3. The total length of the one-bounce signal ray in that diagram (which is to scale) is only 19 percent longer than the direct signal ray. Also, since the velocities measured by the sound velocity meter on all channels during Shot 12 stayed steadily at low values and did not even once go to double the ambient figure, one could hardly suppose that the air in the gap was steadily hot and that directly below it was steadily cooler. Yet this condition is necessary for a continuous refraction of the strong on-axis signals. Therefore, this refraction explanation is considered improbable, and this last applies also to the higher meters at 3- and 6-foot elevations even though longer path lengths might be concocted for these elevations. The case of the off-axis signals has already been considered above. Signal rays certainly can travel over long paths and would be quite important if the strong on-axis signals were lacking for some reason. It would be hard to imagine that this would happen steadily for any period of time, however, especially since on most channels almost every cycle of the carrier can be seen from shortly after zero time until shock arrival on the Shot 12 velocity records (see recorded sound signals, Appendix F).

3.3 ATTENUATION OF THE ACOUSTIC SIGNAL IN THE AIR GAP

It was noted in a preliminary test of the equipment on Shot 8 that some effect, probably thermal, was causing the received acoustic signal to be attenuated (see Section 3.3). This phenomenon also occurred on Shot 12. Since it did not occur in the one channel on Shot 8 where the transducers and air path were replaced by an electrical network, it was assumed that the variations were not related to the electronics but rather to the air medium, the loudspeaker, the microphone, and/or the horns.

The expression for the propagation of a plane sinusoidal sound pressure wave in air is:

$$p = p_0 e^{j\omega \left[t - \frac{x}{c} \right] - \delta x} \quad (3.1)$$

Where: x = the distance from the sound source in cm.

t = the time in seconds.

p = the sound pressure existing at distance x in psi.

p_0 = the sound pressure existing at distance $x = 0$, when $t = 0$ (in psi).

c = the velocity of sound in cm/sec.

δ = the attenuation constant in nepers/cm.

$\omega = 2\pi f$ and f is the frequency in cycles/sec.

There are two types of sound attenuation in the air: attenuation due to molecular absorption, δ_m , and attenuation due to heat conductivity and viscosity, δ_c .

$$\delta = \delta_m + \delta_c \quad (3.2)$$

These quantities are dependent upon air temperature, absolute humidity, and the sound frequency (Reference 9, Pages 64-67).

For the 3,200-cps signal used by Project 1.5 and assuming a 30-percent relative humidity at 20°C, an air temperature change from 20°C to 70°C will cause a change in p , the pressure amplitude, 6 feet from the loudspeaker of approximately 0.5 percent, negligible in comparison to the attenuations measured (see Appendix D for measured attenuations). The attenuation factor δ_m is found from an extrapolation of Kneser's nomogram (Reference 9, Page 65), and δ_c is found from Sivian's attenuation-versus-temperature curve (Reference 9, Page 66). See Appendix D for calculations.

Neither Kneser's nor Sivian's data are for temperatures above 50°C. Furthermore, it is possible that large attenuations of acoustic signals do exist at higher air temperatures. This might imply that Project 1.5 measured the attenuation of its acoustic signals correctly but erred in its velocity computations. However, if the Project 1.5 velocities should be correct, then the associated air temperatures are so low that presently known acoustic-attenuation phenomena alone cannot account for the small pressure amplitudes measured. This again suggests the phenomenon of destructive interference of multiple-path signals. For a highly turbulent condition, it has been found in experiments at NEL that great attenuation can occur even when the signal is following the minimum path between transducers. A test was performed in which velocities were measured over flaming pans of gasoline. In order to be certain that the acoustic signals were following the direct path between transducers, an asbestos baffle was placed

halfway across the gap with a hole in it aligned with the transducer horns (see Figure 3.4). It should be clear that multiple-path signals in a certain sense always occur, since more than one ray passes through the baffle hole; but at least very-long-path signals are eliminated in such a setup.

For the test depicted in Figure 3.4, the measured signal amplitudes and calculated sound velocities are plotted versus time in Figure 3.5.

Clearly, there was little velocity change, and yet there was considerable amplitude variation. There also was an interval of 0.05 second where the signal was not only greatly diminished but also was highly distorted. Velocity measurements in this 0.05-second period were difficult to make because the identity of a certain phase (the maximum



Figure 3.4 Sound velocity meter three feet above flaming gasoline. Asbestos baffle at midpoint of path.

value of the modulation envelope) could not be determined with an accuracy of better than two or three cycles of the carrier. However, it should be remarked that a crude measurement that would give arrival times accurate within 16 percent could have been made even during 0.03 second of this 0.05-second interval. During the other 0.02 second, the signal was indeed completely unreadable.

Looking at Figures 3.4 and 3.5, one might wonder whether the velocity meter was functioning properly if such a small velocity change was measured since the air medium between the transducers must have experienced a sizable temperature increase. First of all, it is not likely that Figure 3.4 corresponds to any instant of the 0.40-second recorded interval of Figure 3.5. Furthermore, there were 100 measurements of velocity made every second. Each of these $\frac{1}{100}$ -second intervals covered 6 inches on a Brush

recorder paper tape in the final record. The task of choosing the most representative section of an original 30-second recording interval is out of proportion to its importance, when one realizes that the corresponding paper record is more than $\frac{1}{4}$ of a mile in length. So possibly the best sample of velocity record was not chosen for analysis. However, the question still arises as to why the signal amplitude changed so much when the sound velocity did not and whether the sound velocity was measured with sufficient accuracy under such circumstances.

In the following paragraphs of this chapter several more controlled experiments will be described which indicate the reasons why the attenuation occurred and why, in spite of the attenuation, the velocity meter could measure velocity at such times with a sufficient degree of accuracy.

Before describing these experiments and in order to clarify the picture, the following summary of the attenuation phenomenon theory is given, based on the assumption that

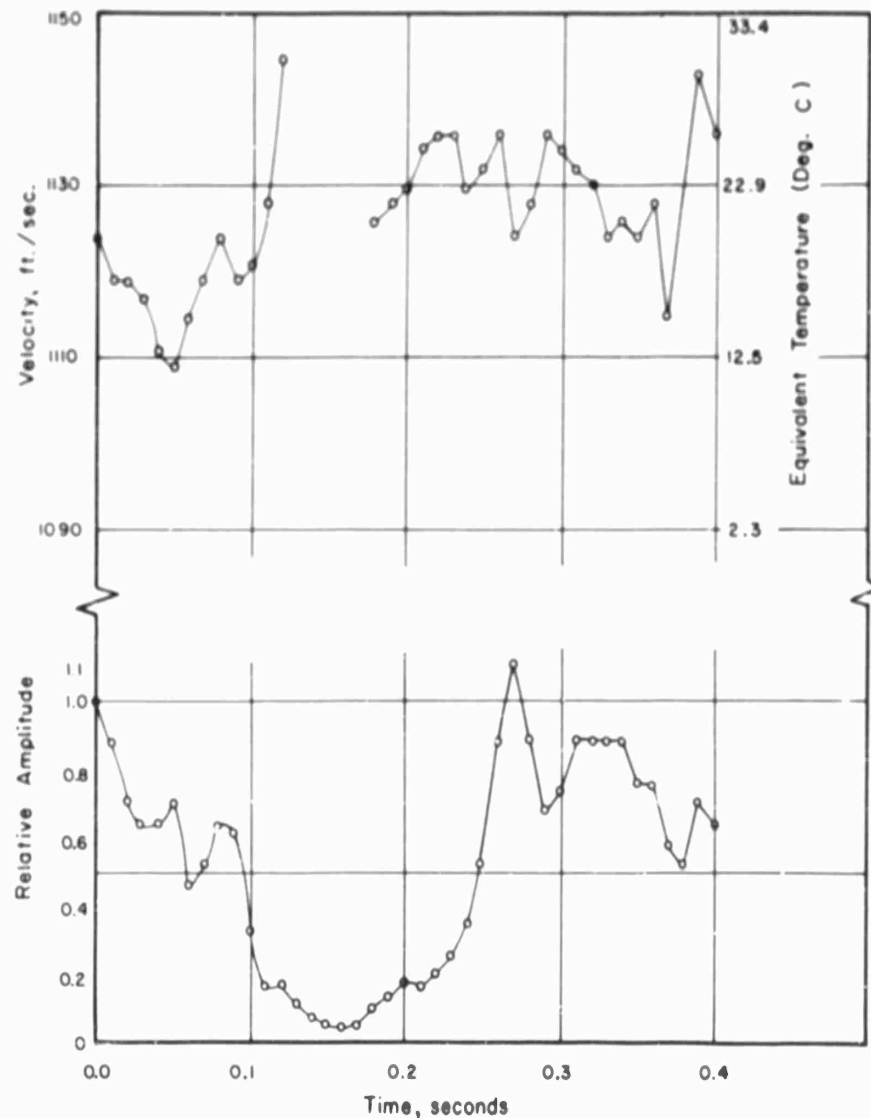


Figure 3.5 Measured sound velocities and signal amplitudes three feet above flaming gasoline tins. Baffle at path midpoint. (See Figure 3.4).

the velocity measured is reasonably correct — substantiation of this important tenet will follow.

1. The attenuation measured is not due primarily to changes in the attenuation constant δ because at the temperatures corresponding to the velocities recorded the change in δ is infinitesimal (see Appendix D).

2. The attenuation is not due to long-path signals interfering with minimum-path signals at the microphone, because the amplitude at the microphone of any long-path signals would be too small due to horn directionalities for this to be important.

3. Attenuation is not due to refraction of the strong on-axis acoustic rays out of the straight-line path because this implies hot air in this path with cooler air surrounding it.

4. The attenuation is partly due to uneven heating of the air medium causing destructive interference in the direct path signals. The bundle of acoustic rays passing through the baffle hole in Figure 3.4 is affected by contiguous zones of hot and cold air. But the zones of hot air do not need to be very hot, for with distance of 4.6 feet between horn mouths a change in temperature from 20°C to 44°C would be sufficient to change the number of carrier cycles in this distance from 13.1 to 12.6 (i. e., a change of $\frac{1}{2}$ wavelength at the microphone). It is not difficult to imagine two acoustic rays crossing the air gap through the baffle hole, with one passing through air of an average temperature of 20°C and the other passing through air at an average temperature of 44°C. The two would completely cancel each other, and yet the velocity meter, when recording either, would have correctly indicated values of only 1.125 or 1.170 ft/sec, respectively.

5. The attenuation is also due partly to the microphones' horns being exposed to intense thermal radiation and hence rising to very high temperatures. Sound signal rays traveling along the hot air layer near the horn would arrive at the horn throat out of phase with those which had taken the route of the cooler air path near the axis. This effect is most pronounced for frequencies at which the sonic wavelengths are about the same size as the horn dimensions, or smaller. This is discussed further in Section 3.6 to follow. If the above theory is correct, it does not seem surprising that attenuation of acoustic signals occurred in the air medium during the Nevada Teapot tests when the measured sound velocity changes were averaging only 9-percent increase above ambient.

3.6 OTHER MEASUREMENTS OF VELOCITY

The question exists as to whether the velocity meter really did measure velocity. First, there has never been a test where a string of thermocouples has been placed across the acoustic air path to verify the velocities measured in terms of their corresponding temperatures. However, there have been instructive tests made on the instrumentation under controlled conditions as follows.

1. When the transducer diaphragms were spaced 3 feet apart instead of 6 feet, the travel time of the acoustic signal was cut in half, and the recorded value of velocity was therefore doubled. Similar results occurred for other spacings as expected.

2. When the sound velocity meter was situated in a paint oven at NEL and the temperature in the oven was raised from 90°F to 130°F and then to 160°F, the velocities measured by the meter at the three temperatures were as given in Table 3.1. The oven temperatures were measured by a thermocouple situated in the back wall of the oven and projecting on a stud into the air about 6 inches from the wall. The accuracy of the thermocouple is not known. The oven was heated by electrical coils in the ceiling and fans blew the hot air toward the floor. It is reported by those who use the oven that for

a temperature reading of 160°F there is a differential between ceiling and floor of 20°F along the back wall. Although the results of this test are not as convincing as those recorded for two velocity meters used on Tumbler (Table 4.2, Reference 1), this is attributed partially to the lower frequency carrier used on Teapot (3.2 kc instead of 10 kc) which caused annoying reflections from the hard walls of the oven whose scaled length, width, and height had now decreased by a factor of three. Unfortunately, an oven 27 times as big was not available. Furthermore, it should be remembered that this same thermocouple appeared to be in error in the Tumbler pre-Nevada tests when two velocity meters in the oven agreed more closely with each other than with the thermocouple (see Reference 1, Table 4.2). It was found when running this test that one had to hold the oven temperature at a certain level for perhaps a minute before the

TABLE 3.1 RESULTS OF TEST OF PROJECT 1'S VELOCITY METER IN PAINT OVEN

Thermocouple Temperature Reading		Sound Velocity Calculated from Thermocouple Temperature	Sound Velocity Measured by Sound Velocity Meter	Difference in Sound Velocity in Two Methods	Relative Error in Sound Velocity Assuming Oven Thermocouple Correct	Air Temperature Calculated from Velocity Measure- ment made by Velocity Meter	
°F	°C	ft/sec	ft/sec	ft/sec	percent	°F	°C
90	32	1,146	1,146	0	0	90	32
130	55	1,190	1,172	18	1.5	112	45
160	71	1,216	1,290	72	5.9	236	113

velocity meter readings stabilized. This was attributed to air temperature gradients which vanished after the temperature really became stable. The thermocouple used apparently had great thermal inertia as would be expected for a paint oven.

3. At the Nevada Test Site, it was noticed that the air temperature change between night and morning was recorded by the sound-velocity meters. A change of phase of $\frac{1}{3}$ of the carrier wavelength occurred when the temperature changed from 50°F to 70°F, and this was observed on all channels daily.

4. When the wind blew at Frenchman Flat, the resultant qualitative changes in sound velocity were recorded by the meters.

5. When a flat board was placed as an obstacle across the air path the recorded signal level would drop to almost zero. However, when shovelfuls of sand were dropped through the gap there was no discernible variation in velocity (see Reference 2, Section 3.1).

3.7 ATTENUATION OF ACOUSTIC SIGNALS CAUSED BY HEATING VARIOUS PARTS OF THE MICROPHONE

As mentioned in Section 3.4, the sound-velocity meter transducers in Teapot Shot 12, as well as in Tumbler Shots 3 and 4 and Upshot-Knothole Shots 9 and 10², were oriented with their axes along the blast line. In every case the microphone unit which was

²Except for cross-the-line channels in the particle velocity meter used on Upshot-Knothole Shots 9 and 10.

to receive the acoustic signal had its horn pointing toward ground zero. Also, in the throat of the horn there was a copper screen; behind this screen was another conical horn which was a part of the transducer itself and which connected to an acoustical labyrinth, eventually terminating in the chamber where a 2-mil-thick, shiny, dural diaphragm was situated. The aforementioned labyrinth was the acoustical equivalent of an extension of the transducer horn, and consequently, the cross-section horn area where the labyrinth joined the diaphragm chamber was extremely small. To the knowledge of the author, or anyone of the Project personnel (who served in three tests), there never was an instance where a diaphragm was adversely affected by the thermal radiation; there were, however, numerous cases where fine dust was blown onto the diaphragm by the blast wave. This left a shadow picture of the labyrinth opening on the diaphragm, but no

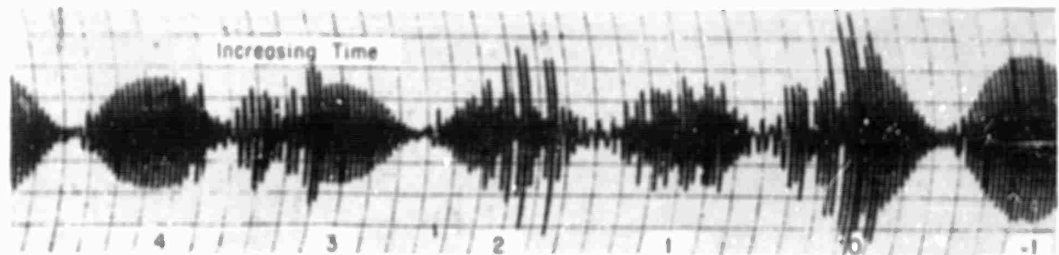


Figure 3.6 Effect of burning copper screen in horn throat on microphone.

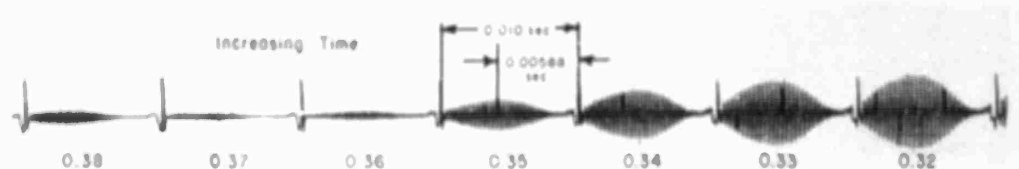


Figure 3.7 Effect of applying a blowtorch flame to horn of microphone.

shadow picture due to thermal radiation was ever observed. However, the aforementioned copper screens in the throats of the large conical horns were invariably charred, the amount depending upon the magnitude of incident thermal radiation.

After Shot 12, tests were conducted at NEL to determine what would happen to the acoustic signal's amplitude while the copper screen in the microphone unit was burning. To accomplish this, a 180-volt B-battery supply was short-circuited through the screen while the velocity meter was operating. Judging by the effect on the screen, this test was more severe than its equivalent on an ordinary Nevada test. Also, a transient condition existed some two to four times as long as those observed on Teapot Shot 12. However, at the end of this period (40 msec) the amplitude of the signal was 66 percent of ambient and 90 percent of ambient, 10 msec later. After the 40-msec transient, there was no detectable sound-velocity change as measured over a 6-foot path length (see Figure 3.6).

Another test was conducted at NEL to determine the effect of heating the horn of the microphone, in order to simulate the usual Nevada test condition. For this, a blowtorch flame was applied to the microphone horn while the complete system was operating (see Figures 3.7 and 3.8).

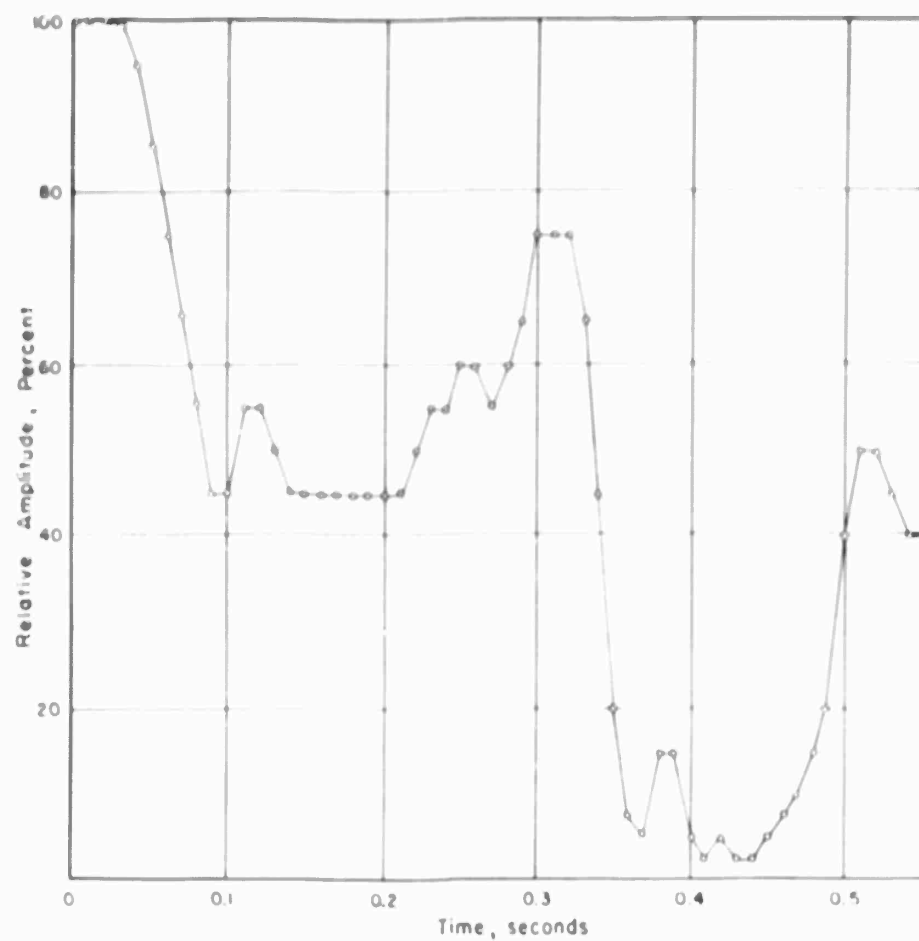


Figure 3.8 Signal amplitude versus time for condition where blowtorch is played over microphone horn.

It is clear from an examination of Figure 3.7 that there is practically no shift in the phase of the recorded signal's envelope with respect to the reference time spikes. Yet the signal's amplitude in this same period dropped to as little as 3 percent of its original value.

Chapter 4

DISCUSSION

The preshock sound velocities measured by Project 1.5 during Shot 12 did not agree with preshock sound velocities calculated from pressure data taken by other agencies (References 5, 6, and 8) and using current blast-wave theories. In all cases the Project 1.5 velocity values were low by the order of a factor of two. Also, these directly measured sound velocities were almost the same at the 1,000-foot range as at the 2,000-foot range on both the asphalt and desert surfaces. In addition, there was little difference between the values recorded over different surfaces (desert, asphalt, water, fir boughs, and concrete) and small differences at the various elevations (1 1/2, 3, and 6 feet).

Yet in 23 out of 24 channels the velocity-meter instruments seemed to perform adequately. Subsequent tests at the Navy Electronics Laboratory (NEL) indicated that the meters were working as they should be and that they would measure velocity under laboratory conditions within an accuracy of 6 percent at air temperatures up to 160°F.

Direct preshock temperature measurements were made on Shot 12 by Project 8.4e (Reference 12) and over the same surfaces as those where Project 1.5 measured sound velocities.

Temperature is related to sound velocity by:

$$c = KT \sqrt{} \quad (4.1)$$

Where: c = sound velocity ft/sec.

T = absolute temperature.

K = a constant for a given medium of constant molecular weight.

It was hoped that an agreement between the measured c and T values would help explain the precursor phenomenon. Unfortunately, the Project 8.4e data agreed neither with the Project 1.5 data nor with the blast data. Several unusual phenomena were noteworthy in the 8.4e data:

1. Over the plots of fir boughs, ivy, concrete, and wood (this last plot was not instrumented by Project 1.5) the temperatures appeared to increase with elevation up to 10 feet. This certainly was not expected over concrete and does not agree with sonic velocity data or current blast theory.

2. High elevation channels showed temperature increases before the low elevation channels did in many cases. This is contradicted by the sound-velocity data and current blast theory also.

3. High preshock maximum temperatures were reached in many cases; this agreed at least qualitatively with present blast theories, although it was not supported by the Project 1.5 data which consistently showed low velocity values on all channels. However, the Project 8.4e temperature value invariably dropped after these maxima to very low magnitudes before shock arrival. This was not reconcilable with any known theory.

4.1 CALCULATIONS OF PRESOCK SOUND VELOCITY FROM PEAK-PRESSURE, SHOCK-VELOCITY, AND PRECURSOR-ANGLE DATA

There are several methods currently used for calculating the presock sound velocity at low elevations on a precursor shot from the blast data. The first of these (explained in Reference 7, Chapter 6) involves the measurement of the angle of the precursor wave front with the horizontal and the knowledge of the ambient air sound velocity above an assumed heated air layer. It is calculated from:

$$\sin \theta = \frac{c_0}{c} \quad (4.2)$$

Where θ = the angle between the precursor wave front and the horizontal.
 c = velocity of sound in the heated layer.
 c_0 = velocity of sound in the cool air above it.

This theory does not take account of a temperature gradient in the thermal layer. A more refined treatment which considers a thermal gradient is suggested in Chapter 4 of Reference 8. Here Equation 4.2 is supplanted by:

$$\frac{\sin \theta}{\sin \phi} = \frac{c_0}{c} \quad (4.3)$$

Where ϕ = the acute angle which the wave front in the thermal layer makes with the thermal boundary.

Equation 4.2 is a special case of Equation 4.3 where the thermal Mach wave is at right angles to the boundary, i.e., $\sin \phi = \sin 90^\circ = 1$. By experimentally measuring θ and ϕ , using high-speed photography, and knowing in advance the value of c_0 , the quantity c can be calculated. For $\theta < \phi < 90^\circ$, c will be less than values calculated using Equation 4.2 but will always exceed c_0 . The use of Equations 4.2 and 4.3 is limited by the accuracy with which θ and ϕ can be measured.

A second technique for calculating sound velocity arises from the assumption that the direction of wave propagation is horizontal very close to the ground, i.e., the wave front is perpendicular to the ground. In this method the presock sound velocity is related to the blast-wave velocity. Although the pressure wave is of a complex type which does not lend itself well to straightforward mathematical analysis, nevertheless, from the measured peak pressures which can be calculated within reasonable limits, an approximate relationship between the blast-wave velocity and acoustic velocity can be established.

A third technique for determining presock sound velocity consists of measuring the time of arrival of a blast wave at two gages separated from each other by a known distance vertically, e.g., a few feet (Reference 10, Page 134). Assuming the angle this wave front makes with the horizontal is ϕ , the gage spacing is h feet, the difference in arrival times at the two gages is Δt (seconds), and the velocity of propagation along the ground is c' (ft/sec), then the presock velocity c of the wave in ft/sec is:

$$c = c' \sin \phi = c' \left[1 + \left(c' \frac{\Delta t}{h} \right)^2 \right]^{-1/2} \quad (4.4)$$

A modification of this method is used in this report. Project 1.5 obtained shock-arrival data from Project 1.10 and used these in an application similar to that of Equation 4.4. The difference was that the pressure gages were not in vertical arrays; but this was no particular handicap since their relative locations were known. Arrival times were known within 0.5 msec.

Velocities, temperatures, and wave-front angles were calculated using these data and are given in Table 4.1. Assuming that 95 percent of the measurements of time

TABLE 4.1 BLAST VELOCITIES AND CORRESPONDING AIR TEMPERATURES

Calculated from use of Equation 4.4 technique. Gage elevations were 0 and 3 feet. Deviations of the angle ϕ is the dispersive range of the velocity c and the temperature T . The term ϕ , which is determined by arrival times at two gages, has its dispersion fixed by a time measurement error of as much as ± 0.5 msec at each gage.

Ground Range and Surface	Range in Which True ϕ Should Occur 94 pct of Time	Range in Which True Blast Wave Velocity c Should Occur 94 pct of Time	Range of Temperature T Corresponding to Velocity Range
feet	degrees	ft/sec	°C
1,500 desert	33 — 71	1,955 — 3,406	613 — 2,415
2,000 desert	34 — 59	1,230 — 1,706	78 — 403
2,500 desert	73 — 96	1,215 — 1,252	69 — 90
3,000 desert	79 — 90	1,177 — 1,200	49 — 61
1,500 asphalt	25 — 46	1,504 — 2,596	254 — 1,204
2,000 asphalt	47 — 41	1,704 — 2,319	403 — 973
2,500 asphalt	56 — 42	1,347 — 1,610	147 — 326

at either of two pressure gages will fall within 0.5 msec of the true arrival time and assuming that these measured times form a normal distribution, it can be shown that the time difference Δt will also form a normal distribution where 84 percent of the measurements will be within 0.5 msec of the true Δt . The following tables assume this 0.5 msec error in the measurement of Δt .

Judging from the slow pressure rise of the waves from which these arrival-time data were taken (Reference 6), it appears that they are acoustic rather than shock. This being so, the quantity, c in Table 4.1 would be an acoustic velocity. Clearly these values of c far exceed those recorded in a direct measurement of sound velocity levels at between $1\frac{1}{2}$ feet and 6 feet by Project 1.5. Except for the values at the 2,500-foot and 3,000-foot desert ranges, the temperature values in Table 4.1 encompass the values found by the first two methods of temperature and velocity calculation described at the beginning of this section and plotted in Figure 2.28, Reference 11. In this last plot, Equation 4.2 is presumably used rather than Equation 4.3 for the Naval Ordnance Laboratory (NOL) data.

If Equation 4.3 had been used, the velocity and temperature values would be reduced depending upon how small an angle ϕ was. Although possibly ϕ was not measured photographically in Shot 12, it was measured by the Project 1.10 pressure gages within the limits imposed by arrival-time errors of ± 0.5 msec. Using the range of values of ϕ from Table 4.1 in Table 4.2, one can calculate the minimum and maximum sound velocity values c_{\min} and c_{\max} by use of Equation 4.3. The gages which determined the angle ϕ in Table 4.2 were at 0- and 3-foot elevations at each location and therefore

part, if not all, of the wave front would be in the heated air layer by almost any current theory.

In considering whether the shock-arrival technique would give the same wave front angle as the measured photographic record, the range of angles calculated from shock arrivals using the ± 0.5 -insec possible error at each gage yielded values agreeing very well with those recorded on film by Project 1.2 (see Table 4.3). Because of this correlation, it is expected that the use of the technique for determining ϕ at the very low elevations (0 and 3 feet) is also valid, although admittedly the shape of the wave front at these altitudes is known with considerably less certainty.

In Tables 4.1 and 4.2, ranges of velocities are tabulated which depend upon the accuracy with which the wave-front angle ϕ can be measured. Table 4.1 also depends

TABLE 4.2 BLAST VELOCITIES

Blast velocities calculated from use of Equation 4.3 where θ is angle measured by Project 1.2*, ϕ is angle obtained from blast-wave arrival times at Project 1.10 gages, c is ambient sound velocity = 1,124 ft/sec

Ground Range and Surface	θ	$\sin \theta$	ϕ_{\min} from Table 4.1	$\sin \phi_{\min}$	ϕ_{\max} from Table 4.1	$\sin \phi_{\max}$	$c_{\min} = c \frac{\sin \phi_{\min}}{\sin \theta}$	More likely c_{\min}	$c_{\max} = c \frac{\sin \phi_{\max}}{\sin \theta}$
feet	deg		deg		deg		ft/sec	ft/sec	ft/sec
1,500 desert	29.6	0.494	33	0.545	71	0.950	1,240	1,240	2,160
2,000 desert	43.8	0.692	38	0.632	89	0.956	1,027†	1,124	1,390
1,500 asphalt	26.5	0.445	25	0.422	46	0.720	1,067†	1,124	1,920
2,000 asphalt	37	0.600	47	0.730	81	0.988	1,371	1,371	1,854

* Except for 2,000 asphalt, see text

† These values of c_{\min} are less than ambient. This results from taking too much of an error range for ϕ so that $\phi_{\min} < \theta$. If ϕ_{\min} is arbitrarily set equal to θ , one obtains a more sensible c_{\min} as in Column 9

upon the velocity c' with which the blast wave is propagated along the ground. Table 4.2 depends upon the measurement of the blast wave angle θ above the thermal layer. It will be noted in Table 4.2 that there are data given for the 2,000-foot range on the asphalt line. Moreover, θ was not measured at this range by Project 1.2. However, because of the good correlation of the angle θ measured by Projects 1.2 and 1.10 (see Table 4.3) and the fact that θ from the photographs at 1,500-foot desert, 2,000-foot desert and 1,500-foot asphalt ranges agreed with the low angle values of θ derived from the Project 1.10 data, it is felt to be a reasonable assumption to use an angle of 37° for θ at the 2,000-foot range on the asphalt line (see Table 4.3). With this value of θ and the values of ϕ_{\min} and ϕ_{\max} calculated from arrival times at the 0- and 3-foot elevation Project 1.10 gages, c_{\min} and c_{\max} are calculated and tabulated. Combining the results listed in Tables 4.1 and 4.2, one obtains a range of probable values for the preshock sound velocity for ground distances of 1,500 and 2,000 feet on the desert and asphalt lines (see Table 4.4). The velocity ranges listed in Table 4.4 should therefore be consistent with the measured blast-wave velocity along the ground and the angles of the blast-wave front, both within and above the thermal layer.

The small value of ϕ for the 1,000-foot asphalt location leads to smaller sound velocities being indicated at the 1,000-foot asphalt location than would ordinarily be expected. The small ϕ indicates a large thermal gradient at this range.

4.2 PROJECT 1.5 SOUND-VELOCITY DATA

4.2.1 Teapot Instruments. Clearly, the measured sound-velocity data, with the exception of the 2,000-foot desert location, do not agree with the figures tabulated in Table 4.4. Many tests on the sound-velocity meters have been made to see if the 23 channels which recorded data could have been malfunctioning (see Chapter 3)—it is

TABLE 4.3 WAVE FRONT ANGLE COMPARISON

Comparison of wave front angle measured photographically by Project 1.2 and wave front angle measured by Project 1.10's 3- and 10-foot elevation gages, assuming arrival-time errors of 0.5 msec each gage

Ground Range and Surface	Project 1.2 Angle	Project 1.10 Angle Range
feet	degrees	degrees
1,500 desert	29.6	29.0 — 30
2,000 desert	43.8	41.2 — 49.4
1,500 asphalt	26.2	29.0 — 37.0
2,000 asphalt	Not measured	36.7 — 44.8

believed that they were not. It is further believed that most of the attenuation of the acoustic signals which was observed was caused in a relatively small part of the acoustic path; that is, in the microphone horn. It is felt that destructive interference occurred in these horns, which were apparently long enough to allow phase shifts of as much as $\frac{1}{2}$ wavelength between different sonic rays traveling by hot and cold paths but only rarely a shift of one wavelength. If the latter had happened, signals would have been augmented instead of diminished, and although this did occur in isolated cases, it was a very rare occurrence. Yet hundreds of cycles of the sine waves which left the loudspeakers crossed the air path and entered the microphones and were clearly recorded. These waves are depicted in Figures F.1 and F.24. These records were obtained by playing back the original magnetic tapes and photographing the amplified signal from the tape as it appeared on a cathode-ray tube. These data will enable anyone interested to roughly determine that no great velocity change occurred on any channel (employ the technique described in Table 4.2). A more refined method was used by the analysts at NEL for this determination. The magnetic tapes, which were run at speeds of 15 in/sec when recording the original data, were played back at approximately $\frac{1}{100}$ this speed, thereby converting the carrier frequency from 3,200 cps to 32 cps. This signal was then passed through a dc amplifier and recorded on a Brush oscillographic paper recorder run at 6 in/sec. In this way the scale was greatly expanded, notes could be made upon the record and a very-accurate cycle-by-cycle analysis of phase shifts made.

4.2.2 Data Comparisons with Previous Precursor Shots. There are very few velocity data available from other precursor-shot tests to use for comparison with the 1.5 Teapot data. The best would be the Tumbler Shot 4 velocities at $1\frac{1}{2}$ -foot elevation at ground range of 1,342 feet. Preshock velocities in this case roughly averaged 2,500 ft/sec, not greatly different from the calculated values given in Table 4.4 for the 1,500-

foot desert location in Teapot Shot 12. There does not seem to be any reason to question the validity of this particular Tumbler Shot 4 meter's data. But scrutinizing the Teapot Shot 12 velocity records and the Tumbler Shot 4 velocity records in general, exclusive of other data and theories, one would tend to be more skeptical of the Tumbler instrumentation at close-in ranges because of the frequent loss of data points (see Appendixes C and D, Reference 1). It is believed today that the attenuation of the acoustic signals which was measured in Teapot occurred also in Tumbler and Upshot-Knothole but could not be observed because of the recording techniques used in those tests. The Tumbler and Upshot-Knothole data were derived data. Zero crossings with positive slope of the modulation frequency sinusoid (after demodulation) were made to form signal spikes which were recorded on magnetic tape along with reference timing spikes.

TABLE 4.4 PRESHOCK SOUND VELOCITIES

Preshock sound velocities are compatible with measured values of the interval velocity c' , the acute angle θ between the wave front in the thermal layer and the thermal layer boundary and the acute angle ϕ between the wave front in the air above the thermal layer boundary and the boundary

Ground Range and Surface	Preshock Sound Velocity Range	Corresponding Air Temperature
feet	ft/sec	°C
1,500 desert	1,955 — 2,160	613 — 808
2,000 desert	1,230 — 1,390	78 — 175
1,500 asphalt	1,500 — 1,920	254 — 494
2,000 asphalt	1,700 — 1,950	403 — 527

Velocities were calculated from the shifts of the signal spikes with respect to the timing spikes (Reference 1). Changes in signal amplitude could cause spurious shifts in the signal spikes, could make them vanish, or could even generate extra ones. All of these phenomena have been observed.

In summary, it must be said that the people who have been closely associated with the sound velocity meters in Tumbler, Upshot-Knothole, and Teapot consider the Teapot instruments to be much more reliable than those used in the other two tests. However, the data taken in Tumbler and Upshot-Knothole are still considered reliable in those periods where several signal spikes in succession indicated similar values of sound velocity, but cases of isolated high-velocity points after several cycles of no signal should be treated with great skepticism, whether they agree with current theory or not.

The Teapot velocity data by themselves imply the following:

1. Since blast-wave arrival times are shortest on the asphalt line, next on the desert line, and longest on the water line (and these are measurable from the Project 1.5 data), the velocity of propagation in the horizontal direction on the three lines is greatest on the asphalt, next on the desert, and least on the water line.
2. Since measured sonic velocities at $1\frac{1}{2}$ -foot, 3-foot and 6-foot elevations increased approximately 9 percent above ambient from detonation to shock-arrival time at the 1,000-foot and 2,000-foot ranges, and irrespective of the surface, for Paragraph 1 above to be true, the thermal layer of consequence must have been between the ground level and some elevation below $1\frac{1}{2}$ foot, say 6 inches or 1 foot, unless the measured sound velocities are not related as assumed to the blast-wave propagation velocities.
3. If the preshock velocity of sound in the air was really some high value such as those calculated for Table 4.4, then the velocity meter simply does not work—although it will in most cases record every sine wave which leaves a loudspeaker, crosses a 6-foot air path, and enters a microphone (see Figures F.1 through F.24).

4. From the theories on the instrumentation presented in Chapter 3, there is a chance of the velocity meter's erring in its velocity measurement because of the cool air remaining in the transducers. This error is a function of the temperature of the air through which the acoustic signal passes (being 0 percent at ambient). However, it is also possible to err in the other direction, if the horns are heated red hot and the air in front of them becomes hot and thereby causes a more rapid advance of the acoustic signal. The Project 1.5 data imply that the total preshock-sound-velocity increase is small above an elevation of $1\frac{1}{2}$ feet. Also the magnitudes are similar at the 1,000-foot and 2,000-foot ranges and even over different surfaces. This might mean that the only velocity increase of significance measured was that due to the hot air near the transducer horns. This leads to the conclusion that the velocity measured by the meters was possibly too large rather than too small. Some small measure of credibility is lent to this supposition when one looks again at Figure 2.1 and observes that the water-line meter channels, where the reflectance of the surface was highest, measured a somewhat higher sound velocity than did the asphalt and desert channels. Certainly no one would predict a higher air temperature over the water surface.

Chapter 5

CONCLUSIONS AND RECOMMENDATIONS

The sound velocity meter appears to be capable of recording thousands of cycles of acoustic signals at ground ranges of 1,000 and 2,000 feet from detonation to shock arrival for the test conditions of Shot 12 (see Appendix F). These acoustic waves did not enter the microphones as soon (except for the water surface) as current blast-wave theory predicted that they should. No satisfactory explanation seems to be available as to where these acoustic signals could have spent their time.

It can only be concluded that if current precursor blast theory is correct, some unknown phenomenon is causing unreasonable velocity magnitudes to be deduced from otherwise reasonable-appearing data. If, however, the data are correct, some modifications in the present theory concerning the preshock medium status will need to be made.

If the precursor phenomenon is to be investigated further, it is recommended that additional effort be expended to obtain the contour of the blast-wave front near the ground surface, e.g., below 10 feet. Few reliable data are presently available in this region. It is to be hoped that these data would do much to explain the differences in high air temperatures and sonic velocities deduced from current blast-wave theory and the lower values recorded by instruments which measured these phenomena directly.

Appendix A

INSTRUMENTATION

A.1 BACKGROUND

The Naval Electronics Laboratory's measurement of sound-velocity changes again relied on a system in which sound transit time between two fixed transducers in an air medium was observed (Reference 1).

A 3,200-cps carrier, amplitude modulated approximately 90 percent with a 100-cps sinusoid, was transmitted across the transducer air gap. Measurements proved that signal crosstalk between balanced signal pairs was negligible in a multi-conductor cable of considerable length. Hence, it was decided to send the signal information from the instrument van to the field, through the air gap, and back to the instrument van where it was recorded directly on magnetic tape along with its timing-spike reference.

Basically, the records so obtained were analyzed by transcribing them onto some readable medium such as paper tape or photographic film. The peak of the modulation envelope gave a reference point from which to measure to the reference spike. The latter was added to the signal information upon its return to the instrument van. As the signal delay through the complete electronic system from generation to recording was constant, changes in air-path transit time were evidenced by changes in time differences between the reference spike and modulation peak. Such time differences were convertible to sound velocity, given predetonation air temperature.

Most sound-velocity records obtained in Nevada showed appreciable signal attenuation and some distortion; hence, the Teapot system of instrumentation was an improvement over previous NEL versions which relied on additional spike generation from the demodulated air-path signal. Obvious troubles would arise if the modulation envelope were not well preserved.

A.2 BASIC INSTRUMENTATION

A.2.1 Master Generator. The master generator, the heart of the sound-velocity system, consisted of three units (see Figure A.1). It utilized a very stable oscillator of proven design to generate a carrier frequency of 3200 cps. This oscillator in turn drove a synchronized frequency step-down oscillator which generated the 100-cps modulation frequency. The 100-cps signal so derived was fed to a balanced modulator which in turn provided the 100-cps modulated carrier drive for the bridging amplifiers that furnished the signal for the field units. The 100-cps oscillator also provided drive for the reference spike generator. The spike generator ran in synchronism with the 3,200- and 100-cps generators and provided an output variable in phase over 360 degrees of the 100-cycle modulation envelope, and sufficiently sharp to provide resolution, if necessary, within a fraction of a cycle of the carrier.

The above three described units were monitored by a safety unit which would switch in immediately an identical master generator should any of the output signals fall below a minimum operating level.

The bridging amplifiers provided a balanced signal output to the field units via the field cables. A considerable amount of work was done in attempting to eliminate the zero time electromagnetic transient induced in the equipment via field cabling. The use of twisted and electrically balanced signal pairs and careful selection of electrically balanced transformers that worked into and out of the field line enabled a reduction of the induced transient to a negligible amount. Also the time duration of this transient was less than 10 msec in all channels of the system, thus no signal information was obscured (see Figure A.2). However, a very good zero marker was so obtained. The number of bridging amplifiers used (one for every three field channels) was greater than power requirements would demand for driving the field amplifiers, so that a failure would not effect the loss of too many channels of information.

A.2.2 Transducer Power Amplifiers. One driver unit provided voltage step-up and bandpass filtering and drove three power amplifiers from the low impedance line. The power amplifiers in turn drove the transducers sufficiently hard to give a good signal-to-noise ratio, thereby overriding acoustical noise signals arising from any apparatus in the vicinity.

The direction of acoustic signal transmission was selected to give minimum crosstalk between transducers for the three elevations at the same surface location. Both theory and equipment tests showed crosstalk effects were quite negligible.

A.2.3 Mike-to-Line Amplifier. The receiving transducer drove a mike-to-line amplifier. This latter unit made up for air-path signal attenuation in order to send the signal back to the instrument van with

ample signal-to-noise ratio. The mike-to-line amplifier and all subsequent equipment were sufficiently broadbanded to allow for frequency change of the air-path signal during any possible rapid air-temperature changes.

In the Line-to-Tape Unit, the last link in the chain of instrumentation, the reference spike was added to the incoming signal; the resultant composite signal was applied to the magnetic tape.

A.3 DISCUSSION

Direct calibration of the system is difficult to achieve. However, a good approach to the measurement of air temperature was achieved in the laboratory's paint-drying oven which was sufficiently large to

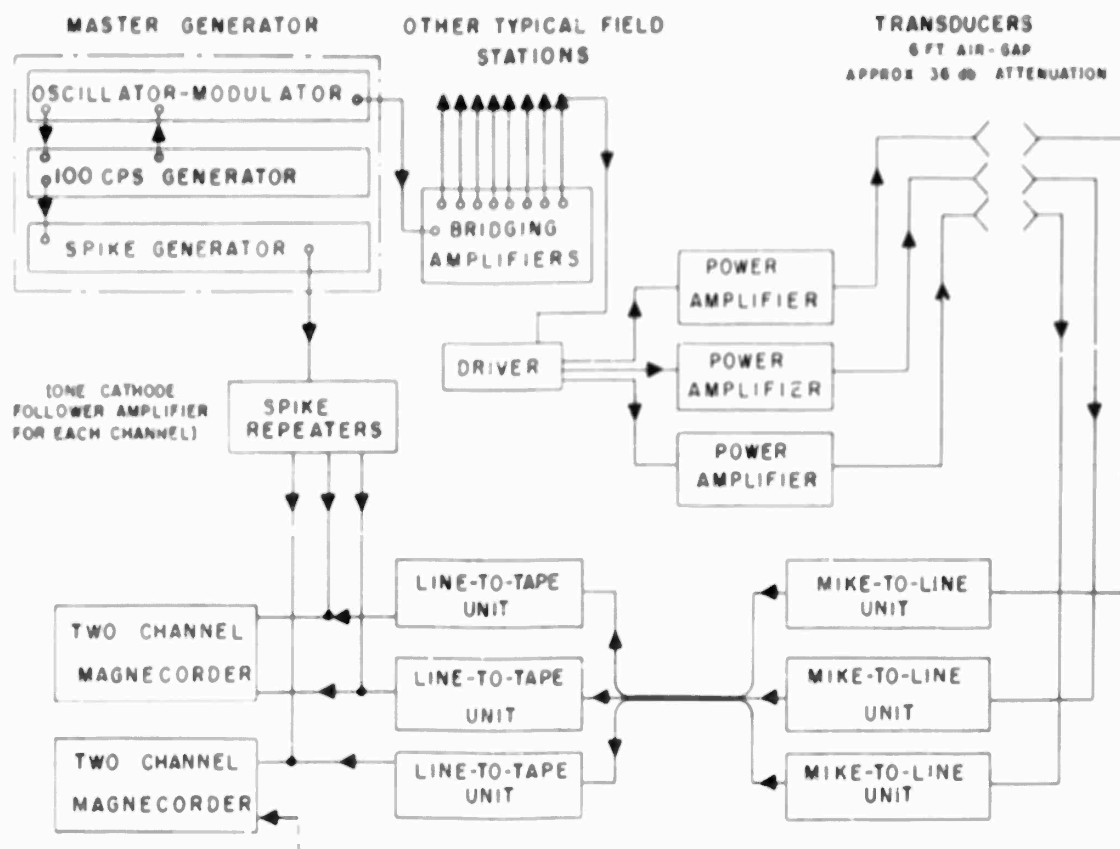


Figure A.1 Electronics for one typical field station, three channels.

house the transducer pairs. Fair correlation between air temperature and signal phase shift was obtained though certain difficulties were experienced. The oven was limited to a temperature of approximately 300 degrees Fahrenheit from which a phase shift of about four carrier cycles could be expected. The degree of resolution was troubled somewhat by signal reflections off the oven walls and by convection currents within the fairly large enclosure. Thus it was difficult to read the data with a note of finality to within a fraction of a carrier cycle when the above effects produced variations of phase shift which could be observed at any given temperature. However, in general, phase shift correlated with the corresponding temperature throughout the temperature ranges investigated.

Suspicion of coupling between the transducers through the supporting cross-arm was ruled out by other tests at NEL.

As certain proof that the signal was being acted upon only in the transducer air path, in one channel a dummy air gap was substituted for the actual air path in one of the preliminary Nevada shots. The remainder of the electronics in the dummy channel was identical to that of the air-path channels; the dummy attenuating pad was equivalent to the air-path loss. Results showed no change in data before, during, or after shot time for the dummy channel, whereas the air-path channels exhibited signal phase shifts indicative of air-temperature and sound-velocity increases.

A later refinement in data analysis removed the necessity of locating the modulation peak which was sometimes difficult to do in view of the signal attenuations and distortions often present. Instead, a reference point was chosen in the pre-thermal record from which it was possible to count through the continuous record (cycle by cycle) through thermal conditions, using the subsequent reference points found every 32



Figure A.2 Recorded acoustic signal showing effects of electromagnetic transient at detonation. Note delayed transient due to distorted loudspeaker signal received by microphone after time delay in air path.

cycles to make measurements to the reference spike. However, both methods gave substantially comparable results.

It is believed the system is capable of measuring sound-velocity changes in air (or whatever the medium may be); it functioned in all channels but one up to shock arrival.

The records can be analyzed in a straightforward manner (except over the two surfaces of ivy and fir where turbulence made some data unreadable). It is believed the system measured, with an accuracy of at least 8 percent, sound-velocity changes near the ground in the vicinity of a nuclear detonation.

Appendix B

PHASE AND AMPLITUDE CHANGES DUE TO INTERFERENCE OF SOUND WAVES

When two sinusoidal waves are added, the resulting wave is another periodic function. If the original two waves have the same frequency but differ in phase by an angle ϕ , the sum of the two will be another sinusoid with the same frequency but with a different phase angle θ . Consider the two functions:

$$x = A \sin \omega t$$

$$y = B \sin(\omega t + \phi)$$

Then:

$$\begin{aligned} x + y &= A \sin \omega t + B \sin(\omega t + \phi) \\ &= A \sin \omega t + B \sin \omega t \cos \phi + B \cos \omega t \sin \phi \\ &= (A + B \cos \phi) \sin \omega t + B \sin \phi \cos \omega t \end{aligned}$$

Now, let the sum of the sinusoids be of the form:

$$\begin{aligned} x + y &= C \sin(\omega t + \theta) \\ &= C \sin \omega t \cos \theta + C \cos \omega t \sin \theta \end{aligned}$$

Then:

$$C \cos \theta \sin \omega t + C \sin \theta \cos \omega t = (A + B \cos \phi) \sin \omega t + B \sin \phi \cos \omega t$$

By separating terms in $\sin \omega t$ and $\cos \omega t$:

$$C \cos \theta = A + B \cos \phi$$

$$C \sin \theta = B \sin \phi$$

Therefore:

$$\begin{aligned} \tan \theta &= \frac{B \sin \phi}{A + B \cos \phi} \\ \theta &= \tan^{-1} \frac{B \sin \phi}{A + B \cos \phi} \\ C &= \{(A + B \cos \phi)^2 + B^2 \sin^2 \phi\}^{1/2} \end{aligned}$$

To find the maximum θ , let:

$$\frac{d\theta}{d\phi} = 0$$

Then:

$$\frac{d\theta}{d\phi} = \frac{AB \cos \phi + B^2}{A^2 + 2AB \cos \phi + B^2}$$

Therefore:

$$0 = AB \cos \phi + B^2$$

And, for θ to be a maximum:

$$\cos \phi_{\theta \max} = \frac{-B}{A} \text{ and } \sin \phi_{\theta \max} = \frac{(A^2 - B^2)^{1/2}}{A}$$

Then:

$$\theta_{\max} = \tan^{-1} \frac{B(A - B^2)^{1/2}}{A(A - \frac{B^2}{A})}$$

$$\theta_{\max} = \phi_{\max} - 90^\circ$$

$$\theta_{\max} = \cos^{-1} \frac{B}{A} - 90^\circ$$

For example, let $B = 1$ and $A = 16$. Therefore,

$$\frac{B}{A} = \frac{1}{16}$$

Then:

$$\cos \phi_{\max} = -0.0625$$

$$\phi_{\max} = 93^\circ 35'$$

Therefore:

$$\theta_{\max} = 3^\circ 35'$$

The maximum value which C can have occurs if $\phi = 0^\circ$, then:

$$C = A + B$$

Its minimum value occurs if $\phi = 180^\circ$, then:

$$C = A - B$$

In summary, the maximum phase shift which can occur when two sinusoids of the same frequency are added (as in interference of sound waves) is:

$$\theta_{\max} = \cos^{-1} \frac{B}{A} - 90^\circ$$

Where:

A and B = their amplitudes

For $B = 1$ and $A = 16$, $\theta_{\max} = 3^\circ 35'$. That is, the sinusoid resulting from the addition of two sine waves cannot differ in phase from its larger amplitude component by more than θ_{\max} — in this case $3^\circ 35'$. The amplitude of the resulting sinusoid cannot differ from the amplitude of its largest component by more than B parts out of A — in this case one part out of sixteen.

Appendix C OPERATIONS

Bad weather caused considerable hardship and delay during the entire Teapot operation. Extremely low temperatures, high winds, snow and rain damaged the equipment, caused sickness of the personnel and generally hurt morale.

Under such circumstances, any equipment which facilitates field operations is always welcome. To house fragile electronic equipment on the blast line at ranges as close as 1,000 feet, the Operations Division at NEL developed a steel instrument shelter (see Figures C.1 through C.3). Navy dock pontoons were modified for this purpose. A watertight hatch was welded to the top of the pontoon, and mounting brackets for holding electronic chassis were welded to the inside ribs. Watertight packing glands for admitting

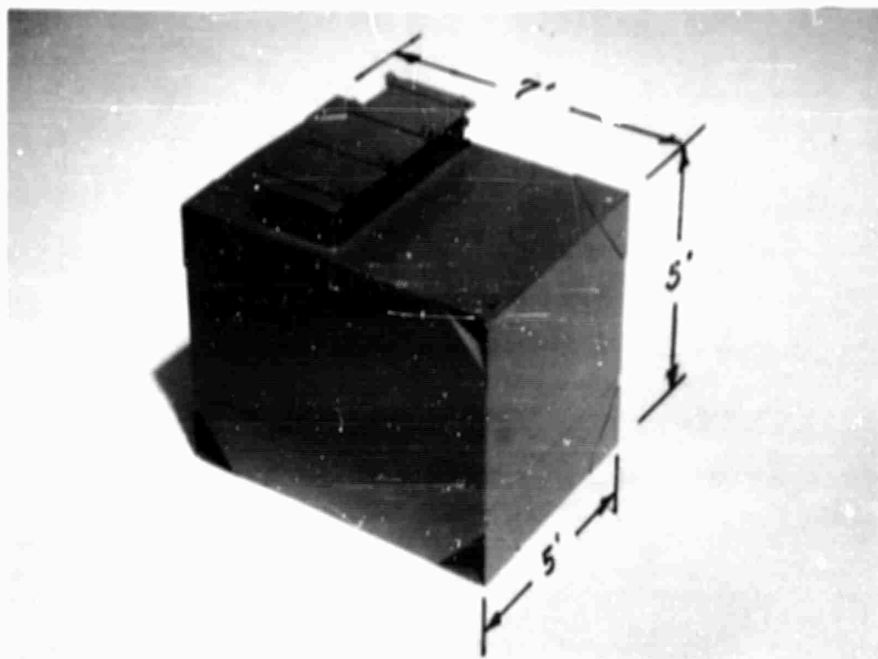


Figure C.1 Model of NEL instrument shelter with dimensions of full-size shelter depicted.

cables were welded to the sides of the shelter, and ladder rungs were tack-welded inside.

When personnel worked inside the shelters, a transparent door made of lucite replaced the steel hatch cover which was swung back out of the way. The units were painted with aluminum paint inside and out; the visibility inside during the day and without artificial illumination was quite suitable even when a dust storm was raging outside.

The shelters did not leak when other types of shelters were flooded during a rain storm, and a minimum of dust seeped into the equipment.

The units were light enough in weight to enable transportation by truck from the home laboratory in San Diego. Consequently, electronic equipment was fitted into the shelters in advance, eliminating the need for costly changes in the field.

Many used pontoons are now available at Navy bases and can be outfitted for little more than the cost of cleaning, welding, and painting. This alteration work was done at NEL for approximately \$300 per unit.

Complete specifications and drawings for these shelters can be obtained by writing:

Commanding Officer and Director
U. S. Navy Electronics Laboratory
San Diego 52, California
Attn: Mr. J. N. Shellabarger

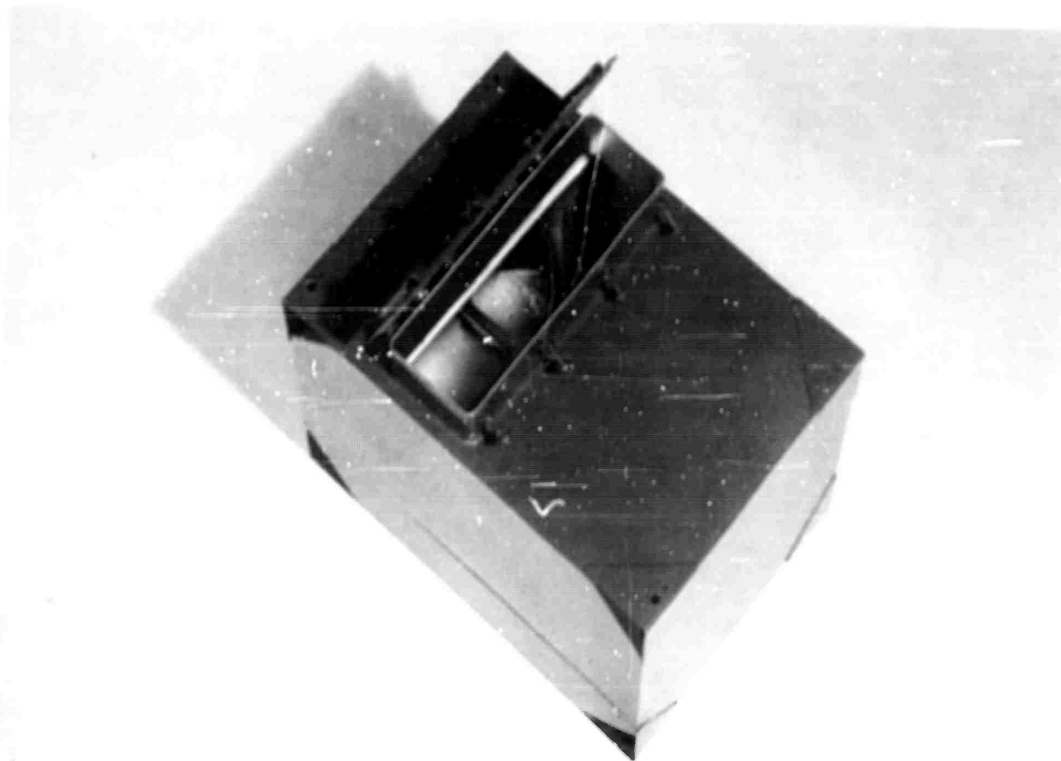


Figure C.2 Model of NEL instrument shelter.

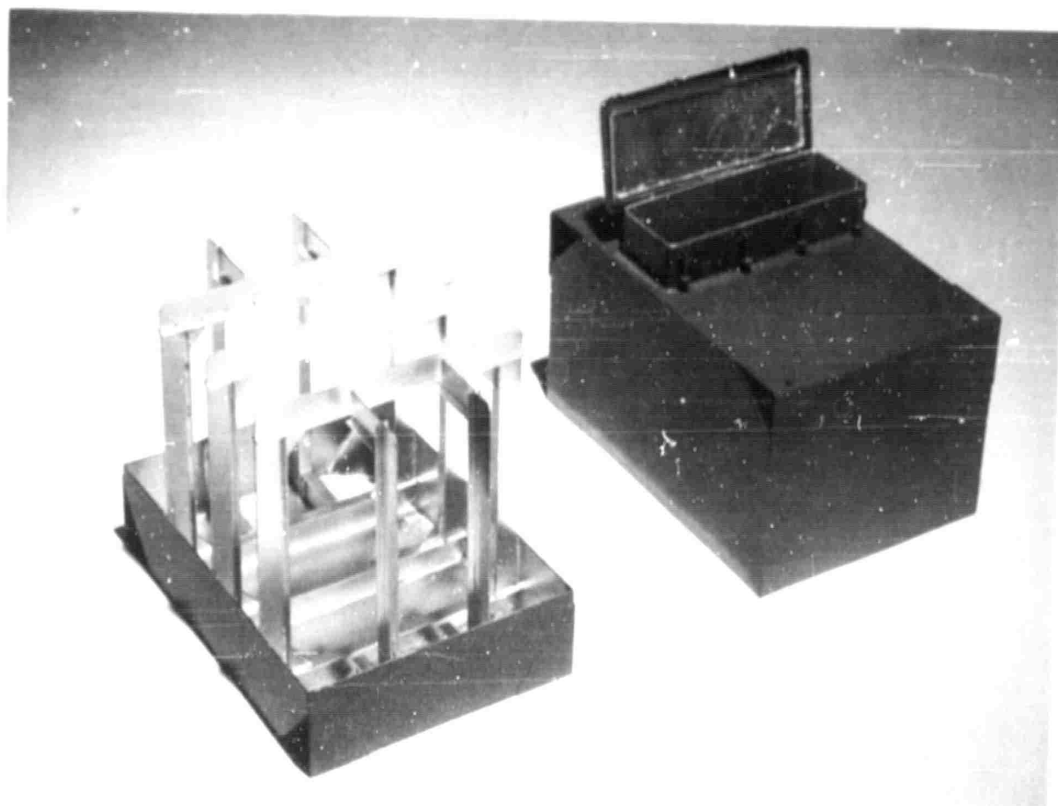


Figure C.3 Details of NEL instrument shelter model.

Appendix D

CALCULATIONS OF ATTENUATION OF SOUND IN AIR

There are two properties of the medium which cause attenuation of a sound wave in air. The first of these attenuations is caused by viscosity and heat conduction in the gas, the other is brought about by molecular absorption and dispersion in polyatomic gases involving an exchange in translational and vibrational energies between colliding molecules.

Sivian (Reference 9, Page 67) gives an expression for the decrement due to heat conduction and viscosity,

$$\delta_c = 0.143 \frac{A}{\lambda^2} \text{ db/ft} = 0.0165 \frac{A}{\lambda^2} \text{ nepers/ft}$$

Where: λ = wavelength in feet

A = (in centimeters) function of the temperature and is found from a graph (Reference 9, Page 66)

Consider two temperatures, 20°C and 70°C. At these temperatures

$$\lambda_{20} = \frac{c_{20}}{f} = \frac{1125 \text{ ft/sec}}{3200/\text{sec}} = 0.352 \text{ ft}$$

$$\lambda_{70} = \frac{c_{70}}{f} = \frac{1217 \text{ ft/sec}}{3200/\text{sec}} = 0.380 \text{ ft}$$

Where: c_{20} = velocity of sound in air at 20°C.

c_{70} = velocity of sound in air at 70°C.

f = frequency of the acoustic signal

Also, from Sivian:

$$A_{20} = 49 \times 10^{-5} \text{ cm}$$

$$A_{70} = 61.5 \times 10^{-5} \text{ cm}$$

Therefore:

$$\delta_{c_{20}} = \frac{0.0165 \times 49 \times 10^{-5}}{(0.352)^2} = 6.54 \times 10^{-5} \text{ nepers/ft}$$

$$\delta_{c_{70}} = \frac{0.0165 \times 61.5 \times 10^{-5}}{(0.380)^2} = 7.01 \times 10^{-5} \text{ nepers/ft}$$

To determine a value for the attenuation caused by absorption and dispersion due to molecular collision, one uses Kneser's nomogram (Reference 9, Page 65) which gives the decrement as a function of temperature, humidity, and frequency. Again taking the two temperatures, 20°C and 70°C, and a relative humidity of 30 percent at 20°C, the nomogram gives:

$$\delta_{m_{20}} = 0.911 \times 10^{-3} \text{ nepers/ft}$$

$$\delta_{m_{70}} = 1.973 \times 10^{-3} \text{ nepers/ft}$$

The total decrement δ then is:

$$\delta = \delta_c + \delta_m$$

And:

$$\begin{aligned}\delta_m &= (0.065 \cdot 10^{-3} + 0.911 \cdot 10^{-3}) \text{ nepers/ft} \\ &= 0.976 \cdot 10^{-3} \text{ nepers/ft}\end{aligned}$$

$$\begin{aligned}\delta_{10} &= (0.070 \cdot 10^{-3} + 1.973 \cdot 10^{-3}) \text{ nepers/ft} \\ &= 2.043 \cdot 10^{-3} \text{ nepers/ft}\end{aligned}$$

For the 4.6-foot gap between horns the attenuation would be:

$$\begin{aligned}\Delta_m &= 4.6 \delta_m = 4.6 \cdot 0.976 \cdot 10^{-3} \text{ nepers} \\ &= 4.50 \cdot 10^{-3} \text{ nepers}\end{aligned}$$

$$\begin{aligned}\Delta_{10} &= 4.6 \delta_{10} = 4.6 \cdot 2.043 \cdot 10^{-3} \text{ nepers} \\ &= 9.40 \cdot 10^{-3} \text{ nepers}\end{aligned}$$

Therefore, the attenuation caused by absorption and dispersion due to molecular collisions and by heat conduction and viscosity increases by $4.90 \cdot 10^{-3}$ nepers when the temperature of the medium increases from 20°C to 70°C.

The increase in attenuation is 0.5 percent, since:

$$\begin{aligned}\frac{P_{10}}{P_m} &= e^{-(\Delta_{10} - \Delta_m)} = e^{-(9.40 \cdot 10^{-3} - 4.50 \cdot 10^{-3})} \\ &= e^{-4.90 \cdot 10^{-3}} \\ &= 0.995\end{aligned}$$

Appendix E
ATTENUATION OF ACOUSTIC SIGNALS
MEASURED IN SHOT 12

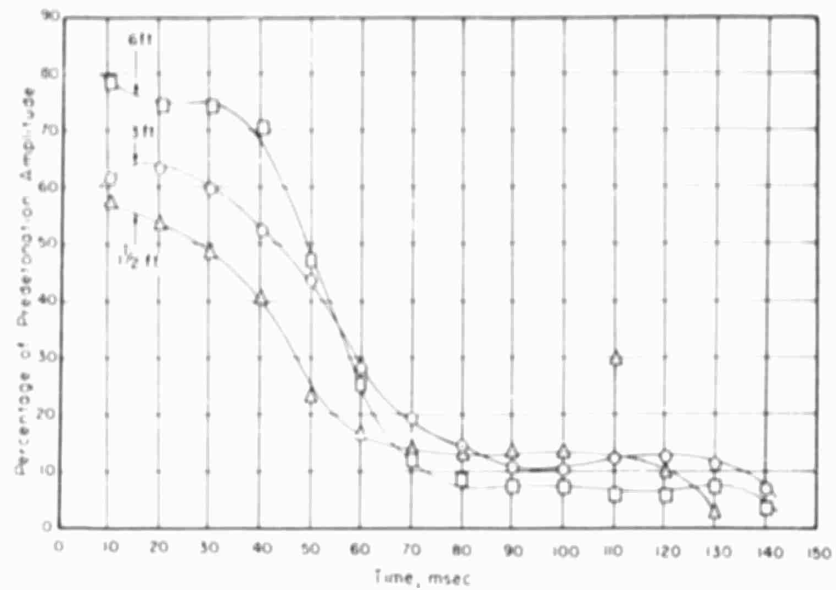


Figure E.1 Relative sound pressure amplitude versus time, 1000-foot desert.

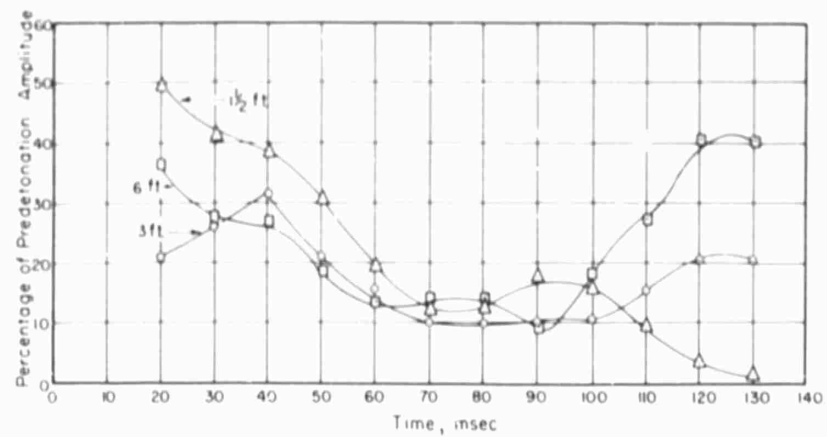


Figure E.2 Relative sound pressure amplitude versus time, 1000-foot asphalt.

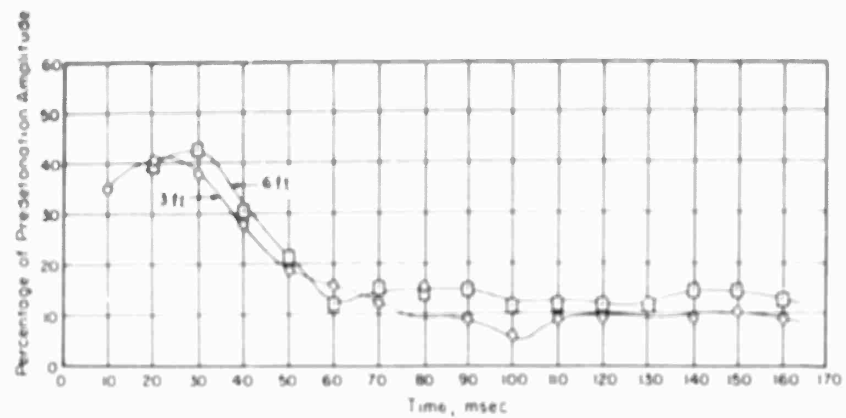


Figure E.3 Relative sound pressure amplitude versus time, 1000-foot water.

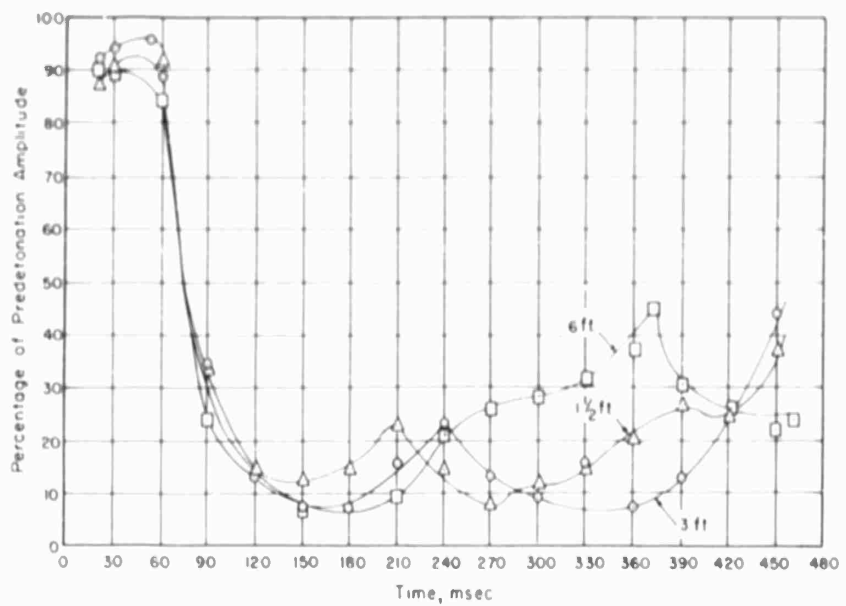


Figure E.4 Relative sound pressure amplitude versus time, 2000-foot desert.

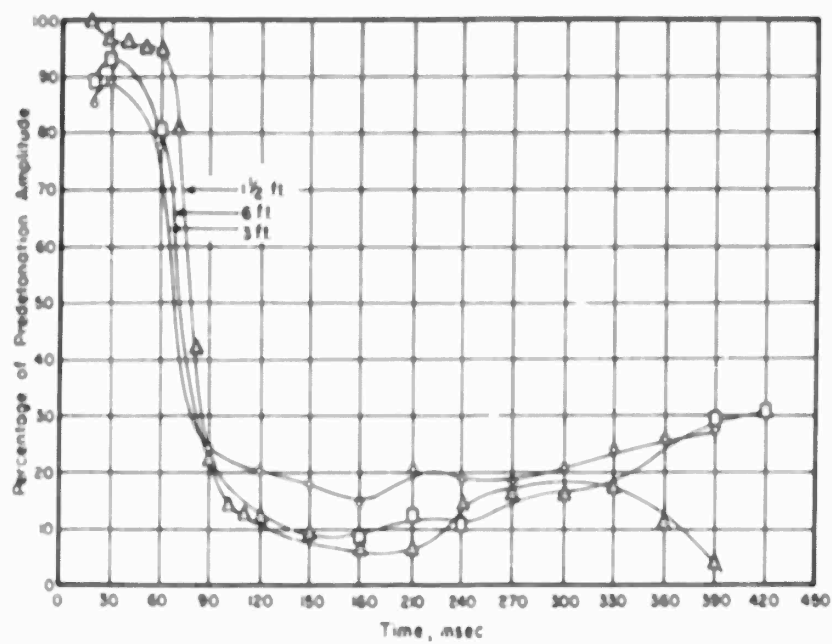


Figure E.5 Relative sound pressure amplitude versus time, 2000-foot asphalt.

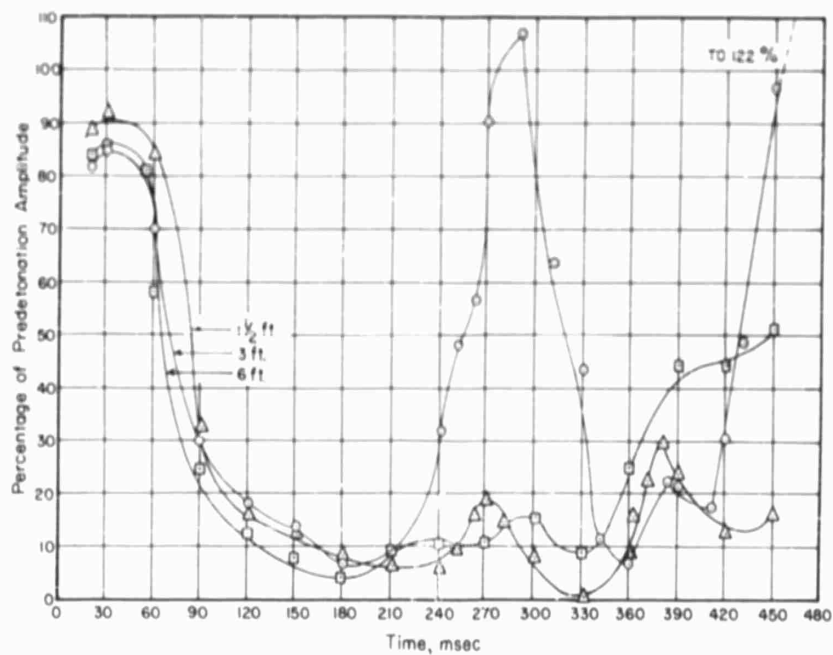


Figure E.6 Relative sound pressure amplitude versus time, 2000-foot concrete.

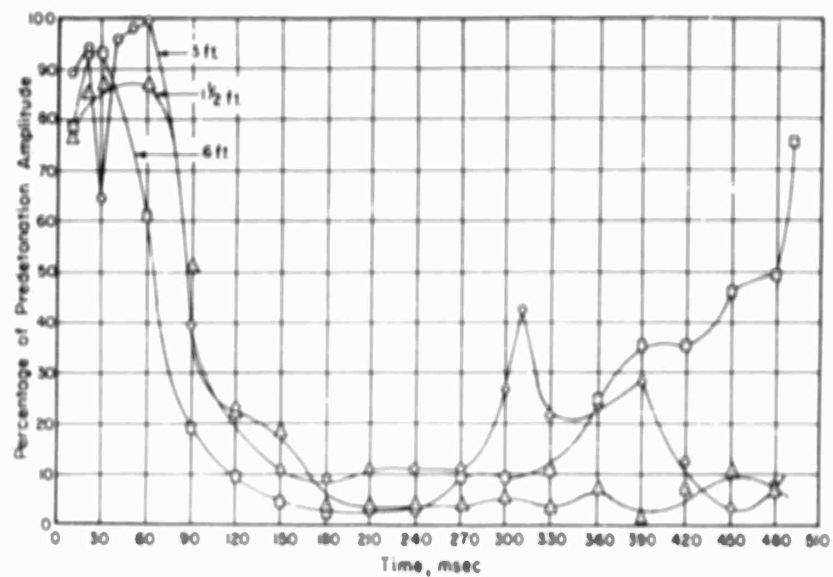


Figure E.7 Relative sound pressure amplitude versus time, 2000-foot fir bough.

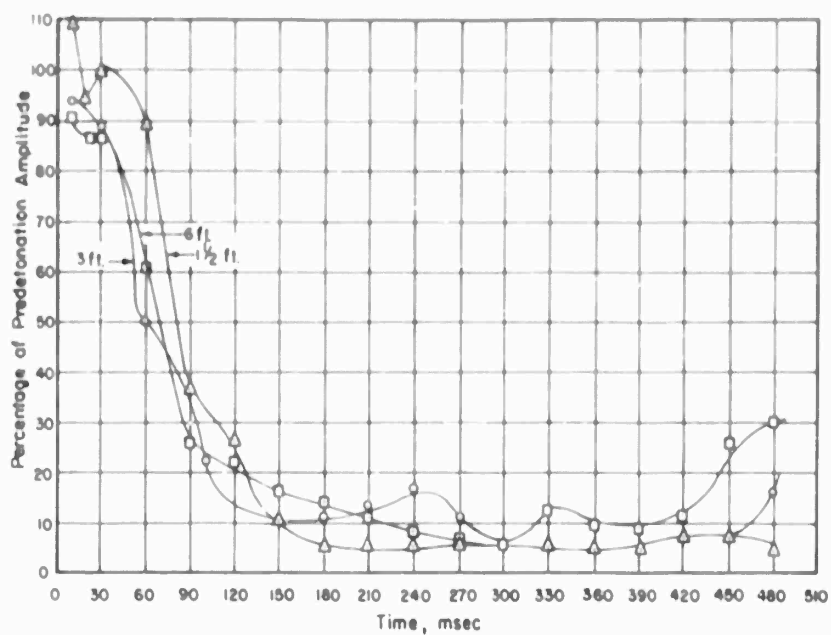


Figure E.8 Relative sound pressure amplitude versus time, 2000-foot ivy.

Appendix F RECORDINGS OF RAW DATA MADE BY PROJECT I.5 SOUND VELOCITY METERS

Time numbers appear on these data curves. To determine time after detonation, multiply number appearing at instant of interest by 10 msec. For greater accuracy use relation that distance between spikes represents 10 msec. Timing spikes are regrettably quite faint in many cases because of rapid beam sweep on cathode ray tube at these times. However, they never appear far from the envelope minima and can generally be seen if one looks carefully for them.

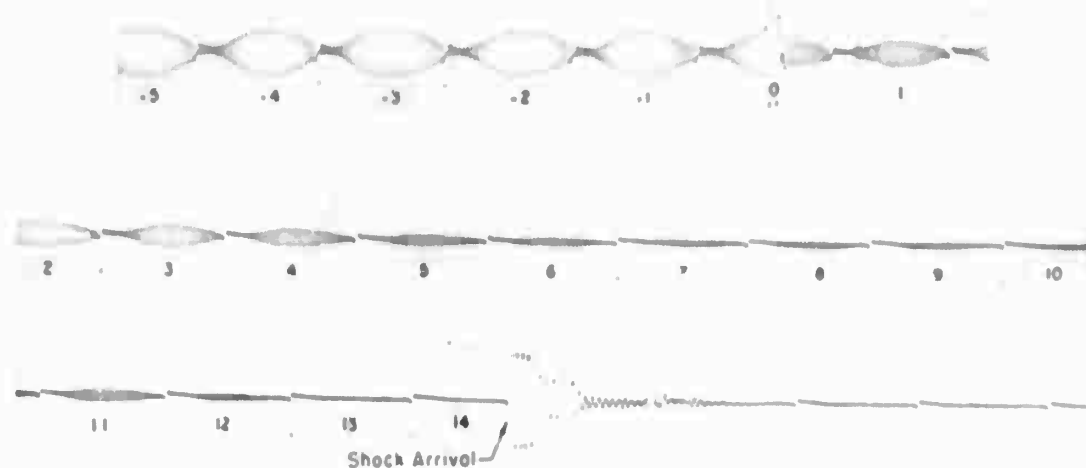


Figure F.1 Channel 10, desert, 1000-foot ground range, 1 1/2-foot elevation.

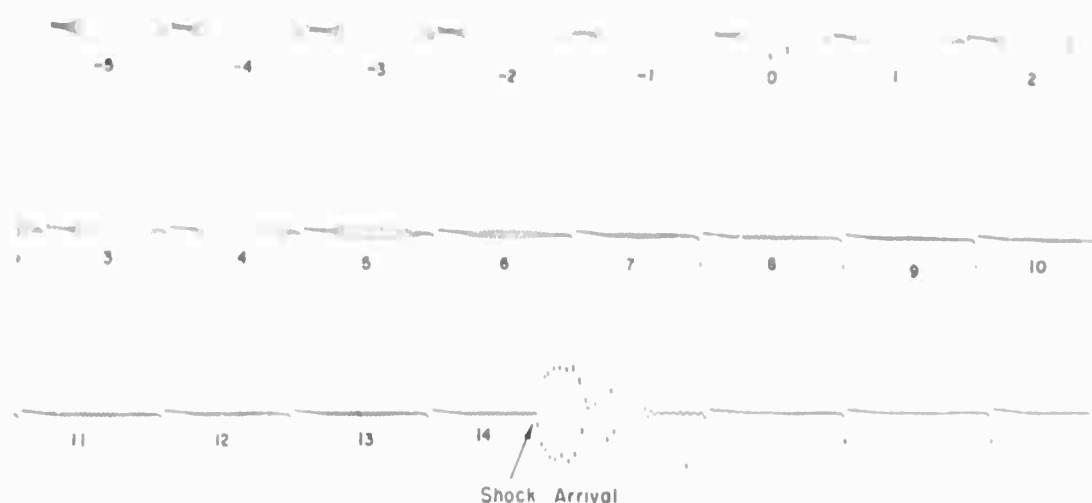


Figure F.2 Channel 11, desert, 1000-foot ground range, 3-foot elevation.

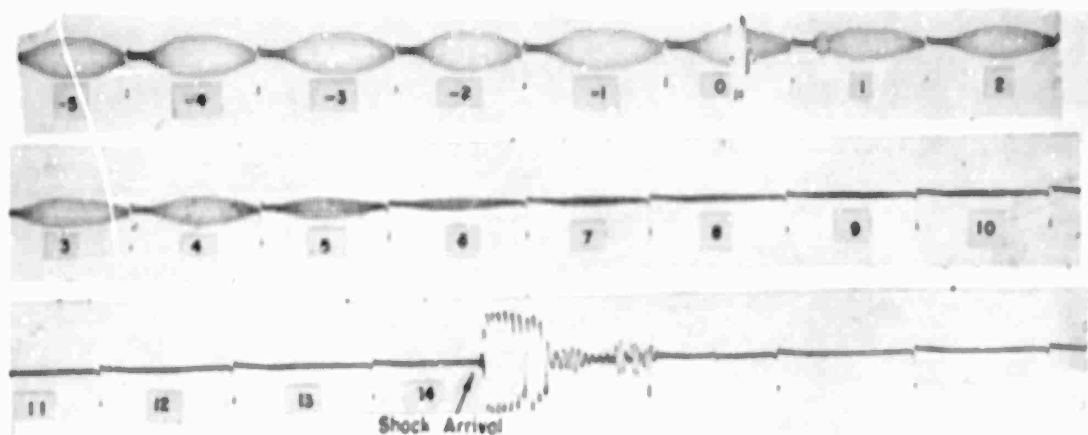


Figure F.3 Channel 12, desert, 1000-foot ground range, 6-foot elevation.

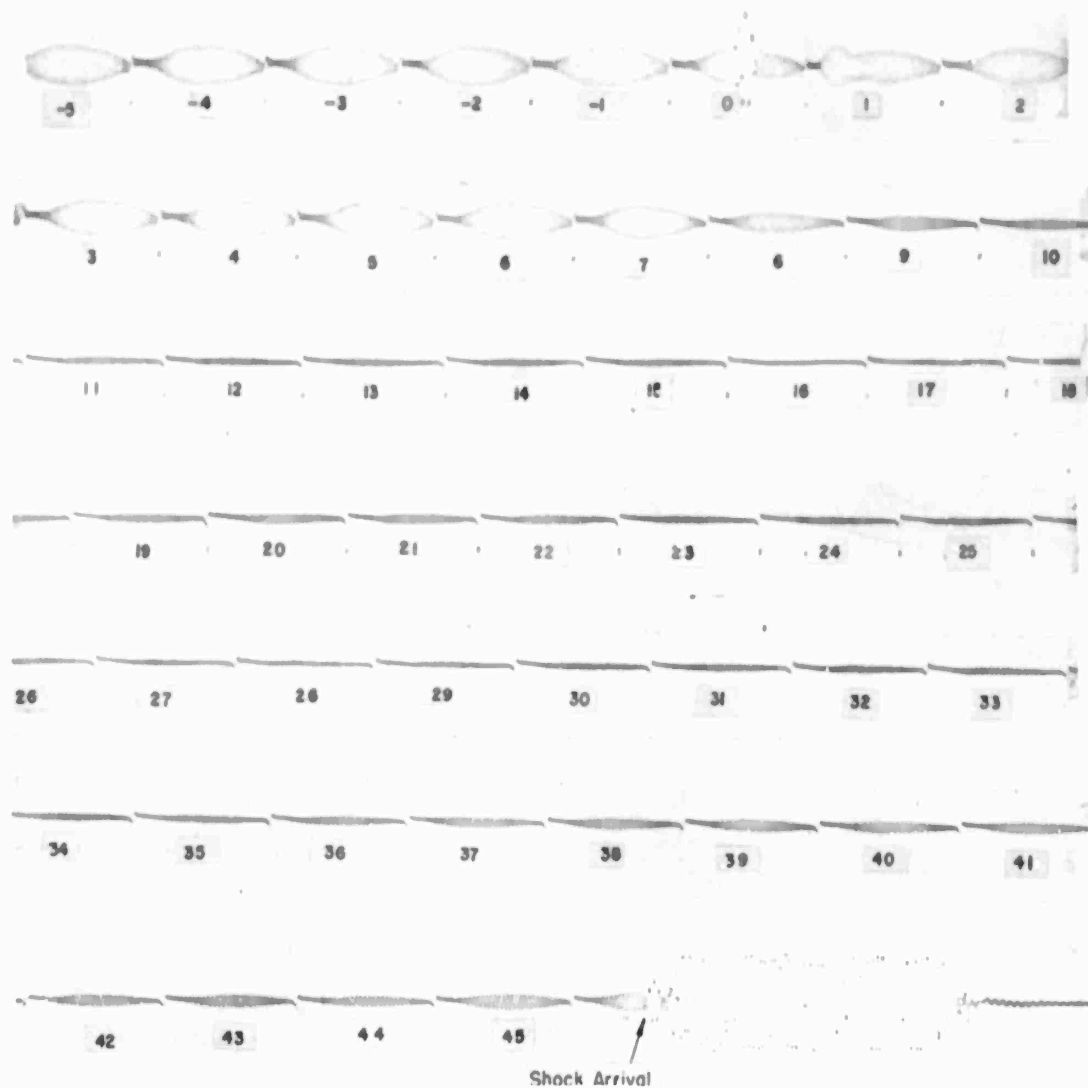


Figure F.4 Channel 19; desert, 2000-foot ground range, 1 1/2-foot elevation.

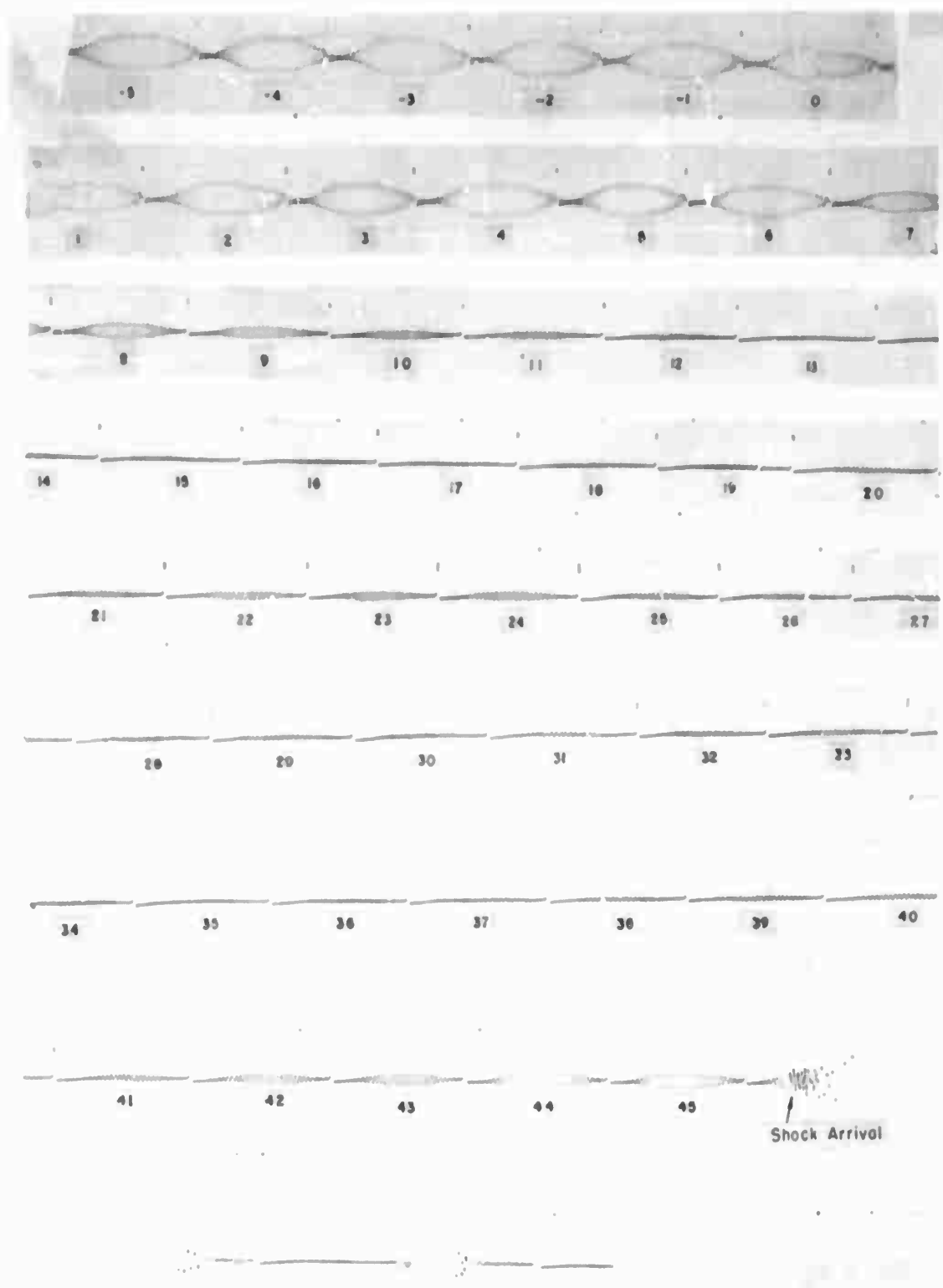


Figure F.5 Channel 20; desert, 2000-foot ground range, 3-foot elevation.

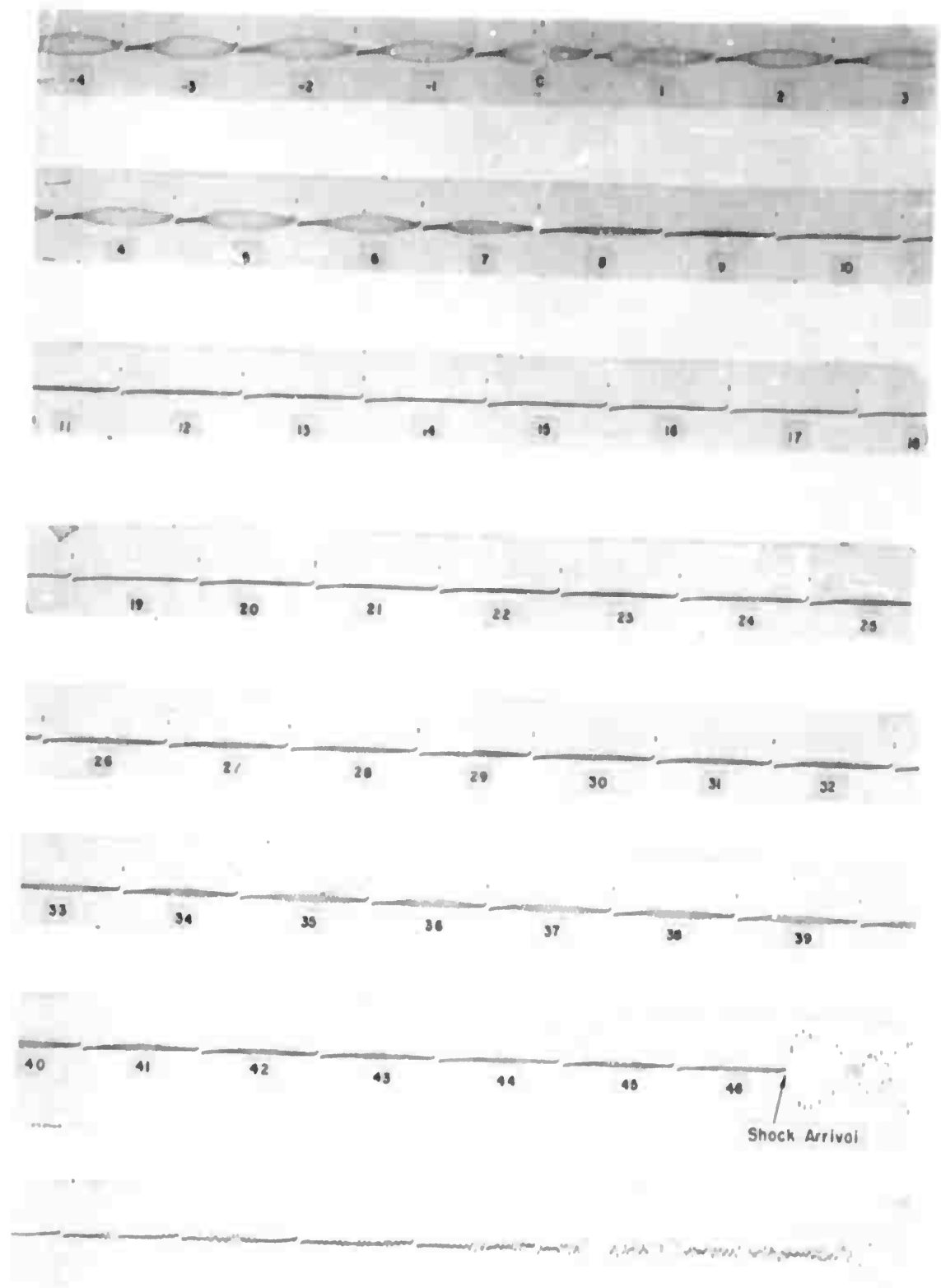


Figure F.6 Channel 21; desert, 2000-foot ground range, 6-foot elevation.

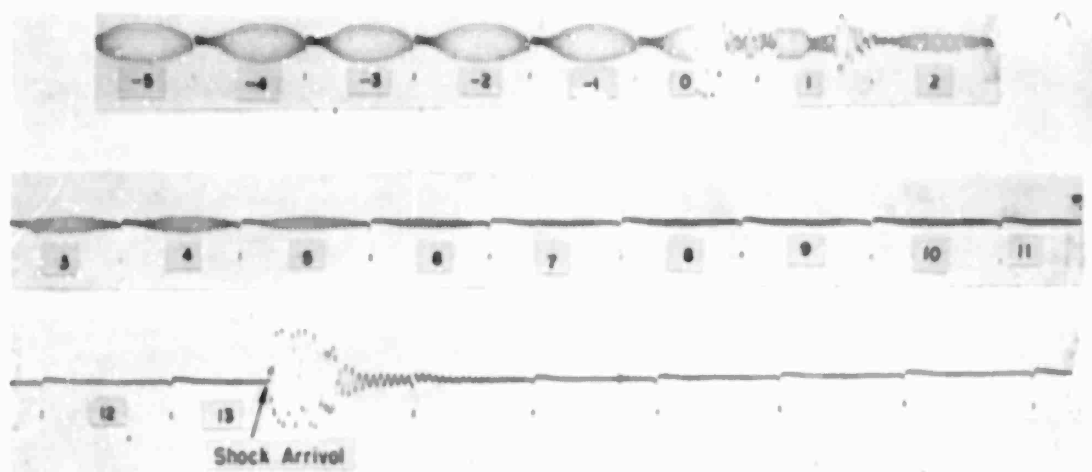


Figure F.7 Channel 4, asphalt, 1000-foot ground range, 1 1/2-foot elevation.

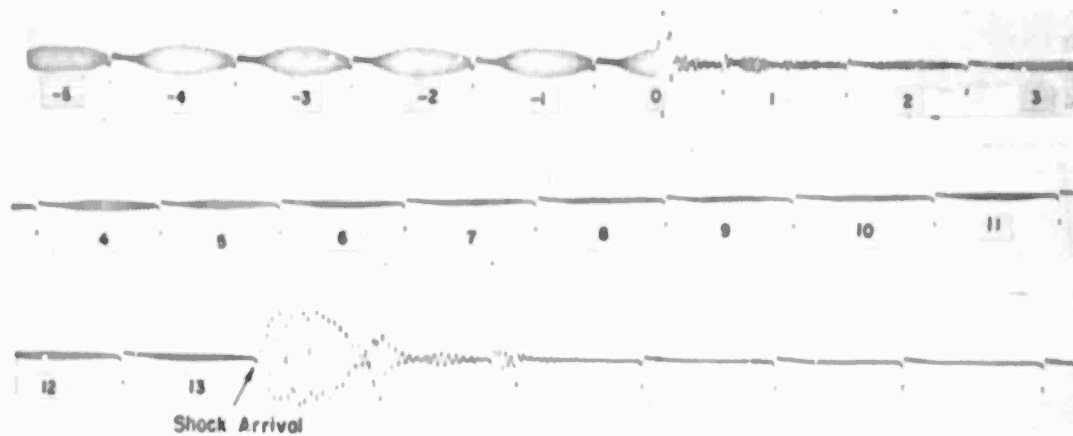


Figure F.8 Channel 5, asphalt, 1000-foot ground range, 3-foot elevation.

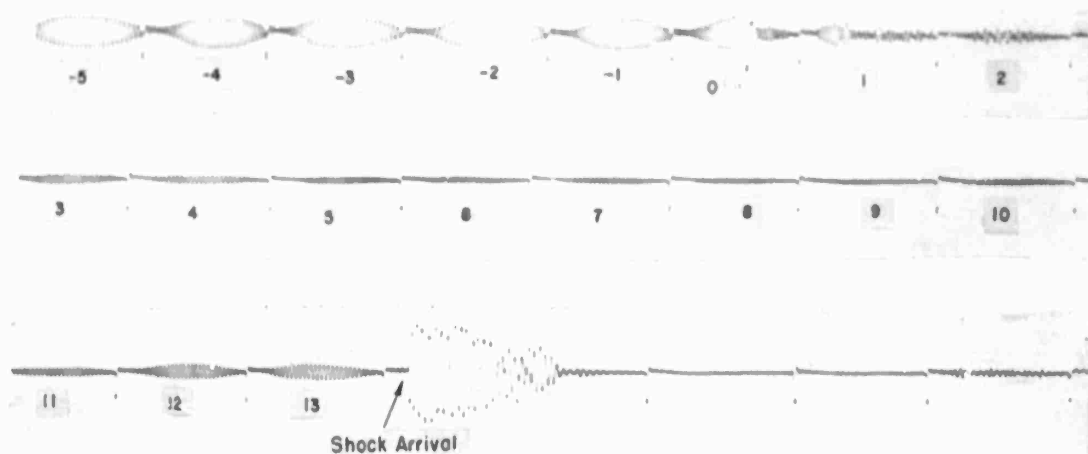


Figure F.9 Channel 6, asphalt, 1000-foot ground range, 6-foot elevation.

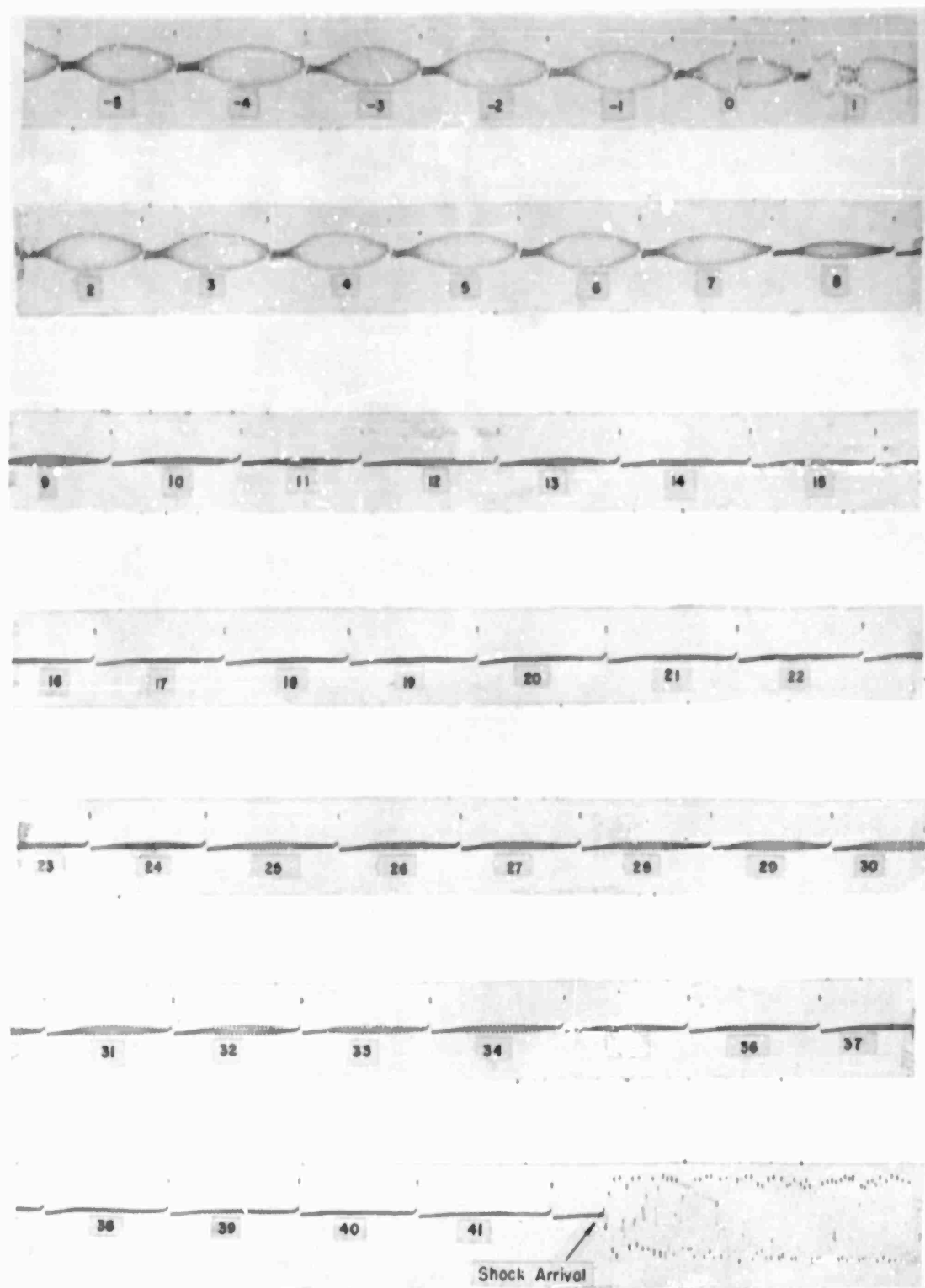


Figure F.10 Channel 7; asphalt, 2000-foot ground range, 1½-foot elevation.

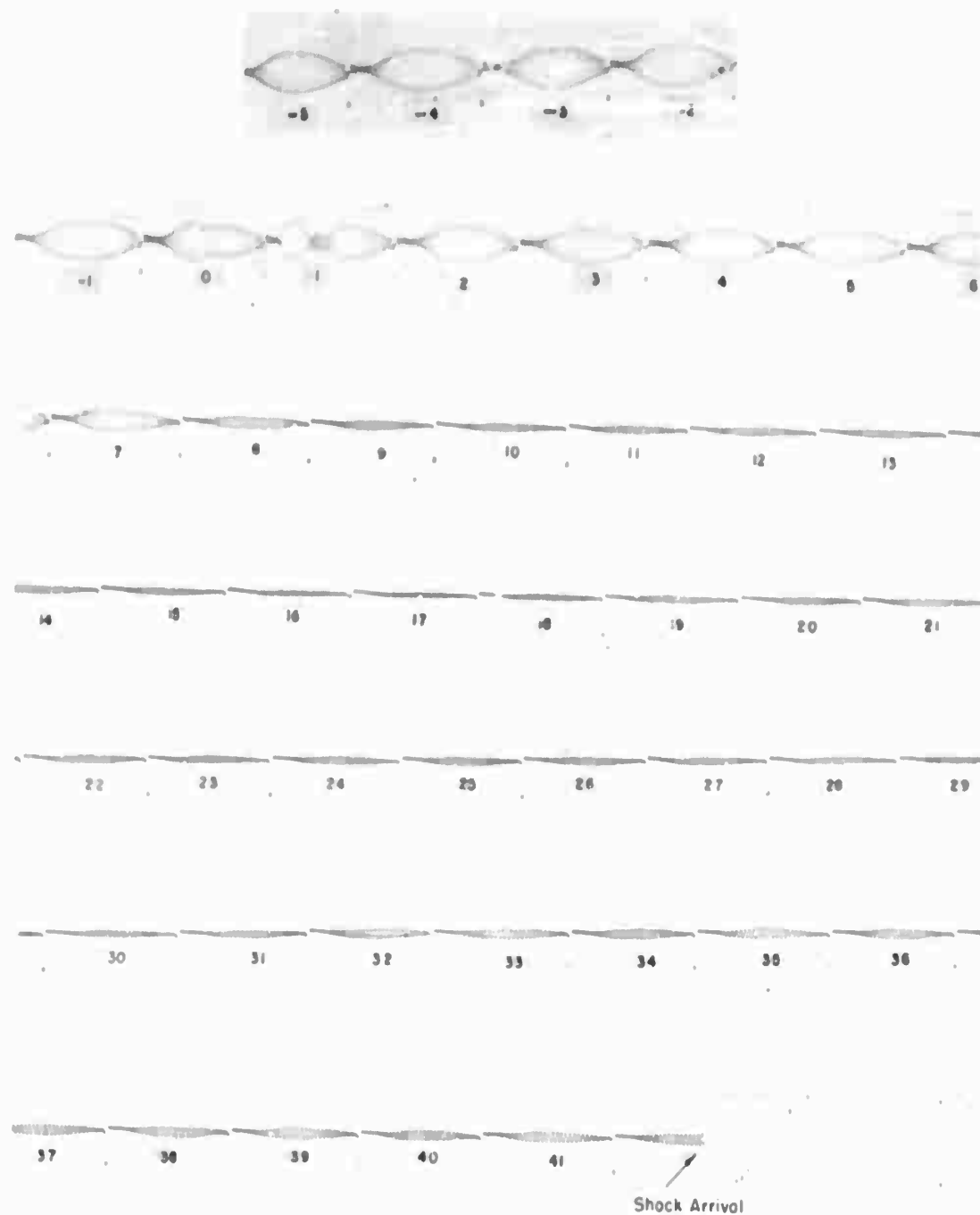


Figure F.11 Channel 8; asphalt, 2000-foot ground range, 3-foot elevation.

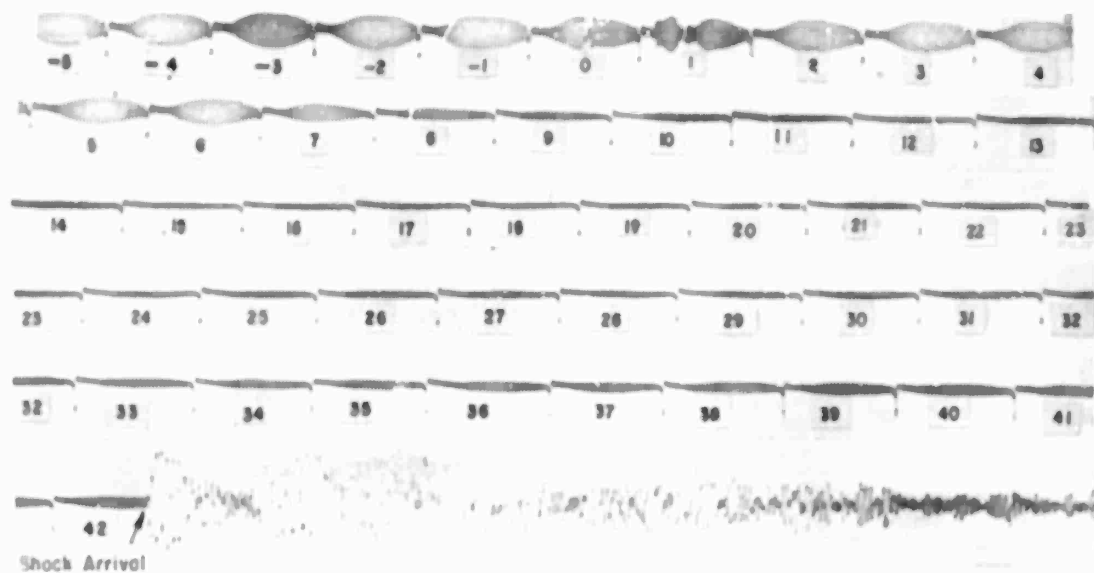


Figure F.12 Channel 9, asphalt, 2000-foot ground range, 6-foot elevation.

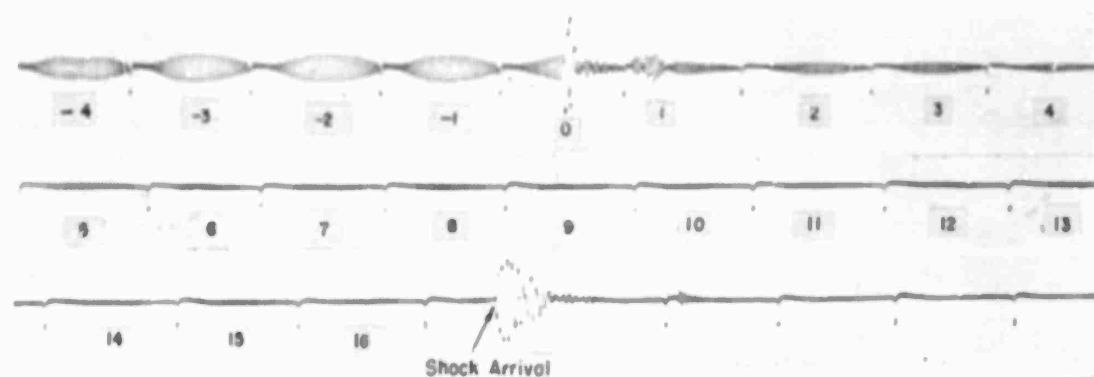


Figure F.13 Channel 2, water, 1000-foot ground range, 3-foot elevation.

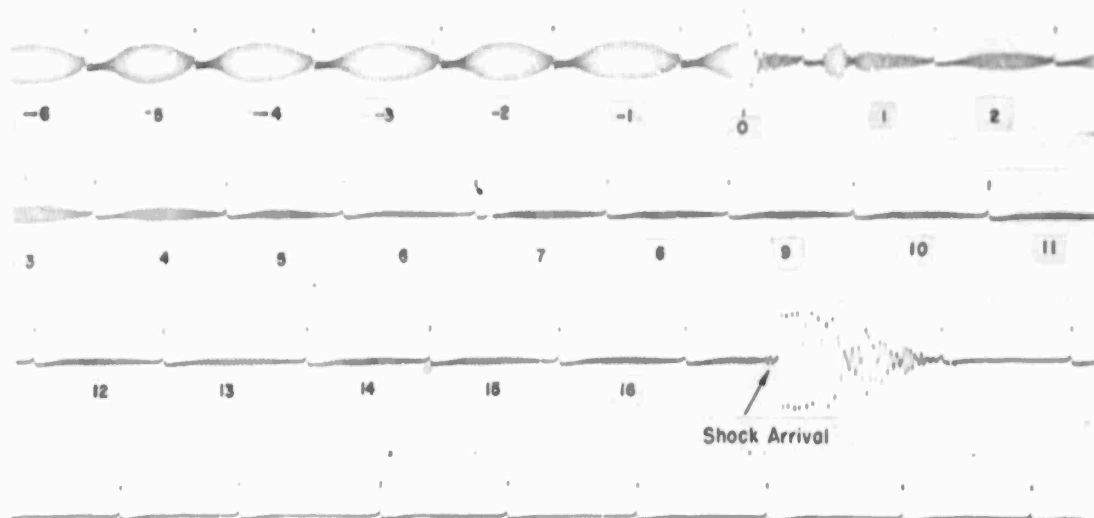


Figure F.14 Channel 3, water, 1000-foot ground range, 6-foot elevation

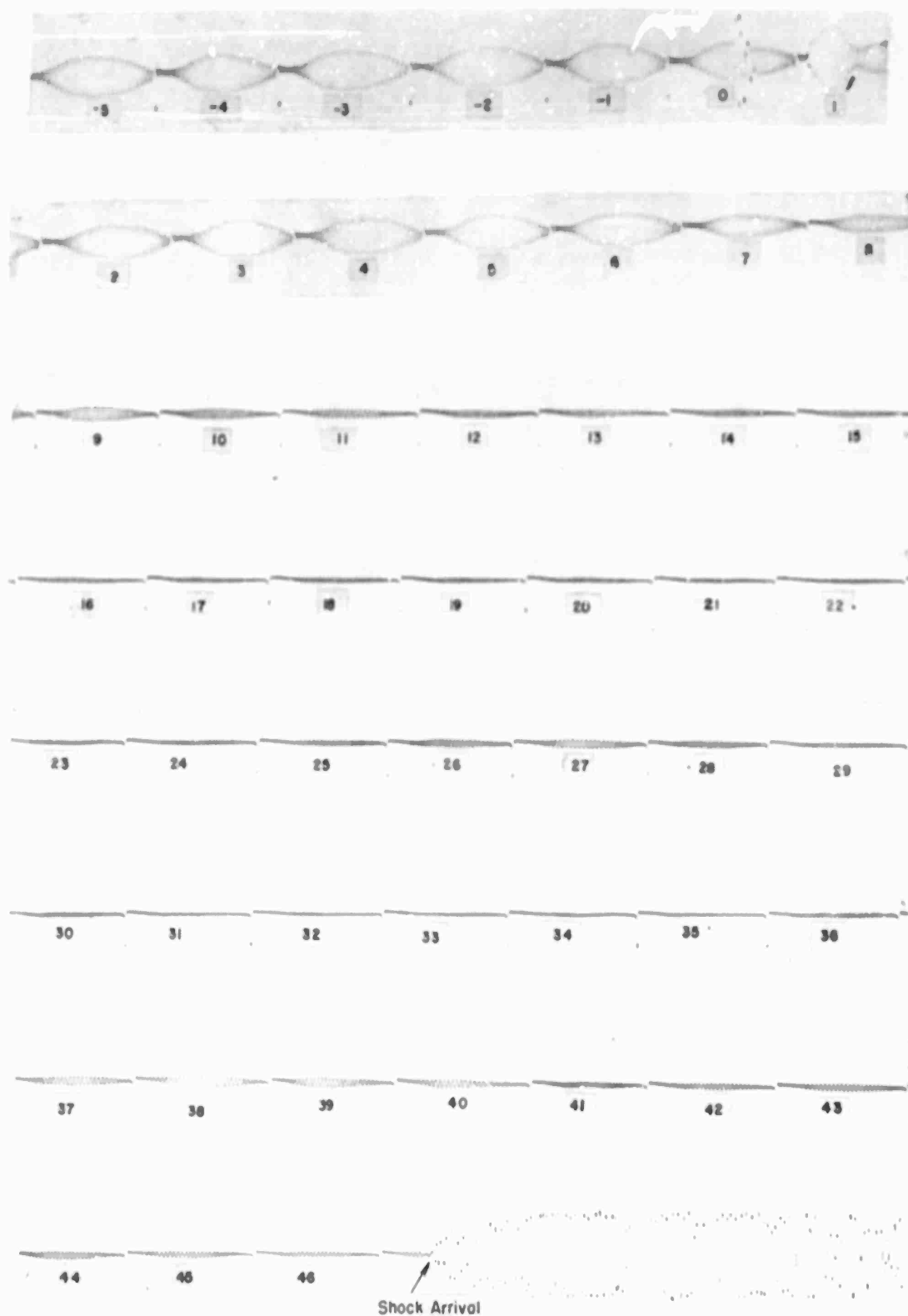
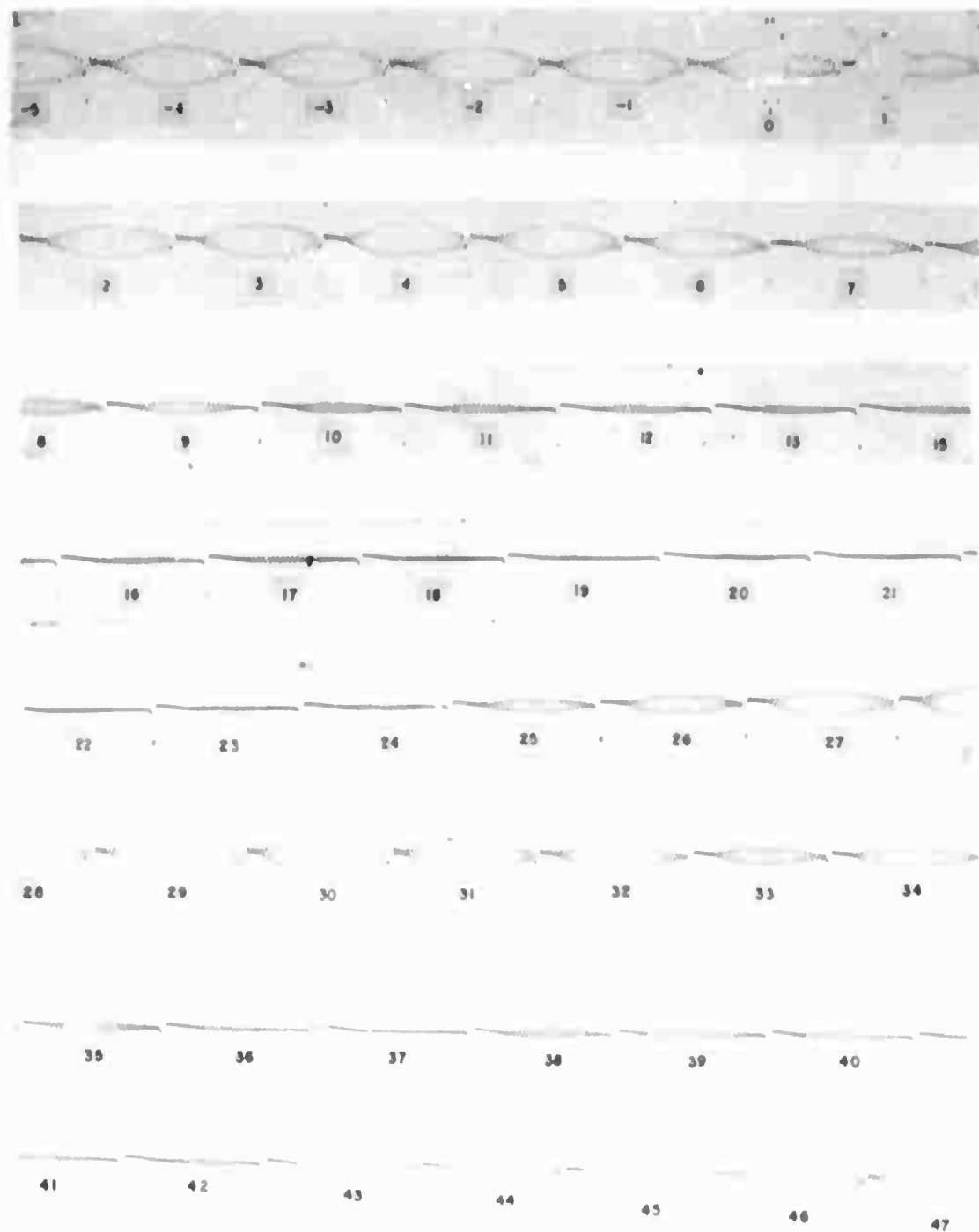


Figure F.15 Channel 22; concrete, 2000-foot ground range, 1½-foot elevation.



Shock Arrival

Figure F.16 Channel 23; concrete, 2000-foot ground range, 3-foot elevation.

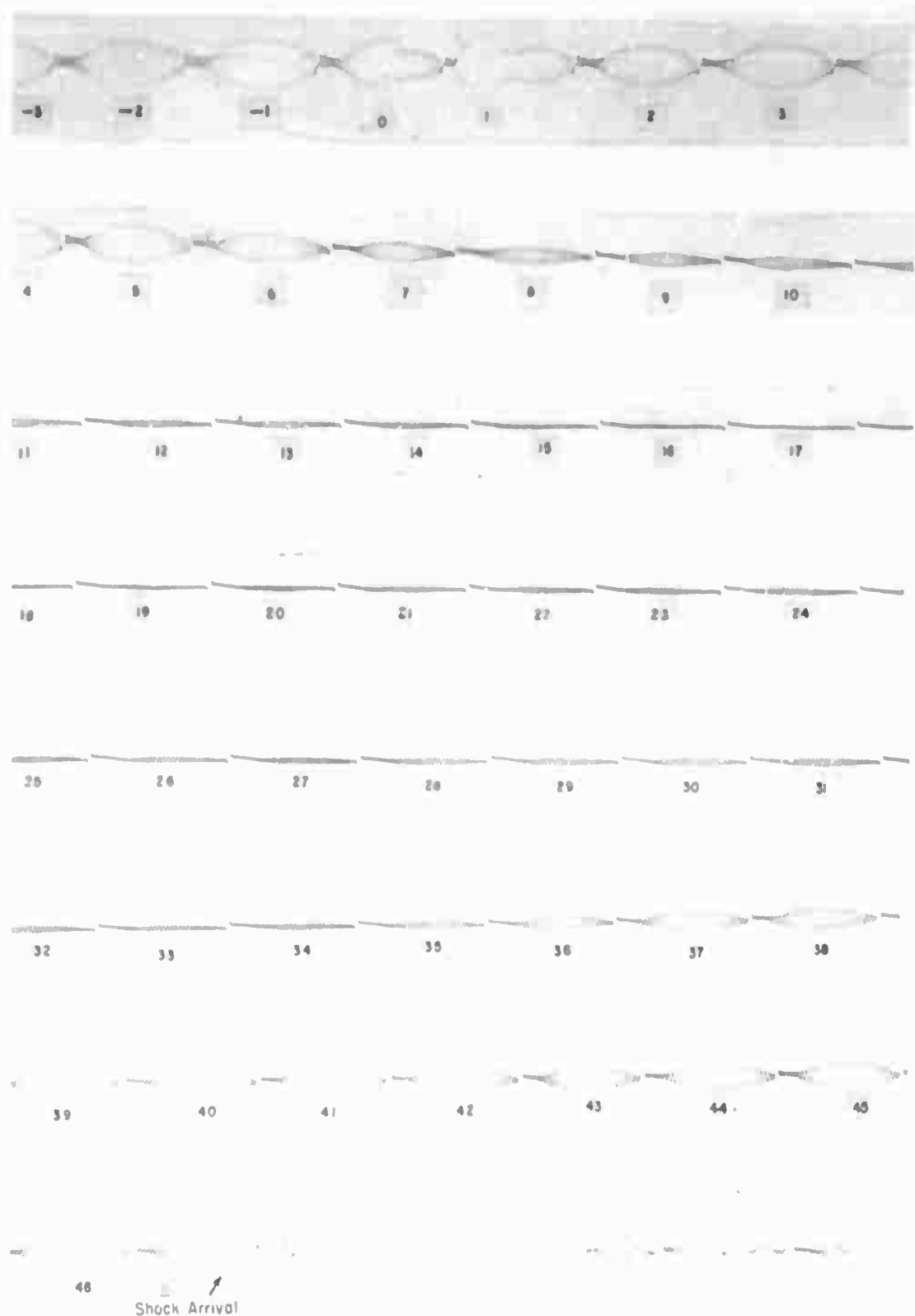


Figure F.17 Channel 24; concrete, 2000-foot ground range, 6-foot elevation.

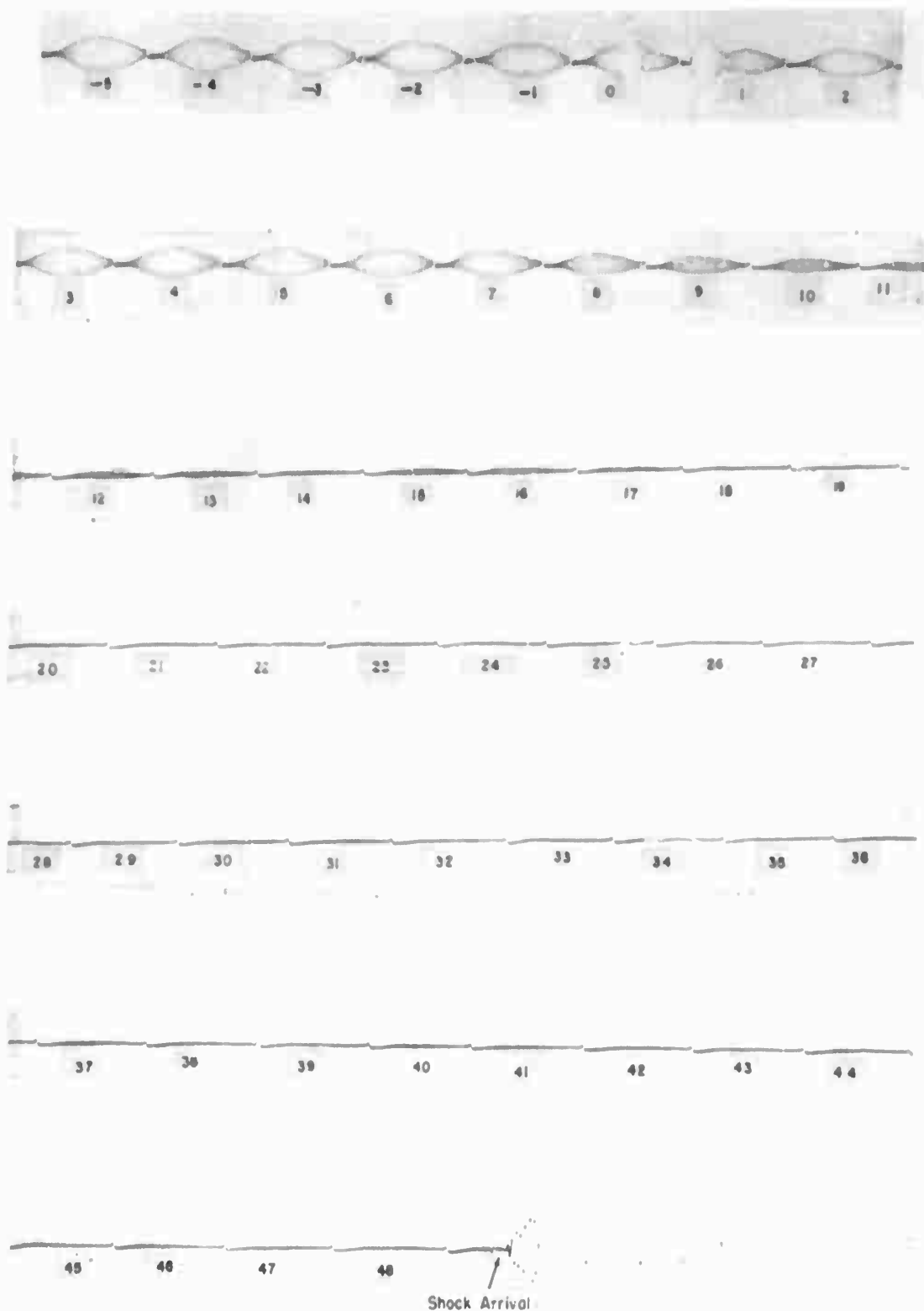


Figure F.18 Channel 16; white fir boughs, 2000-foot ground range, $1\frac{1}{2}$ -foot elevation.

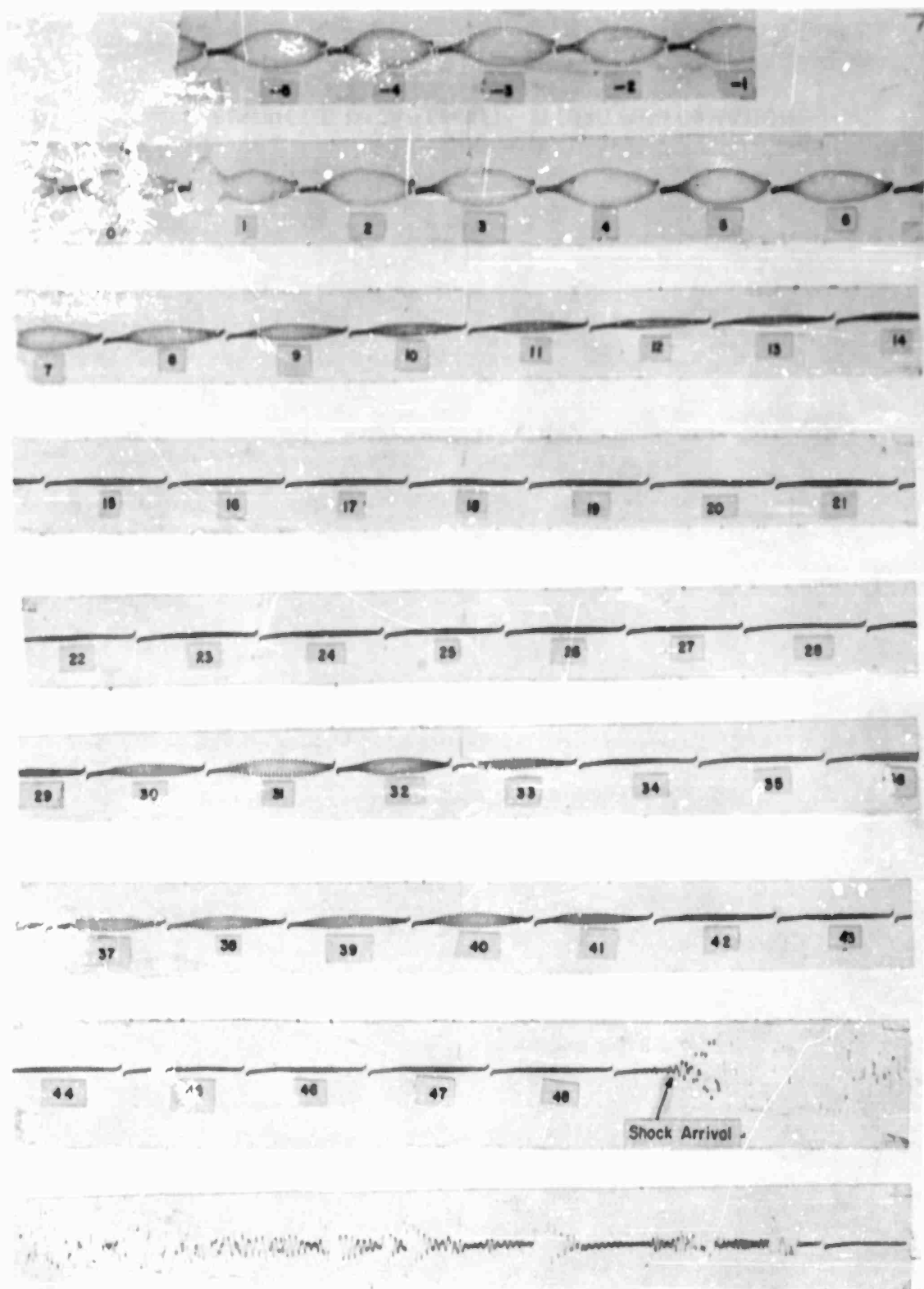


Figure F.19 Channel 17; white fir boughs, 2000-foot ground range, 3-foot elevation.

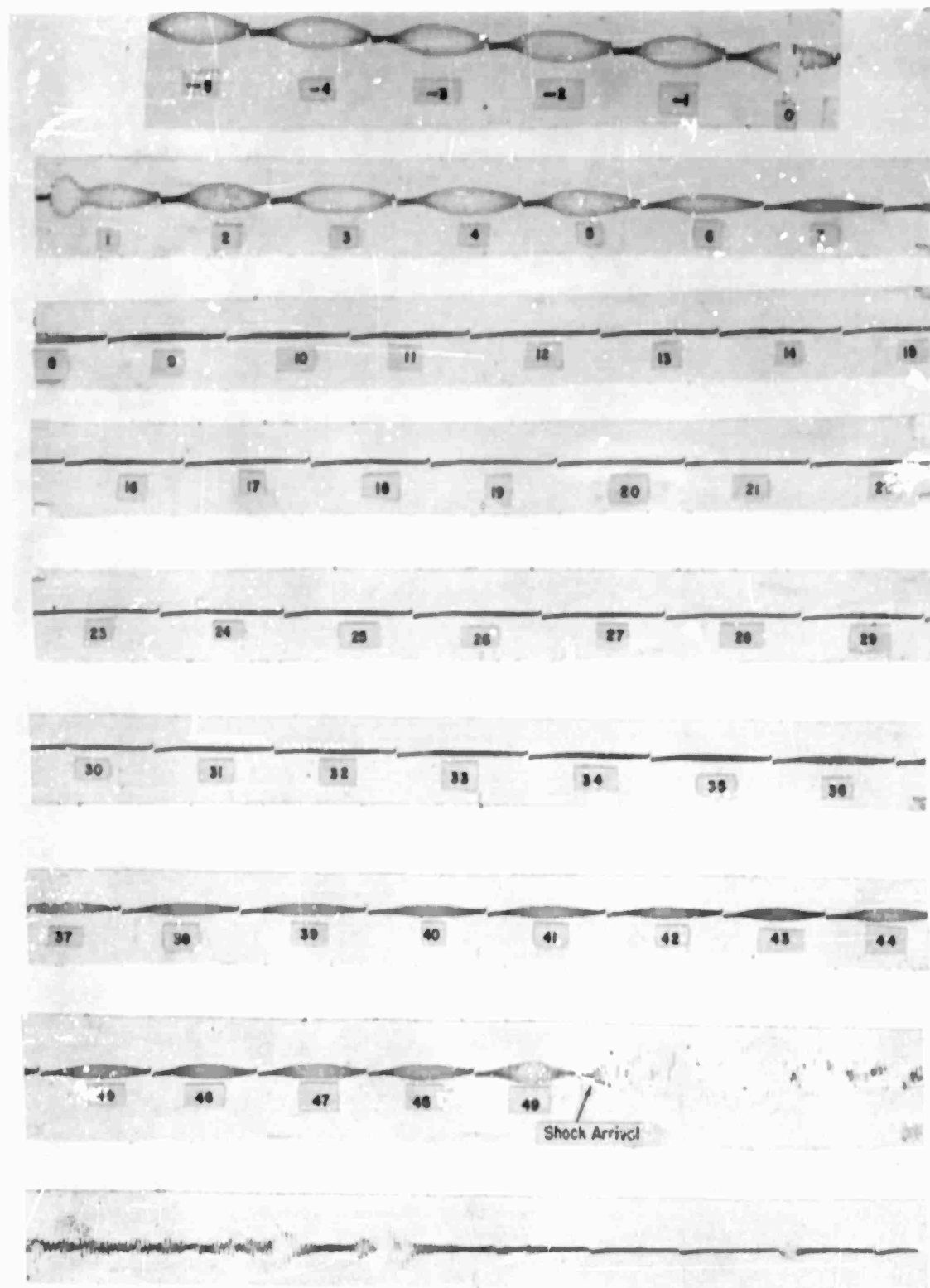


Figure F.20 Channel 18; white fir boughs, 2000-foot ground range, 6-foot elevation.

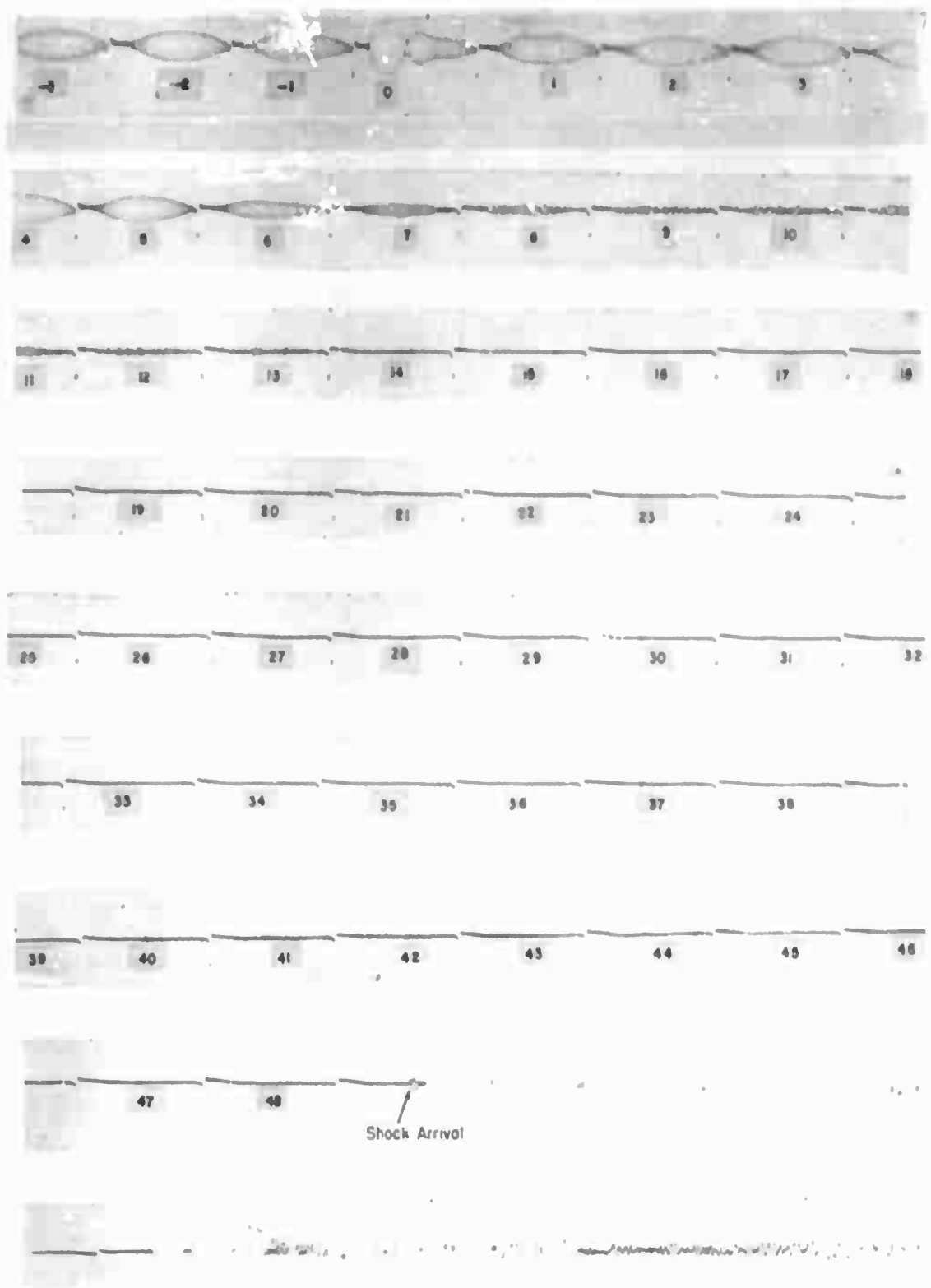


Figure F.21 Channel 13; broad leaf cover (Ivy), 2000-foot ground range, 1½-foot elevation.

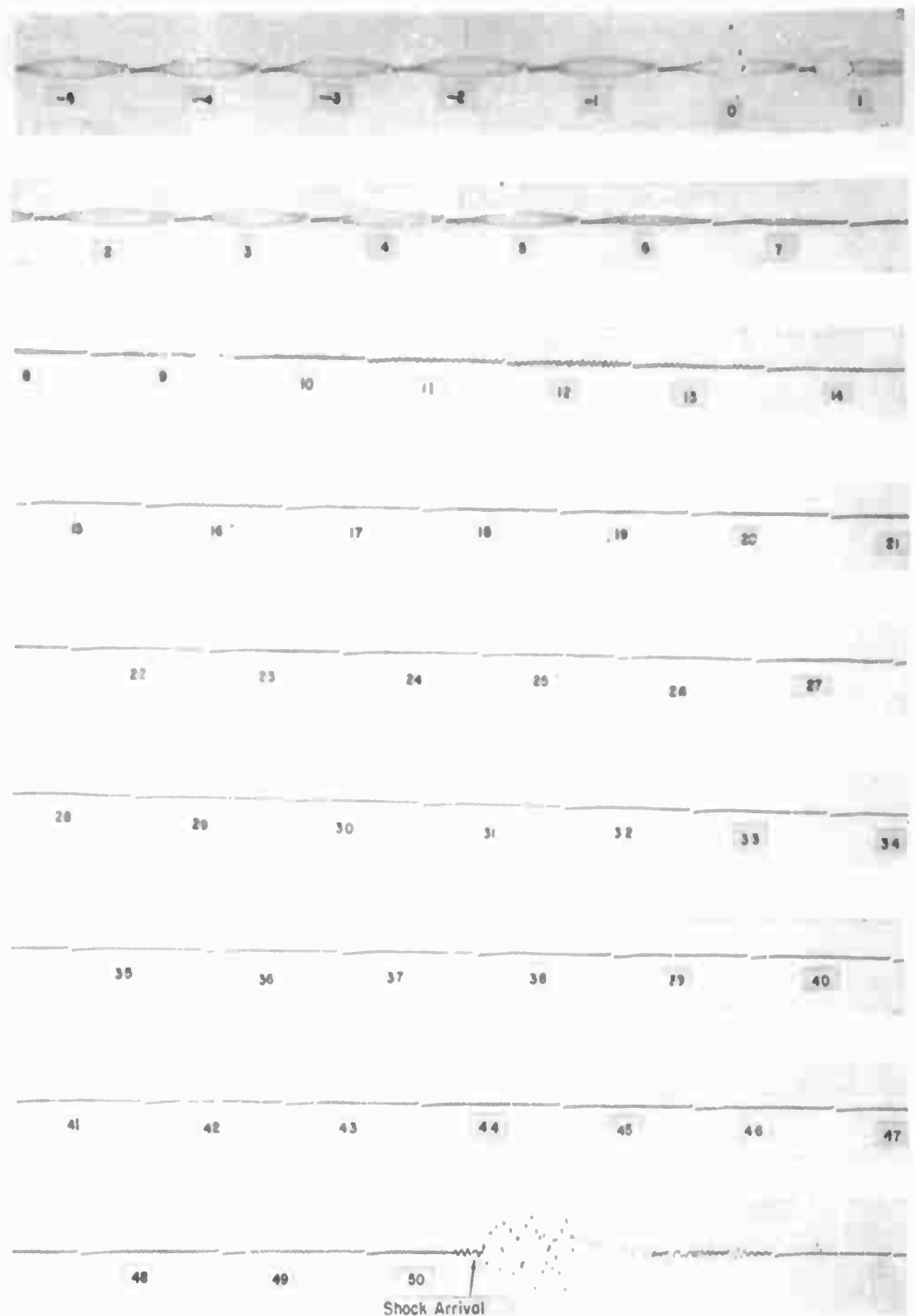


Figure F.22 Channel 14; broad leaf cover (ivy), 2000-foot ground range, 3-foot elevation.

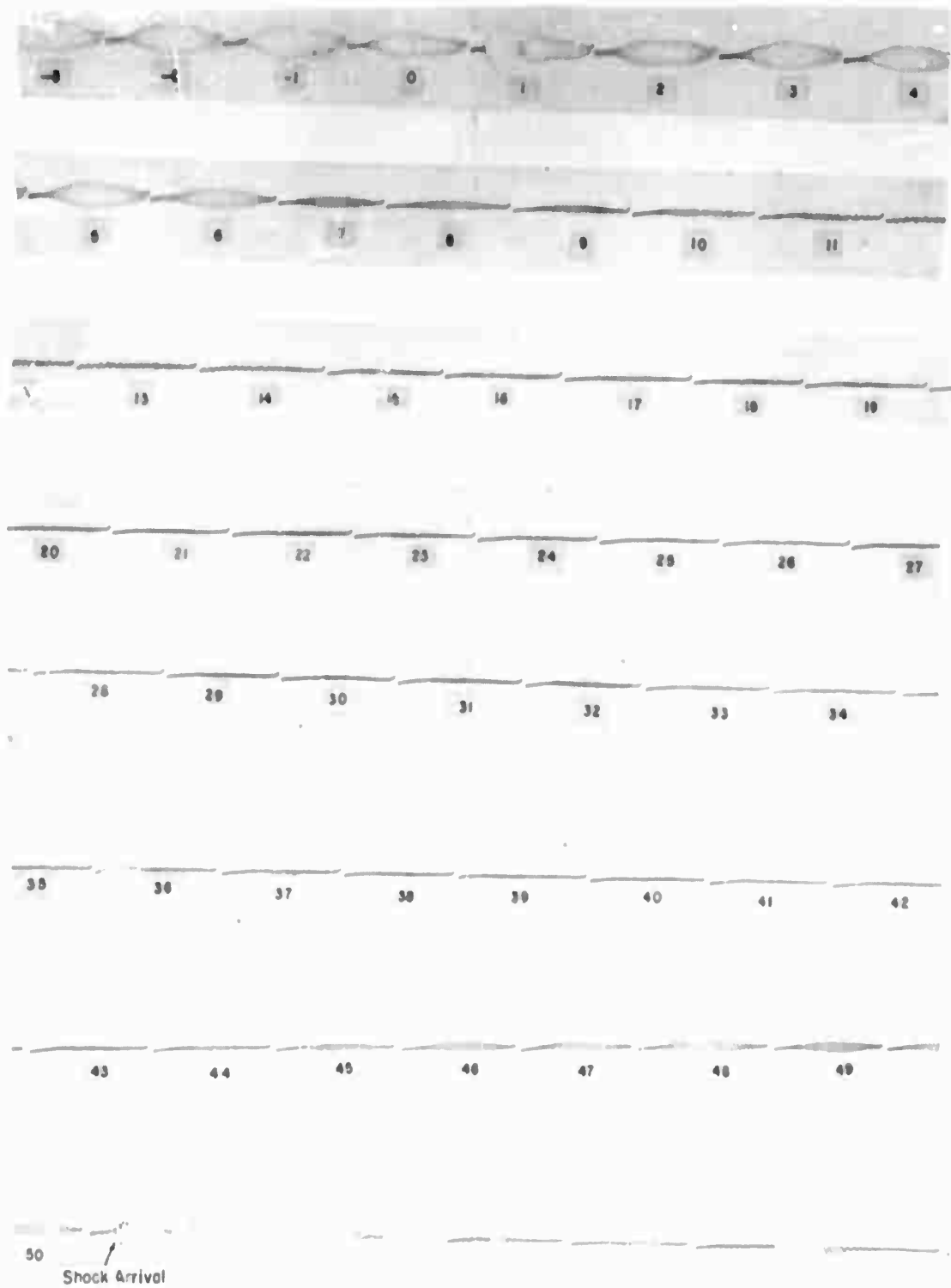


Figure F.23 Channel 15; broad leaf cover (ivy). 2000-foot ground range, 6-foot elevation.

REFERENCES

1. McLoughlin, R. C.; "Sound Velocity Changes near the Ground in the Vicinity of an Atomic Explosion"; Armed Forces Special Weapons Project, Operation Tumbler, Project 8.8, WT-546; Secret Restricted Data.
2. McLoughlin, R. C., and Foustee, F. C.; "Sound Velocities near the Ground in the Vicinity of an Atomic Explosion"; Armed Forces Special Weapons Project, Operation Upshot-Knothole, Project 8.12a, WT-776; Confidential Restricted Data.
3. Broido, T. R., Broido, A., and Willoughby, A. B.; "Air Temperatures in the Vicinity of a Nuclear Detonation"; Armed Forces Special Weapons Project, Operation Tumbler, Project 8.2, WT-842; Secret Restricted Data.
4. Scoville, H. Jr., and others; "Final Summary Report"; Armed Forces Special Weapons Project, Operation Tumbler, WT-514; Secret Restricted Data.
5. Bryant, E. J., Ethridge, N. H., and Keefer, J. H.; "Basic Blast Measurements for Projects 1.14a, 3.1 and 3.10"; Armed Forces Special Weapons Project, Operation Teapot, ITR-1155; Secret Restricted Data.
6. Swift, L. M., and Sachs, D. C.; "Air-Blast Overpressure and Dynamic Pressure over Various Surfaces"; Armed Forces Special Weapons Project, Operation Teapot, Project 1.10, ITR-1109; Secret Restricted Data.
7. Morris, W. E., and others; "Air-Blast Measurements"; Armed Forces Special Weapons Project, Operation Upshot-Knothole, Projects 1.1s and 1.2, WT-710; Secret Restricted Data.
8. Moulton, J. F. Jr., and Walthall, R. E.; "Shock Wave Photography"; Armed Forces Special Weapons Project, Operation Teapot, Project 1.2, WT-1102; Secret Restricted Data.
9. Beranek, L. L.; "Acoustic Measurements"; John Wiley and Sons.
10. Salmon, V.; "Air Pressure Versus Time"; Armed Forces Special Weapons Project, Operation Tumbler, WT-512; Secret Restricted Data.
11. "Summary Report of the Technical Director"; Programs 1-9, Operation Teapot, ITR-1153; Secret Restricted Data.
12. Inn, E. C. Y.; "Air-Temperature Measurements over Several Surfaces"; Armed Forces Special Weapons Project, ITR-1149; Confidential Restricted Data.

Military Distribution Category 5-2.

- 67-12-1. Chief, Staff Officer, Transportation & Station, Ft. Lee, Va.
- 67-12-2. Director, Electronics Laboratory Center, Evans Signal Laboratory, Silver, Md.
- 67-12-3. Director, Underwater Experiment Station, Ft. Belvoir, Mo., ATTN: Library
- 67-12-4. Director, Armed Forces Institute of Pathology, Walter Reed Army Medical Center, 3150 Mink Street, S.E., Washington 25, D.C.
- 67-12-5. Director, Operations Research Office, Johns Hopkins University, 1100 Massachusetts Ave., Chevy Chase, Md. Washington 25, D.C.
- 67-12-6. Commanding General, Quartermaster Research and Development Command, Quartermaster Research and Development Center, Dallas, Texas ATTN: CPM Liaison Officer
- 67-12-7. Chief of Naval Operations, D/X, Washington 25, D.C. ATTN: CP-03
- 67-12-8. Chief of Naval Operations, D/X, Washington 25, D.C. ATTN: CP-03E
- 67-12-9. Director of Naval Intelligence, D/X, Washington 25, D.C. ATTN: CP-03
- 67-12-10. Chief, Bureau of Medicine and Surgery, D/X, Washington 25, D.C. ATTN: Special Weapons Defense Div.
- 67-12-11. Chief, Bureau of Ordnance, D/X, Washington 25, D.C.
- 67-12-12. Chief, Bureau of Ships, D/X, Washington 25, D.C. ATTN: Code 1-8
- 67-12-13. Chief, Bureau of Yards and Docks, D/X, Washington 25, D.C. ATTN: D-440
- 67-12-14. Chief, Bureau of Supplies and Accounts, D/X, Washington 25, D.C.
- 67-12-15. Chief, Bureau of Aeronautics, D/X, Washington 25, D.C.
- 67-12-16. Chief of Naval Research, Department of the Navy, Washington 25, D.C. ATTN: Code 811
- 67-12-17. Commander-in-Chief, U.S. Pacific Fleet, Fleet Post Office, San Francisco, Calif.
- 67-12-18. Commander-in-Chief, U.S. Atlantic Fleet, U.S. Naval Base, Norfolk 11, Va.
- 67-12-19. Commandant, U.S. Marine Corps, Washington 25, D.C. ATTN: Code 403H
- 67-12-20. President, U.S. Naval War College, Newport, R.I.
- 67-12-21. Chief, U.S. Naval Postgraduate School, Monterey, Calif.
- 67-12-22. Commanding Officer, U.S. Naval Schools Command, U.S. Naval Station, Treasure Island, San Francisco, Calif.
- 67-12-23. Commanding Officer, U.S. Fleet Training Center, Naval Base, Norfolk 11, Va. ATTN: Special Weapons School
- 67-12-24. Commanding Officer, U.S. Fleet Training Center, Naval Station, San Diego 34, Calif. ATTN: School
- 67-12-25. Commanding Officer, Air Development Squadron 1, VX-1, U.S. Naval Air Station, Moffett Field, Calif.
- 67-12-26. Commanding Officer, U.S. Naval Advance Control Training Center, Naval Base, Philadelphia 1, Pa. ATTN: AIC Defense Course
- 67-12-27. Commander, U.S. Naval Ordnance Laboratory, Silver Spring 19, Md. ATTN: EE
- 67-12-28. Commander, U.S. Naval Ordnance Laboratory, Silver Spring 19, Md. ATTN: EE
- 67-12-29. Commander, U.S. Naval Ordnance Laboratory, Silver Spring 19, Md. ATTN: P
- 67-12-30. Commander, U.S. Naval Ordnance Test Station, Azusa, China Lake, Calif.
- 67-12-31. Officer-in-Charge, U.S. Naval Civil Engineering Research and Evaluation Lab., U.S. Naval Construction Battalion Center, Port Hueneme, Calif. ATTN: Code 793

SECRET

- 60 Commanding Officer, U.S. Naval Medical Research Inst.
National Naval Medical Center, Bethesda 14, Md.
- 61 Director, Naval Air Experimental Station, Air
Material Center, U.S. Naval Base, Philadelphia,
Penn.
- 62 Director, U.S. Naval Research Laboratory, Washington
25, D.C. ATTN: Mrs. Katherine E. Case
- 63 Commanding Officer and Director, U.S. Navy Electronics
Laboratory, San Diego 72, Calif.
- 64-65 Commanding Officer, U.S. Naval Pathological Infection
Laboratory, San Francisco 24 Calif. ATTN: Technical
Information Division
- 66-68 Chief, Bureau of Aeronautics, U.S. Washington 25,
D.C. ATTN: AFM-45-41/50
- 91-92 Commanding Officer and Director, David W. Taylor Model
Basin, Washington 25, D.C. ATTN: Library
- 93 Commander, U.S. Naval Air Development Center, John-
sville, Pa.
- 94-95 Chief, Fleet Post Office, San Francisco, Calif.
- 96 Commander, Buffalo Naval District, Buffalo 10, N.Y.
ATTN: c/o 100
- 100-101 Commander, Wright Air Development Center, Wright
Patterson AFB, Dayton, O. ATTN: WACB
- 112-113 Commander, Air Force Cambridge Research Center, 12
Randolph Field, Bedford, Mass. ATTN: CMAW-2
- 114-115 Commander, Air Force Special Weapons Center, Kirtland
AFB, N. Mex. ATTN: Library
- 117-118 Commander, Lowry AFB, Denver, Colo. ATTN: Department
of Special Weapons Training
- 119 Commander, DAFPA Special Weapons Squadron, Head-
quarters, USAF, Washington 25, D.C.
- 120-121 The PAED Corporation, 1700 Main Street, Santa Monica,
Calif. ATTN: Nuclear Energy Division
- 122 Commander, Second Air Force, Randolph AFB, Texas. ATTN: Operations Analysis Office
- 123 Commander, Eighth Air Force, Westover AFB, Mass. ATTN: Operations Analysis Office
- 124 Commander, Fifteenth Air Force, March AFB, Calif. ATTN: Operations Analysis Office
- 125 Commander, Western Development Division, 1000
Industrial Drive, 10000 S.W. 10th, W. P. 10000
- ATTN: KRAMBONT, J. JOHN I. AMERICAN
- 126 Asst. Secretary of Defense Research and Development,
DOD, Washington 25, D.C. ATTN: Tech. Library
- 127 Asst. Chief of Staff, Joint Chiefs of Staff, Washington
25, D.C. ATTN: Operations Analysis Office
- 128 Director, Defense Systems Evaluation Board, USAF, Pa.
129 Director, Defense Systems Evaluation Board, USAF, Building
100, 1200 1st Street, Washington 25, D.C.
- 130 Commander, Armed Forces Staff, Building 100, Norfolk 14,
Va. ATTN: Secretary
- 131 Commander, Field Command, Armed Forces Special
Weapons Project, 1000 1st Street, Albuquerque, N. Mex.
- 132 Commander, Field Command, Armed Forces Special
Weapons Project, 1000 1st Street, Albuquerque, N. Mex.
ATTN: Technical Training Group
- 133 Commander, 7th AFSC, 1000 1st Street, Albuquerque,
N.M. ATTN: Deputy Chief of Staff, Weapons
Effects Tests
- 134-135 Chief, Armed Forces Special Weapons Project, Building 100,
1000 1st Street, Albuquerque, N. Mex. ATTN: Documents Library Branch
- 136 Office of the Technical Director, Directorate of Eff-
ects Tests, Field Command, AFSC, 1000 1st Street,
Albuquerque, N.M. ATTN: c/o 100
- ATOMIC ENERGY COMMISSION ACTIVITIES
- 137-138 U.S. Atomic Energy Commission, Classified Technical
Library, 1901 Constitution Ave., Washington 25, D.C.
ATTN: Mrs. J. M. O'Leary (For CMA)
- 139-140 Los Alamos Scientific Laboratory, Report Library, P
Box 166, Los Alamos, N. Mex. ATTN: Helen Pedman
- 141-142 Sandia Corporation, Classified Document Division,
Sandia Base, Albuquerque, N. Mex. ATTN: Martin
Lucero
- 143-144 University of California Radiation Laboratory, 1000
10th, Livermore, Calif. ATTN: Louis J. Gault
- 145-146 Argonne National Laboratory, Technical Information Service
147-148 Technical Information Service Extension, Los Alamos, N.M.
(Duplicate)

SECRET

RESTRICTED DATA